Functional implications of size reduction in molar dentition during human evolution: using 3D printed models

Scott T Camp

MSc by Thesis

The University of Hull and The University of York

Hull York Medical School

April 2019

ABSTRACT

During hominin evolution the size of postcanine dentition has varied. While many researchers have tried to make predictions as to the functional significance of these changes, the effect of tooth size on food breakdown has not been quantified.

This thesis develops a novel physical testing rig to compare the fracture performance of teeth of differing sizes on the breakdown of food replicas to examine the relationship between tooth size, food size and breakdown performance. This work presents the design protocol and sensitivity studies carried out in order to develop the methodology for subsequent investigations into dental mechanics.

To examine the effect of dental reduction during human evolution on hard food breakdown stainless steel dental models of a modern *Homo sapiens* upper and lower dental row were isometrically scaled up. A size series of physical dental rows were attached to a universal testing machine and the efficiency of food breakdown recorded for each (force at initial fracture, energy, displacement and fragmentation), using 3D printed spherical hard brittle food replicas with diameters of 5mm, 10mm, 15mm, and 20mm.

The results of this study suggest that smaller teeth of modern *Homo sapiens* are slightly more efficient at reducing peak forces and energy consumption of initial fracture of food objects than larger teeth. However, compared to the effect of changes in food size and the location of the bite on the tooth, performance differences between the different tooth sizes were minimal. The results suggest that individuals may be able to access different stress resistant food resources by simply changing how they position a food item, but also suggest that dental reduction during human evolution may have had a minimal impact on the ability of the individual to break hard food items of varying sizes. This study highlights the conflicting constraints placed on teeth and considers the evolutionary, developmental and mechanical mechanisms that may have resulted in the reduced molar size we see during human evolution.

LIST OF CONTENTS

The following is a small excision that formed part of Ch. 2 that details the methods used to create the sphere placement devices and a description of the reason they were not used in the project. If the shrinkage problem could be overcome it is recommended any attempt to replicate this study make use of similar devices.

LIST OF FIGURES

machining, (C) Specimen C13. 41 created via Sculpteo via binder jetting, (D) Specimen C13. 41 created via Shapeways via binder jetting. (Image adapted from Hunter 2016).

Figure 2.12 Physical CNC model of an M1 molar tooth of *Cercocebus atys* attached to a universal materials tester.

Figure 2.13 3D printed domes (powder and binder) to be crushed in a sensitivity study of tooth design. (Images adapted from Swan 2016 and Hunter 2016)

Figure 2.14 Boxplot showing peak force (N) recorded during breakdown of solid domes.

Figure 2.15 Force-displacement graphs showing the differences between runs.

Figure 2.16 Examples of different methods used to attach the dentition to the physical testing equipment and load cell. (A) method used in Berthaume et al., 2010, (B) method used in Hunter 2016.

Figure 2.17 The universal materials tester (Mecmesin MultiTest 2.5~i) used in the study. The dental models required a method of attachment to the load cell (left) and the base plate (zoomed in on right) to be established.

Figure 2.18 Circular attachment plate prototypes attached to the universal materials tester.

Figure 2.19 Square attachment plates. (A) The attachment plate for the mandibular teeth with two hole placed for attachment to baseplate. (B) Top view of attachment plate for the maxillary teeth with one hole placed in the centre.

Figure 2.20 Upper and lower dental models virtually attached to the plates. (A) Lower dental model with the plate being lowered vertically into alignment. (B) The upper dental model with the plate being raised vertically into alignment. (C) Final virtual mandibular molar model before merging with plate (D) Final maxillary molar model before merging with plate.

Figure 2.21 Final 3D stainless steel metal print of an upper and lower dental row of a modern *H.sapiens* attached to an attachment plate.

Figure 2.22 Virtual 3d spheres used as food replicas. Spheres vary in size 5mm, 10mm, 15mm and 20mm in diameter (left to right).

Figure 2.23 Multiple attempts to print the 10mm spheres. Prints ended up egg shaped objects rather than spheres.

Figure 2.24 Examples of supports for 10mm diameter spheres. The five supports and spheres to the right were created automatically by ZPrint Pro. The small support second from the left was designed by the author. On the far left is a "sphere" printed without a support.

Figure 2.25 Process for the creation of the sphere supports. (A) Measurements used in the process (B) final 3D based produced. This design minimised material and produced a spherical object post print.

LIST OF TABLES

Acknowledgements

Author's Declaration

I confirm that this work is original and that if any passage(s) or diagram(s) have been copied from academic papers, books, the internet or any other sources these are clearly identified by the use of quotation marks and the reference(s) is fully cited. I certify that, other than where indicated, this is my own work and does not breach the regulations of HYMS, the University of Hull or the University of York regarding plagiarism or academic conduct in examinations. I have read the HYMS Code of Practice on Academic Misconduct, and state that this piece of work is my own and does not contain any unacknowledged work from any other sources.

Chapter 1. Dental Reduction During Human Evolution

During the evolution of our own species, *Homo sapiens*, significant changes in our masticatory and dental morphology have occurred. Given the vital role the masticatory apparatus has in the acquisition and processing of foods variations in masticatory form have often been associated with changes in the mechanical requirements of food breakdown. Indeed, these changes in form, especially overall size of the dentition, also coincide with changes in our ancestor's extraoral food processing capabilities, including hunter gathering and agricultural practices. Thus, changes in dental size could imply, and be related to, some significant dietary shifts. However, the functional significance of these changes has not been investigated.

This chapter will review the trends in dental form evolution within the hominins and examine the different methods researchers have used to elucidate the relationship between dental form and function.

1.1 Masticatory changes During Human Evolution

Hominin evolution has been characterized as a marked trend towards masticatory apparatus reduction accompanying increased retrognathism and bipedalism. Indeed, the panins, represented by the extant species *P. troglodytes* and *P. paniscus* are differentiated in part from the other hominins, from which they separated between 13 and 6 million years ago (Patterson et al. 2006), by their flat, prognathic faces, large anterior teeth and relatively small post-canine teeth (Aiello and Dean 1990). This later relationship is generally mirrored in the other hominins, of which *Homo* sapiens is the only extant member.

1.1.1 Masticatory apparatus within the Australopithecines

The genus *Australopithecus* emerged around 5 million years ago, and is generally considered ancestral to our own (Teaford and Ungar 2000; Irish et al. 2015). Significant differences exist between the masticatory apparatuses of the robust and gracile australopithecines. In addition to massive jaws and larger muscles of

mastication, robust australopithecines such as *P. robustus* and *P. boisei* exhibit significantly larger teeth than the gracile australopithecines like *A. afarensis* or *A. africanus* (see Table 3.1) (Wood and Stack 1980; Aiello and Dean 1990). Current research is uncertain as to the impetus behind these differences. Finite element analysis indicates australopithecines are well adapted to hard object feeding (Strait et al. 2010; Strait et al. 2013). However, physical testing (Berthaume et al. 2010), dental microwear (Ungar et al. 2010), and isotopic evidence do not necessarily support this. The isotopic evidence in particular groups several of the gracile species with *P. boisei* as high C4 eaters, which could indicate hard foods like nuts, while *P. robustus* is contrastingly a C3 eater, associated with tough foods like grasses and sedges (van der Merwe et al. 2008; Lee-Thorpe et al. 2010; Sponheimer et al. 2013). Daegling et al. (2013) suggests that the morphological differences are artefacts of development and phylogeny rather than overt adaptations.

1.1.2 Masticatory apparatus within *Homo* (2.4 mil.- 300,000 ya.)

Our own genus originated some 2.4 million years ago (Wood and Collard 1999; Dunsworth 2010). Several Early *Homo* are distinguished in part from australopithecines by a reduction in size of the jaws and post-canine teeth (Kay 1985; Braice et al. 1991; Teaford et al. 2002). Early *Homo* species also have smaller estimated bite forces (Demes and Creel 1988; Constantino et al. 2010) though this has recently been disputed (Ruiz and Arsuaga 2017). These changes are presumed to be adaptations to a dietary shift towards increased pre-processing of foods and increased exploitation of foods richer in nutrients or more calorically dense (Ungar et al. 2006). Meat consumption in particular is often singled out as a driver for this change (Aiello and Wheeler 1995; Wrangham et al. 1999).

1.1.3 Masticatory apparatus within *Homo sapiens* (300,000 ya. - current)

Our own species, *Homo sapiens*, is relatively young. New evidence from Morocco indicates anatomically modern *H. sapiens* had emerged by 300,000 years ago (Hublin et al. 2017). These early modern humans had teeth much larger than those of modern humans today, with more primitive morphology as well. However, they are smaller than those of other *Homo* species of the time, such as *H.*

neanderthalensis, with a similar jaw shape and other anatomical features. Beginning about 100,000 years ago, human teeth, particularly in the Levant (LeBlanc and Black 1974) and Eurasia began experiencing a marked increase in the rate of size reduction to about 1% in the buccolingual and mesiodistal dimensions every 1000 years. This increased further approximately 10,000 years ago, to about 2% in the buccolingual and mesiodistal dimensions every 1000 years, which coincides nicely with the development of agriculture in this area (Brace et al. 1987; Calcagno and Gibson 1988; Macho and Moggi-Cecchi 1992; Pinhasi and Meiklejohn 2011; Vukelic et al. 2017). This could indicate that decreased food toughness due to increased pre-processing associated with agriculture lead to a smaller dentition. Modern populations nevertheless experience a great variety in tooth size, indeed, to a greater degree than any other Hominin species (Bailey et al. 2017). This appears to be geographically and ecologically determined, with the greatest size reduction seen in populations that consume the most pre-processed diets (Townsend et al. 2012; Freire Fernandes et al. 2013; Pilloud et al. 2014).

1.2 Diet and Food mechanical properties

The goal of mastication is to simultaneously reduce food objects in size so that they can be ingested without causing aspiration or airway obstruction and to increase surface area of the food object to aid in digestion. To do this, fracture must be induced in the food object via deformation (Lucas 2004). Fracture mechanics and behaviours are influenced by both the material properties of the food object and the mechanical properties of the tooth (Kay 1975; Lucas 2004).

The material properties of the food objects can be described in several ways. Some foods are stress limited, meaning they fracture under high stress but low strain, i.e. they are poor at resisting deformation. Other objects are displacement-limited, meaning they can withstand high strain, i.e. high deformation, before fracture (Daegling et al. 2011; Lucas 2004). Foods tend to fall within a spectrum between these two categories.

The mechanical properties of foods can be tested using a universal testing machine, which can subject the food to tension or compression (Williams et al. 2005; Berthaume 2016a). This testing returns a force-displacement curve graphing

the object's performance. By calculating the area bound by this graph and the x-axis, the energy absorbed by the material up to, and thus required to induce, fracture can be determined (Swan 2016).

Modern humans tend to have a highly processed diet, with a mix of stress and displacement limited foods. However, the universal testing machine is best able to simulate a diet of hard object feeding.

1.3 Chewing efficiency measures

As mentioned, mastication is designed to increase food object surface area while reducing the object to manageable size for swallowing. This requires the object to be highly fragmented. Additionally, teeth are also used for processing, particularly of hard objects. Hard objects like nuts are cracked so the seed can be consumed and the shell discarded. Mastication can only be regarded as efficient if the amount of energy expended processing the food object is less than the amount of energy gained by consuming the food. This efficiency can be achieved in several ways. For example, limiting force by properly distributing it to achieve fracture, or maximizing the amount of fragmentation in order to maximize the energy returned in digestion.

1.4 Conclusion

This chapter has outlined the general trend in hominin evolution. Tooth size reduction has been a hallmark of this evolution, with a marked increase since the middle Palaeolithic and an additional increase since the Mesolithic. This size reduction is often interpreted as a reflection of changes in diet indicating increased pre-processing and decreased toughness of food.

Chapter 2. The Development and Creation of Human Dental Models for Physical Testing Experimentation

2.1 Introduction

Computational models used in Finite Element Analysis (FEA) and Multibody Dynamic Analysis (MDA) have frequently been employed over the last few decades to investigate the relationship between primate and hominin masticatory form and function (Sellers et al. 2004; Curtis et al. 2008; Strait et al. 2009, 2010; Shi et al. 2012). While these models are of significant value, especially in their ability to be easily manipulated to perform virtual experiments, some aspect of their performance capabilities are difficult, if not impossible to capture. This is especially the case for investigations looking into the relationship between tooth form and food breakdown. For example, some researchers (Anderson and Rayfield 2012, Berthaume et al. 2010) have previously used FEA to study the energy required to fracture a food item and the points of potential failure (of the food or tooth). However, modelling the material and mechanical properties of food items is highly challenging and fragmentation is impossible to accurately predict (Khodabakhshian and Emadi 2014; Zhang et al. 2018).

Other studies have tried previously to relate the size of molar teeth to the performance of food breakdown (Laird et al. 2016) using live individuals and recorded data during feeding experiments (Laird 2015). Problems with interpreting such data exist due to the variability of feeding patterns between individuals and the shape variation that exists between teeth. Frequently it is also the case that in vivo feeding experiments would not be feasible due to ethical reasons or access to the living individual, this is especially relevant for the fossil hominins.

The majority of previous work investigating the relationship between dental form and food breakdown has thus been conducted using either theoretical or physical experimental methods. Physical experimental methods generally consist of creating dental replicas (tool blades, points, or metal tooth replicas) and attaching

them to a physical load cell/force transducer. The dental replicas are compressed into a food item and the force, displacement and fracture performance are recorded (Anderson 2009, Berthaume et al. 2010; Crofts and Summers 2014). Some studies have created stylised blades and points (Anderson 2009, Swan 2016). Others have used 3D models to create dental replicas of specific species (Berthaume et al. 2010; Hunter 2016). With recent advances in 3D computer modelling and 3D printing it is now possible to create virtual dental replicas and manufacture them in almost any material. This presents a great opportunity to combine physical testing with virtual experimentation, creating a series of teeth with can be modified in morphology virtually and physically 3D printed to test various form-function related questions, such as the effect of dental size on food breakdown.

Physical experimentation however also poses some additional challenges. Real foods vary significantly in their material and mechanical properties (Williams et al. 2005). This creates a challenge in studies comparing the functional significance of changes in biological form; the variability in the food samples may hide any biological signal in the tooth performance results. Several researchers have thus turned to rapid prototyping to create controlled replica food items (Crofts and Summers 2014; Swan 2016; Hunter 2016). This technique allows for replica food items to be controlled in both material properties and morphology and as such offers an exciting opportunity to not only control the study but to further investigate optimal item size for a given tooth size.

2.2 Aims and objectives

In order to test for any functional significance in molar dentition size reduction during hominin evolution, and to investigate the performance relationship between food size and tooth size, it was necessary to develop a methodology that would allow different food items to be broken down with different sized teeth in a controlled way.

The objective of this stage of the project was therefore to develop a process and method, whereby hypothetical teeth of varying sizes could be created and made

physically compatible with a universal material physical testing machine. To allow a controlled investigation into food breakdown, it was also necessary to create a replica food item. Several attempted methods to acquire dental replicas will be discussed, describing the rationale behind them, detailing the procedures employed, and presenting the final rig design which will be used in subsequent chapters to test several hypotheses related to the significance of tooth size on food object breakdown.

Aims:

1. Create a 3D surface scan of a modern human's dentition suitable for 3D printing.
2. Develop and create mode of attachment for the dental model to the universal testing machine.
3. Develop and create food items that are suitable for materials testing.
4. Develop a method to place the food items between teeth during the experiment.

2.3 The Creation of a 3D surface scan of a modern human's dentition suitable for 3D printing

Attaching real teeth to a materials tester to compare performance would present some significant challenges. Real teeth vary in size and shape, and cannot be increased in size for experimentation. Larger teeth from a different individual would also possess variations in shape and as such real teeth not conducive to a controlled study examining the effects of dental size (Laird et al. 2016). The other problem with real teeth is that they can break, and in doing so the risk to data collection is high. As such the first decision the project needed to make was how to create the dental rig. 3D virtual modelling and 3D printing technologies offer an ideal solution. 3D virtual replicas of teeth can be created, modified in a controlled way to keep shape constant but modify size, and subsequently printed in any material. Similar approaches have been used previously (Berthaume et al. 2010; Crofts and Summers 2014; Hunter 2016; Swan 2016). In these studies, it was decided that the physical models should be stainless steel to resist deformation

due to the nature of repeated testing using a universal material tester. Due to the success of the above studies it was decided that this approach would also be adopted here.

2.3.1 Acquisition of 3D dental replicas

Before any 3D dental model could be printed it was necessary to first create virtual replicas of a human upper and lower dental row. There are a number of alternative imaging modalities by which a virtual replica of the physical teeth of a modern human can be created. Computed Tomography (CT scanning), is an ideal technique for generating 3D virtual models, however due to associated health risks (Schmidt 2012) this technique is limited in its use to bony skulls or cadavers rather than direct from modern living humans. Surface scanning techniques such as photogrammetry and structured light scanning have also been used to digitize teeth before with success (Friess 2012), however they are not suitable for scanning internal materials and as such are limited to bony skulls. Some pre-existing medical CT scans of bony skulls or cadavers were available. However, to be used in this study certain criteria needed to be met, such that individuals possessed a full set of upper and lower dentition, with no signs of orthodontic treatment. Unfortunately all bony skulls and CT scans of specimens available to us at this time had dental conditions unsuitable for this study.

2.3.2 Dental impression from a living modern human

Due to the above constraints it was decided that the dental casts should be obtained from a living modern subject following the protocols used by dental professionals (Nandini et al. 2008). Moulds taken from an individual would be cast in a plaster of Paris and subsequently scanned using a 3D surface scanner (Dalstra and Melsen 2007; Birnbaum and Aaronson 2008; Slizewski et al. 2010; Friess 2012). A living subject could also provide information, not always available from a deceased or medical specimen, regarding age, gender, ethnic and geographical

background, dietary preference, feeding behaviours, and knowledge of any previous orthodontic treatment. Also, if bite force and other mechanical values were needed these could be more readily acquired.

2.3.2.1 Ethics

As such an approach required access to human data ethics were first sought. Appropriate documents were prepared to satisfy requirements set out by the ethics review boards at both the Hull York Medical School and the Biology Department of the University of York. Ethical approval for this aspect of the project was subsequently granted to obtain and scan the dentition of human subjects.

2.3.2.2 Criteria for acceptance in the study

The dentition of modern human populations displays a vast variety of traits, sizes, and shapes. For this reason, a set of criteria approximating an average or standard adult human were selected for final subject selected for the study. The pool from which the subject could be selected would be restricted to students and staff of the Hull York Medical School (HYMS), a condition for the acceptance of the ethics application.

In order for the method of dental casting to be refined one subject was chosen who was an easily accessible member of HYMS. This subject did not satisfy the criteria having M3 agenesis and previous orthodontic treatment which included the extraction of premolars. However, for the purpose of method development they were deemed an acceptable choice to test run the method.

The subject who would be used in the final casting was also identified. Of over twenty students and faculty polled, only three had third molars and no previous orthodontic treatment. Interestingly M3 agenesis, the lack of the development of one or more third molars in an individual, is relatively prevalent amongst modern populations (Alam et al. 2014), and some studies indicate no significant chewing efficiency difference between modern humans with and without third molars

(Laird et al. 2016). However, third molars are included in the ancestral state, and as this project is fundamentally interested in the implications of molar size reduction, the presence of third molars was always the main criterion for acceptance in the study.

2.3.2.3 Dental casting methods and materials

All equipment was first cleaned and sterilized before the procedure began. In order to create plaster casts of the subject's dentition, a mould of the subject's teeth *in situ* was first obtained. This mould was created using an alginate powder derived from seaweed (Xantalgin crono). Approximately 23 g of alginate powder was mixed with 50 ml of tap water in a mixing bowl. A particular feature of Xantalgin crono is its ability to change colour using dies that react to changes in the pH level and reflect changes to the material properties of the alginate. As the water was applied, the powder assumed a lavender colour, which slowly changed to a lighter purple after approximately 40 seconds of mixing. In order to minimise the inclusion of air bubbles in the mix, the bowl was periodically placed on a dental vibrator. For the next 60 seconds the mixture, a thick pink paste, was ready for application to the subject's teeth. Aside from the more obvious, though slight risk of aspiration of and and/or asphyxiation on the alginate or other materials entering the subject's mouth, Xantalgin crono, like any alginate, posed certain potential health risks. According to the associated health and safety sheet Xantalgin crono has a potential for sensitization through skin contact. It is principally composed of 50-75% soda ash flux-calcined Kieselguhr; 5-10% Talc $(Mg_3H_2(SiO_3)_4)$; 0-5% dipotassium hexaflourotitanate; and 0-5% Paraffin waxes and Hydrocarbon waxes; and 0-5% magnesium oxide. The product contains fine quartz powder. Xantalgin crono is classed as having a potential to cause serious eye irritation and may cause an allergic skin reaction. Prolonged inhalation may cause silicosis. As such the subject was given eye protection and instructed to rinse their mouth with water and wash their face and hands, with particular attention devoted to the skin around their mouth before and after the procedure as countermeasures against these risks. In general, contact between the subject and the alginate was limited as much as possible. Prolonged inhalation, skin contact,

and eye contact was also potentially hazardous to the researchers. Protective masks, hypoallergenic gloves and protective eyewear were worn throughout the procedure. There was no reasonable expectation that the project would involve prolonged inhalation of the material.

The alginate paste was scooped into a dental tray which was subsequently applied to either the upper or lower dentition of the subject. After approximately 60 seconds, the tray was removed from the subject's mouth and left to dry for about 15 minutes. The alginate mould dried quickly, losing its original pink, rubbery consistency, and turning into a dry, colourless, brittle, shrunken husk. For this reason, the mould is best used for Plaster of Paris casting within approximately an hour of being made.

Plaster of Paris (Fine Casting Plaster of Paris, Home Pack LTD) was mixed with water (2 cups water: 1 part powder) and poured into the alginate moulds. The first attempts (see Figure 2.1) were either missing features or riddled with air bubbles that made the resulting casts unusable. However, with the use of a dental vibrator (Jintai R&D, Model JT-14), air bubbles were reduced (Figure 2.2). This method was subsequently used to collect upper and lower dental row casts.
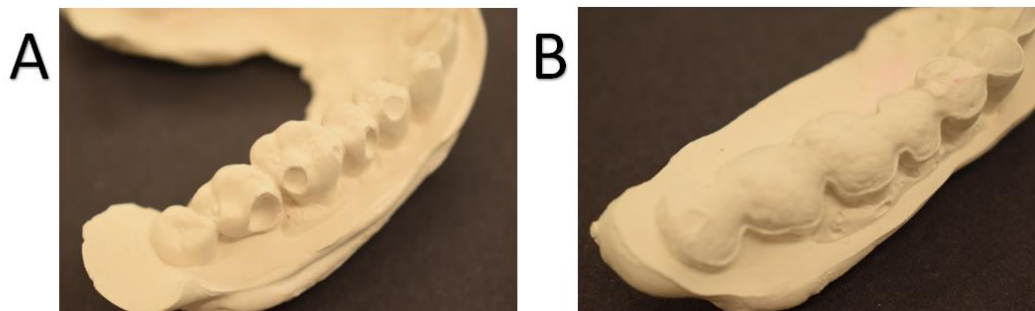
Figure 2.1 Two failed attempts at modern human dental casting using Plaster of Paris taken from alginate dental moulds; (A) suffers from air bubbles, while (B) the plaster failed to properly fill the mould, leaving a featureless cast.

Figure 2.2 Final and most successful modern human dental cast using pPlaster of Paris taken from alginate dental moulds.

2.3.2.4 Surface scanning of the plaster casts

In order to turn the dental casts into 3D virtual models the final casts obtained from the volunteer test candidate (Figure 2.3) were scanned using a structured light scanner. The accuracy of the Breuckmann Smart Scan 3D scanner, and its ability to collect reliable 3D data from teeth has been investigated previously (Slizewski et al. 2010; Friess 2012). The scanner has a 150mm field of view and prior to the scanning the Breuckmann was calibrated to an accuracy of 9 μm. The specimen was placed in a black light photobooth on a turntable and the individual images collected and aligned using the scanner and its associated Optocat software (Slizewski et al. 2010). The scanner had no difficulty imaging the plaster, as unlike real teeth, the material is not transparent or reflective. The casts themselves did have some minor errors (small bubbles) which were unfortunately preserved in the scans but these were not major. Subsequent post processing was carried out using Geomagic Studio (v.11; Dassault Systèmes SolidWorks Corp., MA, USA). Using surface meshing and processing these minor artefacts were automatically filled and the surface cleaned, removing any imperfections (Figure 2.3). Geomagic's 'Fill Holes' tool has three options for 'Fill type'. The 'Flat' option bridges the holes with a flat surface. The 'Curvature' option fills the holes by interpolating a surface that connects the edges while preserving the surrounding curvature. The 'Tangent' option creates a surface that fills the gap but can slightly

alter the curvature of the surrounding polygons, resulting in a fill similar to the 'Curvature' option, but more tapered. As the intent was to preserve the real shape of the teeth as much as possible, the 'Curvature' option was selected. Some error was undoubtedly introduced during this process, but the resulting models were visually similar to the actual teeth. The resulting 3D models are presented in Figure 2.4.

Figure 2.3 Virtual cleaning of mandibular (left) and maxillary (right) virtual models of a volunteer modern human dentition scanned from dental casts. The red shows the areas that required hole filling. Note some obvious inclusions on the lingual face of the maxillary incisors.
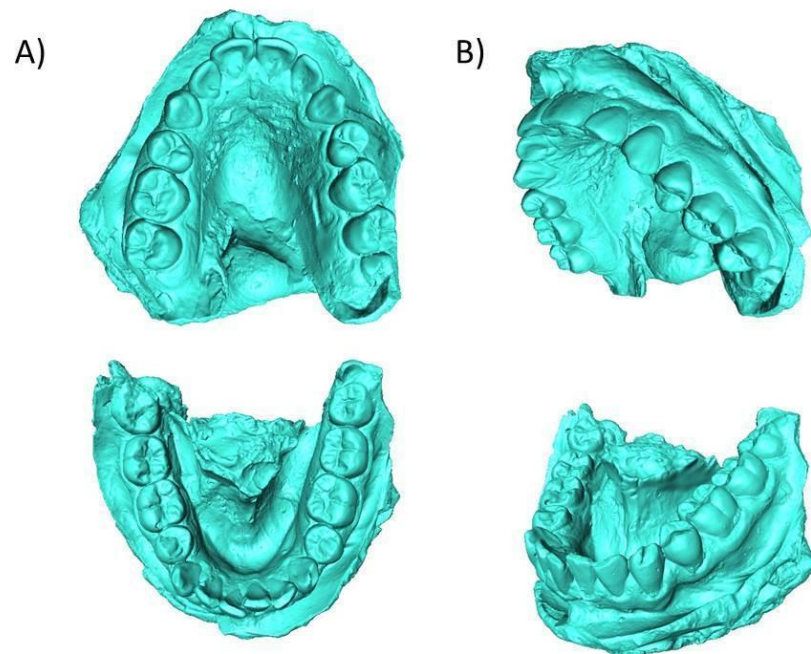
Figure 2.4 Final 3D virtual models of a volunteer *H. sapiens* dentition scanned from dental casts. A) occlusal view of the mandibular (top) and maxillary teeth (bottom); B) oblique view of the mandibular (top) and maxillary teeth (bottom). Note only the upper left M3 is present in this individual, and the specimen lacks second premolars.

2.3.2.5 Abandonment of plaster cast technique

The above approach, surface scanning a plaster of Paris cast of living human dentition, proved successful. Unfortunately, while suitable living candidates were identified at the start of this study, and agreed to participate, they were not available when required for the real data to be collected. As such it was necessary to find an alternative approach to collecting the dental impressions. Fortunately, an alternative approach presented itself; with the new addition of a well-preserved adult male modern *H. sapiens* into the skeletal collection at Hull York Medical School.

2.3.3 Dental scans from a bony skull

The skeleton of a modern human (Figure 2.5) male with complete, unaltered post-canine dentition with an acceptable state of dental wear (fairly unworn) was presented to the Hull York Medical School by the York Teaching Hospital. This skeleton, was thus ideal for this project. As the skeleton was officially a component of the Hull York Medical School teaching collection, there was no requirement to seek additional ethics approval. Some incisors were missing but as this project focuses on molar teeth this was not considered an issue.
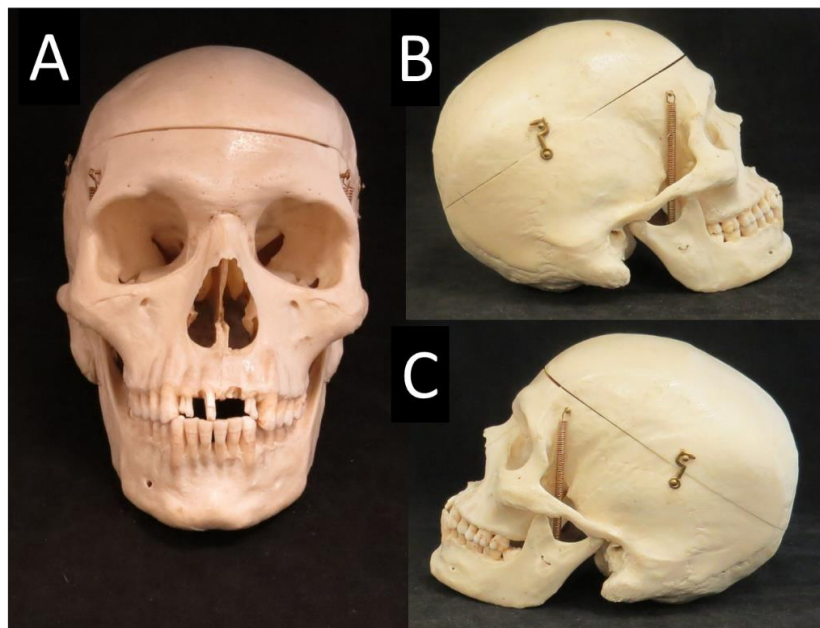
Figure 2.5 Adult modern human male skull used in the creation of the dental replicas. Frontal view (A), right lateral view (B), left lateral view (C).

2.3.3.1 Surface scanning of the skeletal material

Unlike with a living subject, the skull did not require the intermediate processes of mould creation and casting. Instead, the skull itself could be directly scanned. Given the previous success of the surface scanning technique, scans were again obtained using the 150mm field of view lens on a Breuckmann SmartScan 3D scanner. In order to be able to collect data from the occlusal surfaces of the teeth scans of the cranium and mandible were obtained separately (Figure 2.6 A&B). However, it was also necessary to produce a third scan of the teeth in occlusion. This additional scan (Figure 2.6 C) (teeth in occlusion) was needed to subsequently make sure the individual mandible and maxilla virtual surface files, which contained highly accurate dental surface data, could be realigned into occlusion (see below) and thus help create physical replicas with a realistic orientation relative to each other.

To conduct the scans the cranium was first placed in a black, light photobooth, on a turntable and individual images collected from all angles in the region of the maxilla. Special attention was paid to the occlusal surface of the molar teeth but data from more posterior or anterior aspects of the specimen were not deemed important, as such the surfaces in these areas were allowed to be less complete (Figure 2.6). Once scans of all orientations had been gathered the surface was generated and the cranium exchanged for the mandible and the process repeated. Finally, the mandible and maxilla were occluded and re-scanned as a whole (Figure 2.6). The scanner did have some minor difficulty picking up the bone and enamel, but this was ameliorated through application of a white talcum powder to problem areas on the specimen. This powder did not change the topography of the scanned areas. Additionally, some of the maxillary molars were loose, which did cause significant distortions in the scans. The teeth were subsequently lightly glued into their sockets using X60 two-component adhesive (HBM) and the scans were retaken without the distortion.
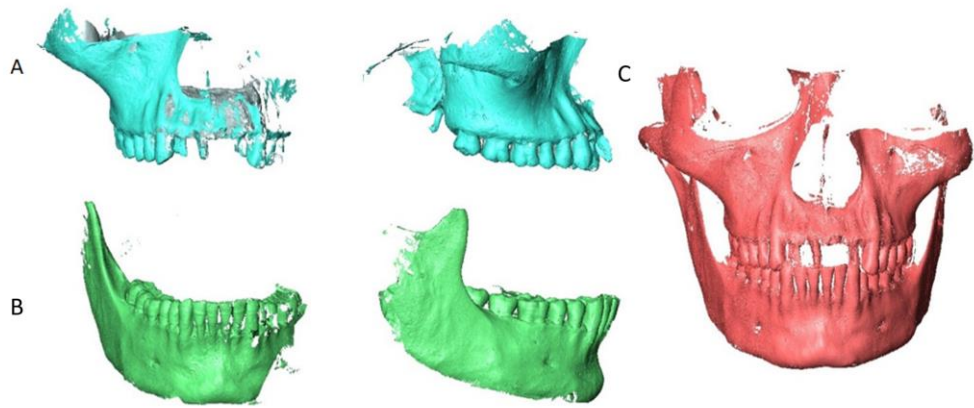
Figure 2.6 Surface scans of a modern human male taken directly from the skull. The maxilla (A) and mandible (B) are first scanned as separate objects and then scanned again as one object in occlusion (C).

2.3.3.2 Alignment and orientation of mandibular and maxillary surfaces

The three scans, the mandible, maxilla, and the teeth in occlusion (mandible and cranium) surface files (Figure 2.6) were imported into Avizo Lite (v 9.2, Visualization Sciences Group, Burlington, MA, USA). To align the individual maxilla and mandible surface files to the "teeth in occlusion" model, 3D landmarks were placed on identifiable features on the mandibular and maxillary surfaces. The same landmarks were also placed on the "teeth in occlusion" model and the maxilla and mandible were individually transformed using a rigid warp to the occluded scan, aligning the individual files to the target location (Figure 2.7).

Whilst the two individual scans were aligned to each other and in occlusion, in relation to the global axis the occlusal plane was not perpendicular to the vertical Y-axis. The consequence of this would have an impact on the subsequent cropping and creation of the physical testing rig. It was therefore necessary to transform the specimens so that the occlusal plane was on the XY plane. Three landmarks were placed on the occlusal surfaces of the right and left M_3 and the right M_1. These landmarks were then transformed to the XY plane with one landmark having an origin of 0,0,0. Avizo was used to apply the transformation to the surface files. In order to facilitate some other future operations and calculations, a landmark was subsequently placed on the centre of the occlusal surface of the right lower M_2, and the surface further transformed so that the 0,0,0 origin of the model was

at this location. The maxilla was also transformed to the same relative degree to preserve occlusion.
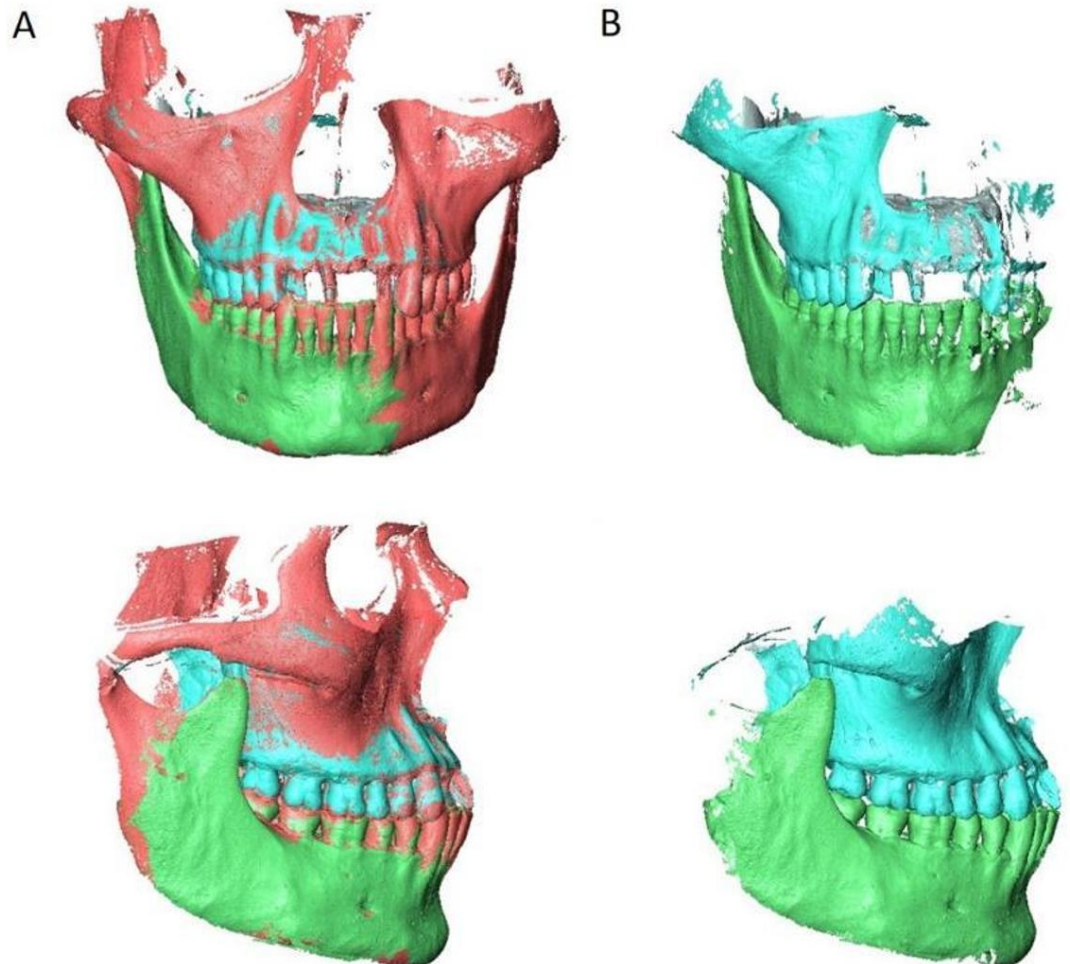
Figure 2.7 Individually scanned surface files of the maxilla and mandible aligned to the skull in occlusion. (A) Maxillary scan (blue) and mandibular scan (green) superimposed onto a scan of the mandible and cranium in occlusion (red). (B) Final mandibular and maxillary scans in occlusion.

2.3.3.3 Post processing of mandibular and maxillary surfaces

Once the maxilla and mandibular scans were aligned they were imported into Geomagic Studio (v.11; Dassault Systèmes SolidWorks Corp., MA, USA) and their meshes cleaned using the 'MeshDoctor' tool. Holes created on the mesial and distal surfaces of the teeth where overlap of the other teeth prevent the surface scanner to obtain data were filled using the 'Fill Holes' tool, again using the 'Curvature' option. These holes were unavoidable artefacts of the scanning

process, but as they were not present on the occlusal surfaces, they were deemed acceptable. The scans were also trimmed, deleting extraneous bone and teeth, so that only the molars and some surrounding bone was left. The need to minimise the additional material was due to the cost associated with 3D printing (see below) and for future ease of attachment to the physical testing rig. The final models in occlusion can be seen in Figure 2.9.
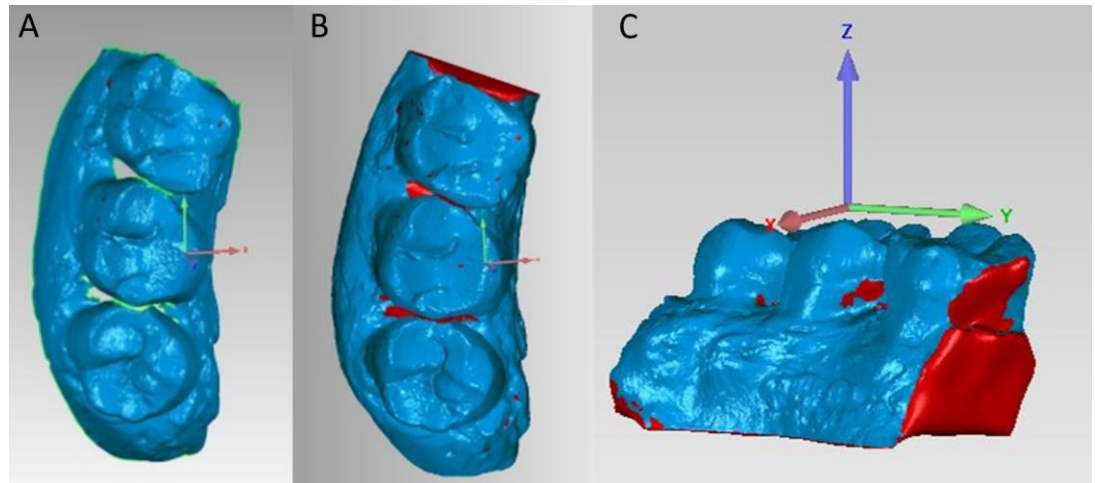
Figure 2.8 Cropped virtual molar row, an example of the trimming and filling stage during the creation of the virtual dental models. The surface files were cropped and holes identified (A), the holes virtually filled (B & C). Note the origin of the model is at the centre of the M2 (C) and the occlusal plane is orthogonal to the vertical.
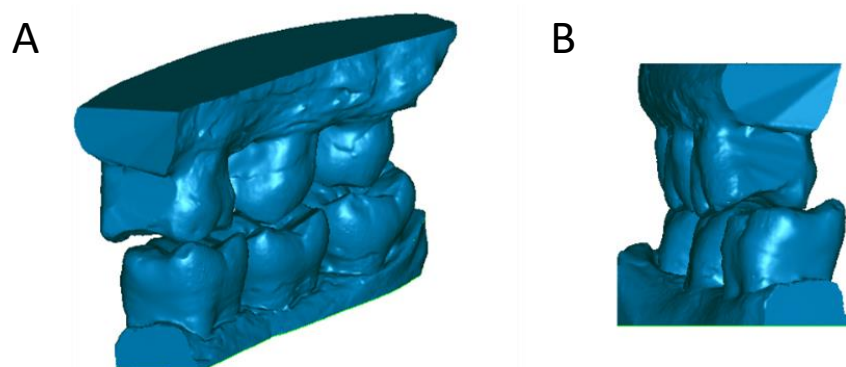
Figure 2.9 Final virtual molar dental models of a modern *H. sapiens,* maxillary and mandibular M1-M3 in occlusion. Lingual view of right side (A) frontal view (B).

2.4 3D printed dental models

Following completion of the dental models and the production of the 3D surfaces (Figures 2.9) it was necessary to create 3D physical replicas of the teeth. The physical replicas created needed to be accurate and able to withstand the forces subsequently applied they also need to be able to be attached to the physical testing rig.

First to check that the 3D prototypes were an accurate reflection of the original morphology the models were printed using the in-house Hull York Medical School's Zprinter 350 (ZCorporation). This printing using additive manufacturing to add layers of powder down in a vertical build chamber and fuse them, where necessary, with a binder. The 3D print material is a combination of zp150 high performance composite powder and zb63 clear binding solution. The power consists of plaster (<90%) and vinyl polymer (<20%). The binder is composed of humectant (<10%) and water (65-99%). It produces a high-performance composite with a resolution of 300 x 450 dpi and layer thickness of 0.09-0.01mm. Following

printing (Figure 2.10) the models were deemed a satisfactory replica of the original.

Figure 2.10 3D printed molar teeth of the human dental model using a powder-based polymer via additive manufacturing.

Whilst the in-house 3D printer was useful to gauge how well the virtual models could be transformed back into the physical one of the requirements of the dental models was withstand high forces and endurance. As such it was deemed necessary to print the final models in a stronger material which could withstand both the large forces and the repetitive loads placed on them. As such an external

company that could create rapid prototypes in stainless steel was needed. A third-party 3D printing company Sculpteo was selected following a brief sensitivity study the details of which are outlined below.

2.4.1 Rapid prototype 3D stainless steel sensitivity study

In order to make 3D physical replicas from virtual models of teeth previous work within the department (Swan 2016, Hunter 2016) have manufactured individual teeth using Computer Numerical Control (CNC) machining. This technique uses automated lathes, drills and saws to produce a 3D replica if the virtual model from a block of material. This approach produced very accurate replicas of the original virtual model (Swan 2016, Hunter 2016) but the cost is high. One tooth at the time of writing this thesis can cost around £150 to manufacture. As such given the large number of models planned to be created in this study an alternative manufacturing technique was sought. Rapid prototyping is a rapidly growing industry, 3D printers are not only commercially available but can be bought for domestic use and print using a variety of polymers, metals and other materials. Whilst there is a rise in its popularity not all 3D printers are capable or the accuracy and durability needed for this project. Some have also reported a significant shrinkage of the material during manufacture.

In order to be suitable for use in this project, the 3D printed teeth must produce accurate replicas and repeatable results. Two previous studies conducted in the department Swan (2016) and Hunter (2016) clearly show that the shape of the teeth has a pronounced effect on fracture mechanics. Therefore, to be suitable the 3D printed teeth used must satisfy two requirements: accuracy and repeatability. Accuracy in this case meant that the 3D printed teeth must be reasonably close in form to the computer model's surface file. Repeatability meant that the printed teeth must be able to withstand repeated compression tests without deformation.

In order to test the 3D prints for reliability and repeatability, it was decided that prior to printing the human dental models a sensitivity study should first be carried. This side study ~~will~~ compares the models created via different printers and techniques (CNC vs. 3D printing) both visually and in terms of physical

performance. As CNC models had already been produced within the department for a primate molar, an M_1 of a *Cercocebus atys*, it was decided, for economic reasons, that a sensitivity study would be carried out using this species tooth rather than create additional models for the human. While this sensitivity study described below is carried out on a single tooth of a different species to *H. sapiens*, the question here is not a biological one but one of 3D printing accuracy and durability.

The aim of this mini sensitivity study was to compare the morphology and fracture performance (force at initial fracture) of a CNC *C. atys* tooth against a number of different models produced via 3D rapid prototyping using the same *C. atys* surface model. In order to test differences between the models compression tests using a universal materials tester were conducted. In order to gauge how different any performance was between the same tooth models (CNC and rapid prototype) an additional M_1 tooth of a different individual was also included and act as an outgroup. If the 3D printed teeth satisfy the two criteria, the results of these tests should group with the results of the similar CNC tooth, and not with the tooth of a different individual. Further, if there is a marked trend in a change in performance (e.g. force at initial fracture or fragmentation) within the results of one 3D printed tooth, this could indicate deformation due to compression and a change in the shape of the contact surface area. Thus, if such a trend was observed, or if the mean was significantly different from the mean of the similar CNC tooth, the 3D printing company would be excluded as unsuitable for this type of project. The model which performed the best (repeatability and accuracy) would be used for the final *H. sapiens* dental models.

Hypotheses to be tested:

H1. There will be no significant difference in the force at initial fracture recorded between an M_1 tooth manufactured in different ways (rapid prototyping vs CNC), and all the results will be significantly different from the force at initial fracture recorded for another individual's M_1.

H2. When comparing results along the repeats there will be no significant increase or decrease in performance (force at initial fracture and fragmentation) for any of the modes of manufacture.

2.4.2 Materials and Methods – Rapid prototype sensitivity study

The two 3D printed teeth models (main and control) used in this sensitivity study were based on the lower right first molar of a male *Cercocebus atys* from a collection of wild-shot skulls obtained in Sierra-Leone c. 1950 and currently housed in the reference collection at the Hull York Medical School's Centre for Anatomical and Human Sciences. This main specimen (referred to as C13.41 CNC) had previously been developed by Swan (2016) and used by Hunter (2016), and thus a premade scan as well as a premade CNC-machined tooth was already available. Another tooth had also been premade via CNC-machined tooth (referred to here as C13.17 CNC), this tooth was of a different individual and more worn, this specimen was selected as a control.
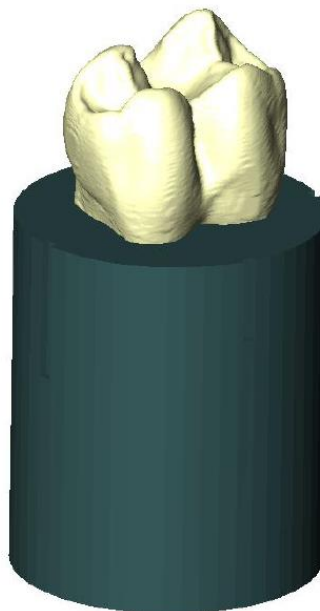
Figure 2.10 Virtual model of molar tooth of *Cercocebus atys* (C13.41) used in the sensitivity experiment to assess reliability of 3D printing options. (image adapted from Hunter 2016)

Using the virtual models CNC teeth were both created using Protolabs, Ltd., UK. In both cases the replicas were made from Carbon Steel (EN8/C45), which has a Young's modulus of 210 GPa and a tensile strength of 500-800MPa (West Yorkshire Steel) (Figure 2.11 A and B). Two additional 3D prints were made using the above surface file for C13.41. Two different companies were chosen, Shapeways (https://www.shapeways.com) (Figure 2.11 D) and Sculpteo (https://www.sculpteo.com/en/) (Figure 2.11 C). These two companies offered reasonably priced prints with minimal shrinkage and a quick turnaround.

Both Shapeways and Sculpteo have several material options, but for this project models the best choice, based on material properties, was a Steel/Bronze 420SS/BR material via binder jetting. This material is a composite of 60% stainless steel and 40% bronze. Stainless steel 420 powder is printed and the bronze is used to strengthen the object. The resulting material has a Young's modulus of 147 GPa and a tensile strength of 500-700MPa. Both companies use the same material and printers, provided by ExOne. Sculpteo advises to expect up to 3% shrinkage with this material, while Shapeways suggests up to 5%. Each company lists minor differences in their tolerances and guidelines, though it is unclear what causes these discrepancies.
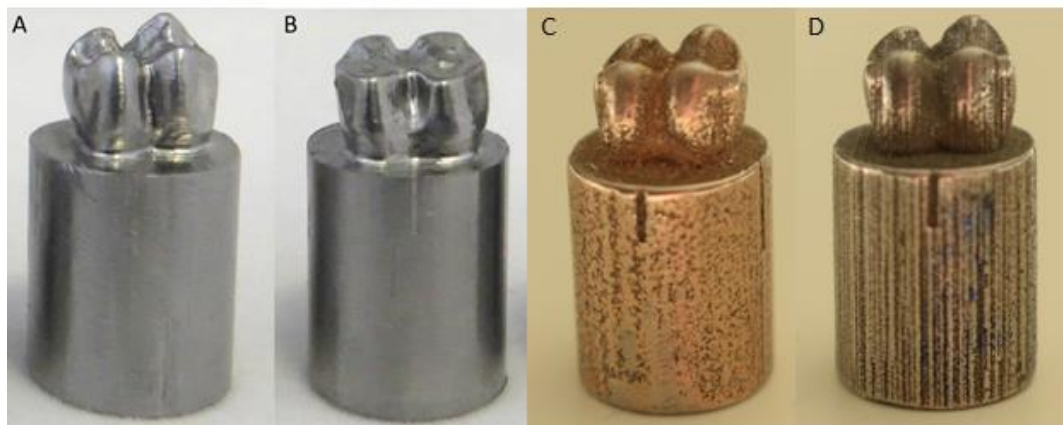
Figure 2.11 Physical models of an M_1 molar tooth of *Cercocebus. atys*. (A) Specimen C13. 41 created via CNC machining, (B) Specimen C13. 17 (the control) created by CNC machining, (C) Specimen C13. 41 created via Sculpteo via binder jetting, (D) Specimen C13. 41 created via Shapeways via binder jetting.

The four 3D models (C13.41 CNC, C13.41 shapeways, C13.41 sculpteo, and the control C13.17) can be seen in figure 2.11. As expected there were some minor differences in the 3D prints vs. the CNC C13.41 models, this can be explained due to the resolution of the print and the shrinkage issue with 3D printing metal, but how this equated to difference in performance however still needed investigating. To investigate the differences in fracture performance the teeth models were subsequently attached to a universal material testing machine (Mecmesin MultiTest 2.5~i) to investigate how variable the results could be based on 3D replica technique (Figure 2.12).
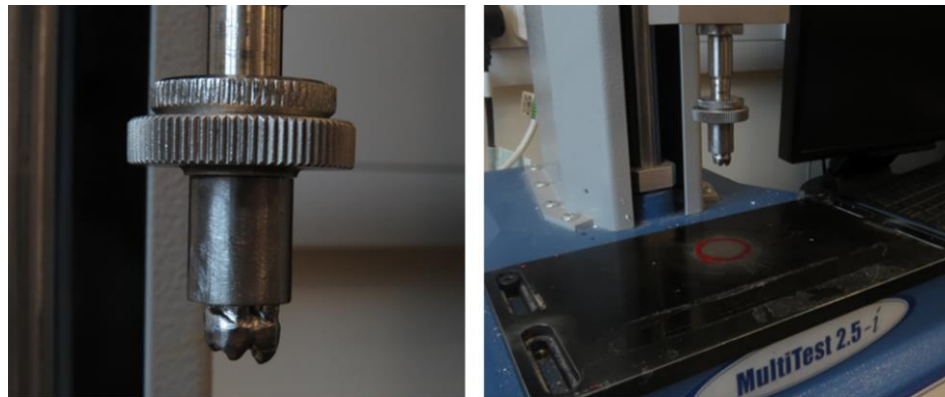
Figure 2.12 Physical CNC model of an M$_1$ tooth of *Cercocebus atys* attached to a universal materials tester.

To control for their performance, as much as possible, the item to be fractured needed to be consistent in form and material properties. As such a solid, 3D printed hemisphere (hereafter referred to as a dome) with a height of 1 cm and a diameter of 2 cm, previously designed and used by Swan (2016), was selected for use as an artificial food object in this study. The domes were printed using the ZPrinter 350 (ZCorporation, SC, USA) 3D printer. As previously described this printer lays down a bed of powder with individual layers of the shape printed using a binding solution. Successive layers of powder and binder and then printed until the object is complete (Figure 2.13).

Figure 2.13 3D printed domes (powder and binder) to be crushed in a sensitivity study of tooth design. (Images adapted from Swan 2016 and Hunter 2016)

The domes were printed in two batches of 70 domes, which were extracted from the printer and immediately placed in a vacuum oven at 75°C and set between 15 and 20 inHg for at least 24 hrs. The domes were then withdrawn from the oven and stored in a desiccator. This stage was completed to create a hard brittle object (Swan 2016). All domes were crushed within 8 hours of withdrawal from the oven.

The sensitivity study was conducted using a universal physical testing machine, Mecmesin MultiTest 2.5~*I*. The CNC-machined tooth models were attached to the crosshead of the testing machine using internal threads, but the 3D printed models lacked this feature. Instead, these were attached to a plate with X60 two-component adhesive (HBM). Efforts were taken to ensure the teeth models were aligned. Swan (2016) found that differences in cusp position produced fairly negligible differences in forces and energy requirements, though differences were apparent in how the fracture was produced and subsequent fragmentation. As such it was felt that as many variables, such as different positioning, should be controlled for as possible. Thus, to control of the position of the tooth between the runs (when the different models were swapped around) at the end of each series of tests for 1 model the 13.41 tooth was lowered into a ball of blue tac, leaving a distinct impression. The tooth was then raised and one of the other C13.41 teeth, either the Shapeways or the Sculpteo model, placed into the impression, taking care to match the cusp positions. Glue was applied to the end of the cylinder attached to the tooth, and a circular flat plate attached to the

crosshead was lowered onto the teeth. The adhesive was allowed to dry, and then testing begun.

A single dome was placed, using the alignment method detailed in Hunter (2016), directly under the crosshead for each run of the test. A program written by Hunter (2016) was slightly modified for this study. In this program which drives the load cell, the crosshead was programmed to be lowered until the tooth model came into contact with the dome and a force of 1N registered by the machine. The force and displacement were then zeroed, and the crosshead continued lowering at a speed of 5mm/min until fracture occurred. This was defined as a break percentage of 30%. The crosshead then returned to a home position. For each of the teeth (C13.41 CNC, C13.41 Shapeways, C13.41 Sculpteo, and the control C13.17 CNC) a sample of n=30 was tested, leading to a total number of 120 trials. The full run of 30 tests was completed for one model before attaching a different model to limit the potential effect of different alignments of the teeth. The software Emperor (v.1.18408, Mecmesin, Sussex, UK) associated with the universal testing machine was used to record force at each moment of displacement at a sampling rate of 500 Hz. The results were output into excel and prepared for statistical analysis in SPSS (v.22; IBM SPSS Statistics, USA).

2.4.3 Results – Rapid prototype sensitivity study

After testing for homogeneity of sample variance and normalcy, an ANOVA was carried out to test for statistically significant differences followed by Tukey's HSD test. All statistical tests were conducted in SPSS (v.22; IBM SPSS Statistics, USA), with a significance of $p < 0.05$. The analysis of variance (ANOVA; $F_{(4, 145)} = 5.466$, $p < 0.000$) showed significant differences when comparing the peak force required to induce fracture between the teeth (Figure 2.14).

The mean peak force of the C13.17 CNC was significantly lower than the mean peak forces required to induce fracture for the C13.41 CNC tooth (Tukey HSD test, $p = 0.002$). On the other hand, when comparing the C13.41 CNC and the Sculpteo tooth (Tukey HSD test; $p = 0.239$) or the Shapeways tooth (Tukey HSD test; $p = 0.732$), there was no significant difference between their means.
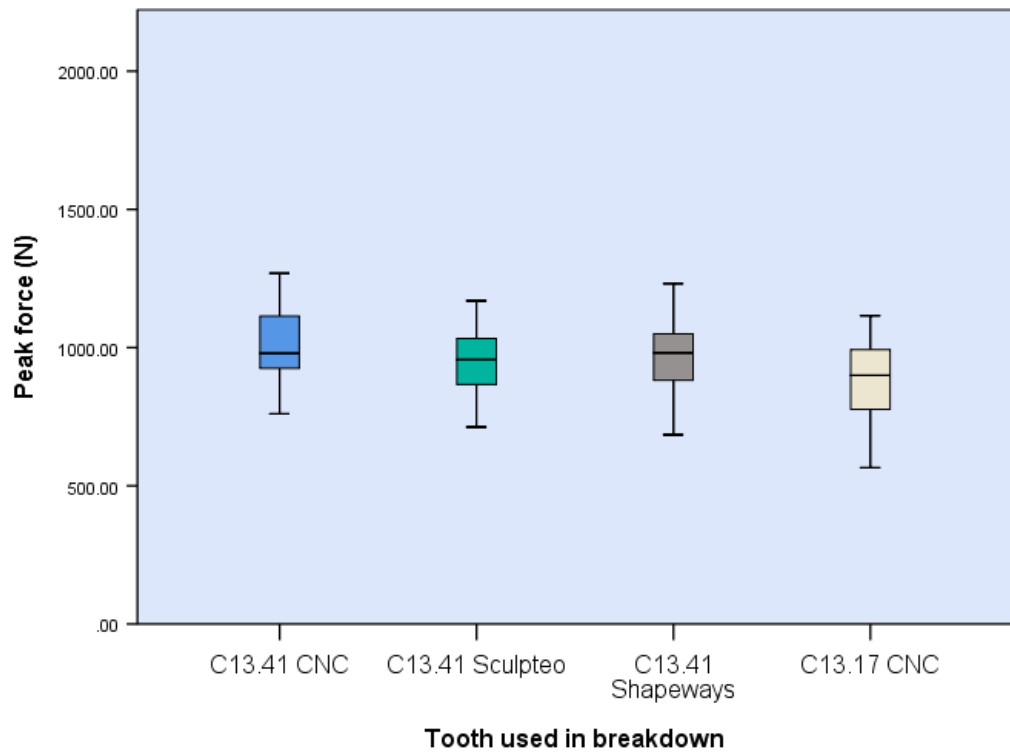
Figure 2.14 Boxplot showing peak force (N) recorded during breakdown of solid domes.

In order to assess whether the dental models themselves were deforming as a consequence of the repetitive loading a comparison of the force displacements graphs was made (Figure 2.15). For no model did a pattern emerge of changes in performance due to repeat usage. If the teeth suffered deformation or wear due to the load it would be assumed that such a change in topography would alter their performance, none was observed.
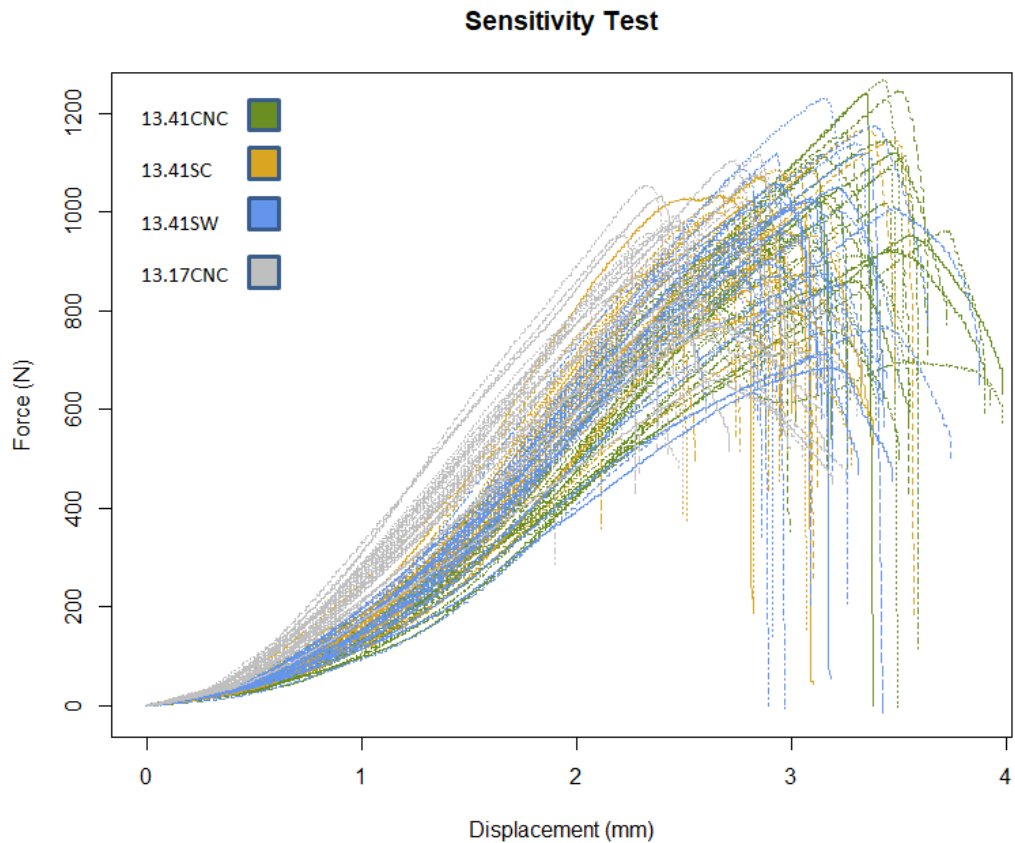
Figure 2.15 Force-displacement graphs showing the differences between runs.

2.4.4 Discussion – Rapid prototype sensitivity study

The results of the sensitivity study validated the use of either 3D printing company for the final models. Though the differences between the C13. 41 3D printed teeth and the control C13.17 tooth were not as pronounced as could be hoped, the 3D printed teeth nevertheless grouped with the original C13.41 CNC tooth, indicating the 3D printed models do replicate the computer model with enough accuracy to deem this approach of 3D model reproduction acceptable for the future study presented here. Additionally, the teeth do not appear to have experienced any deformation, proving they are capable of withstanding the repeated forces they would experience during this project. Ultimately, Sculpteo was selected over Shapeways, as they were slightly more cost effective.

2.5 Development of a mode of attachment for the dental model to the universal testing machine

With the surface files of the upper and lower molars in occlusion created and the method for printing them established it was now necessary to develop a way of attaching them to a physical testing machine. Other studies have previously used clamps (Figure 2.16) which grip the dental row (Berthaume et al. 2010), while others have created threads in the models which can be screwed directly into the rig (Hunter 2016; Swan 2016).
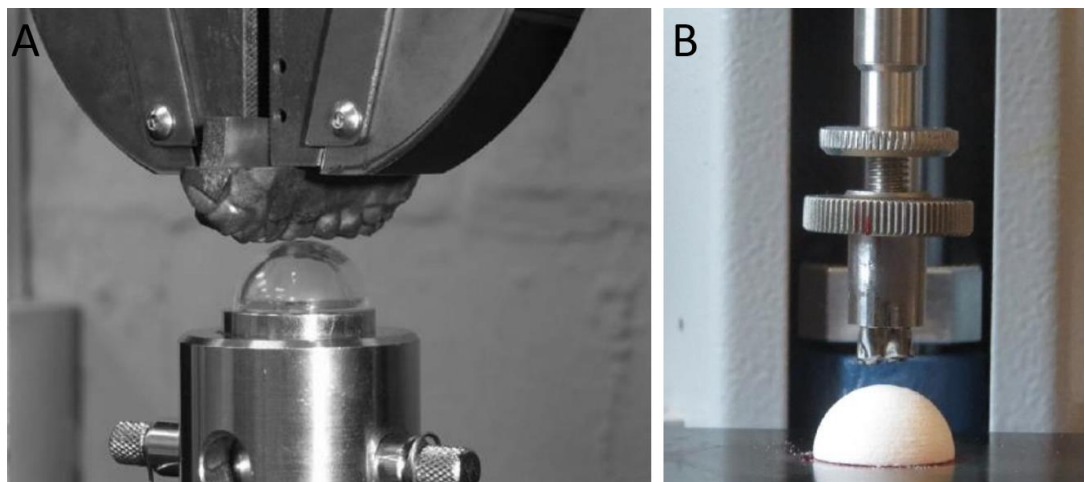
Figure 2.16 Examples of different methods used to attach the denition to the physical testing equipment and load cell. (A) method used in Berthaume et al., 2010, (B) method used in Hunter 2016.

2.5.1 Design of attachment mechanism

The physical testing machine in the department (Mecmesin Universal Testing Machine) has been used previously in the department in several studies (Hunter 2016; Swan 2016). In both these cases single tooth were lowered on to a done (Figure 2.16). In the case of this present study there would be an upper and lower dental row both requiring attachment and attached accurately to avoid losing the perfect occlusion established during the model creation stage. Several methods of attachment were considered. The teeth models could be glued, clamped or threads could be produced to screw them in place (Figure 2.17). However the latter was agreed upon as it was deemed more repeatable and accurate if

specimens needed to be removed and reattached between tests. Using clamps or vice grips would also pose considerable problems for alignment of the teeth in occlusion. As such it was decided that this be done via a single screw beneath the force gauge and a baseplate with a series of threaded holes.
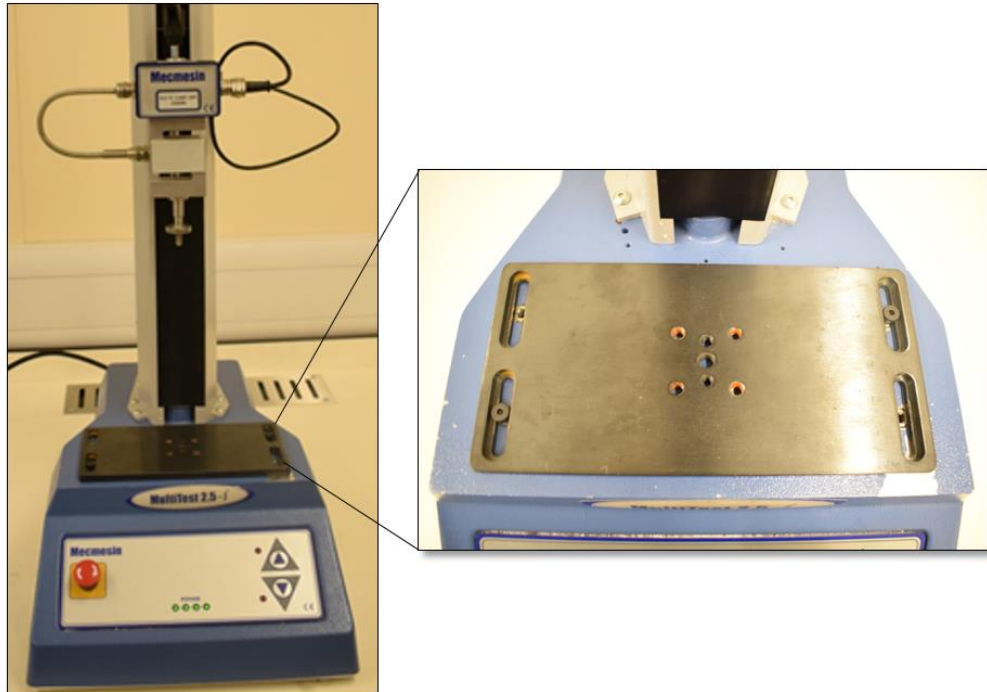
Figure 2.17 The universal materials tester (Mecmesin MultiTest 2.5~i) used in the study. The dental models required a method of attachment to the load cell (left) and the base plate (zoomed in on right) to be established.

The mandibular dental models required attachment to a baseplate on the Mecmesin rig (Figure 2.17). This baseplate already had a series of holes drilled in it. The first step in the design was to create a prototype with a plate containing holes attached to the dental row using virtual software and print using the house Zprinter 350. A circular plate 5cm in diameter was created in Solidworks (Dassault Systemes SoldWorks Corp., MA, USA) with two 6mm holes spaced matching the threaded holes on the baseplate. A similar plate was attached to the maxillary teeth, with a 1cm tall cylindrical extrusion fitted with a M6 internal threaded hole. This would allow the model to be subsequently screwed on directly to the tester (Figure 2.18).

Figure 2.18 Circular attachment plate prototypes attached to the universal materials tester.

Unfortunately, the circular bases (Figure 2.18) were not suitable for subsequent tooth alignment of the upper and lower dental rows when being attached to the rig. With the upper teeth being screwed in place the buccolingual alignment could not be recreated with accuracy. In order to address this a square base was considered. Using the edges and the square corners the pates themselves could easily be aligned and made for subsequent easy and precise alignment between the upper and lower teeth. Using Solidworks (Dassault Systemes SolidWorks Corp., MA, USA) a square attachment plate was therefore created, with length 40mm and a thickness of 5mm, and with two 6mm diameter holes aligned such that when matched to the holes on the Mecmesin baseplate, the exact centre of the attachment plate was directly beneath the force gauge (Figure 2.19, A). A second square plate was then created for the upper attachment. Though also 40mm in length and width, this plate was made 8mm thick, with an additional 2mm thick cylindrical extrusion of directly over the centre of the plate, giving this area a

thickness of 10mm. The extended cylinder was required so that a long enough grub could be threaded into the plate and not damage the dentition. A 6mm diameter hole was sunk 8.5mm into the centre of the plate, extending into the cylindrical extrusion.
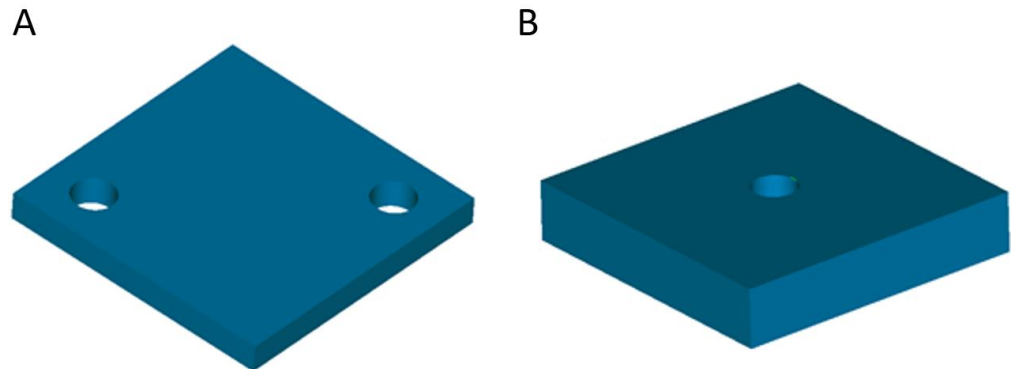
Figure 2.19 Square attachment plates. (A) The attachment plate for the mandibular teeth with two hole placed for attachment to baseplate. (B) Top view of attachment plate for the maxillary teeth with one hole placed in the centre.

2.5.2 Merging the dental models and attachment plates

The scanned models (Figure 2.9) and the attachment plates (Figure 2.19) were imported into Geomagic Studio (v.11; Dassault Systèmes SolidWorks Corp., MA, USA) for attachment. The plates were rotated to the desired orientation, so that the holes were in position for attachment, and the plates were translated so that the centres of the plates were positioned directly on the origin, and thus on the centre of the lower M2. The plates were then raised (for the upper dentition) or lowered (for the lower dentition) in relation to the teeth models, leaving the entirety of the teeth exposed, as well as some portions of alveolar bone, maintaining an unbroken connection between the tooth scans and the plates. The cylinder in the upper attachment plate was sunk into the teeth models to increase stability as. The plates and the teeth were then merged using a Boolean merge (Figure 2.20).
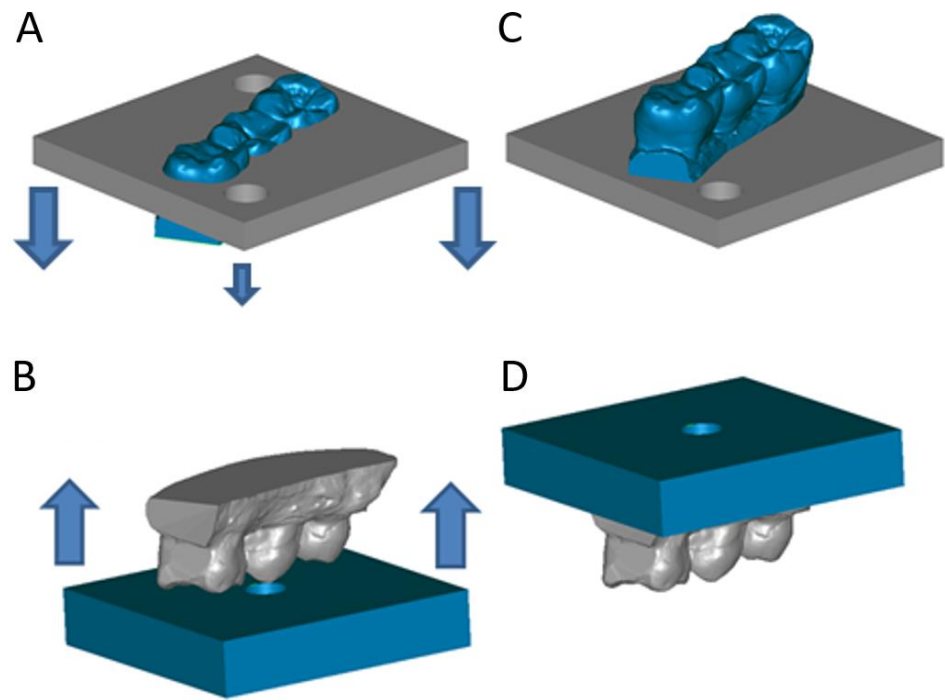
Figure 2.20 Upper and lower dental models virtually attached to the plates. (A) Lower dental model with the plate being lowered vertically into alignment. (B) The upper dental model with the plate being raised vertically into alignment. (C) Final virtual mandibular molar model before merging with plate (D) Final maxillary molar model before merging with plate.

Once the final models were merged to the attachment plates the surface files were submitted to 3D Sculpteo for 3D printing. Following the results of the sensitivity study we opted to use the same material for this model as we had previously tested, a Steel/Bronze 420SS/BR material via binder jetting printing. The final 3D printed model of a modern *Homo sapiens* molar dental row upper and lower can be seen in Figure 2.21. The methodology behind the design of these dental rows meant that the original virtual models can easily be modified in morphology and subsequently re-printed to test any form function hypothesis (see chapter 3).
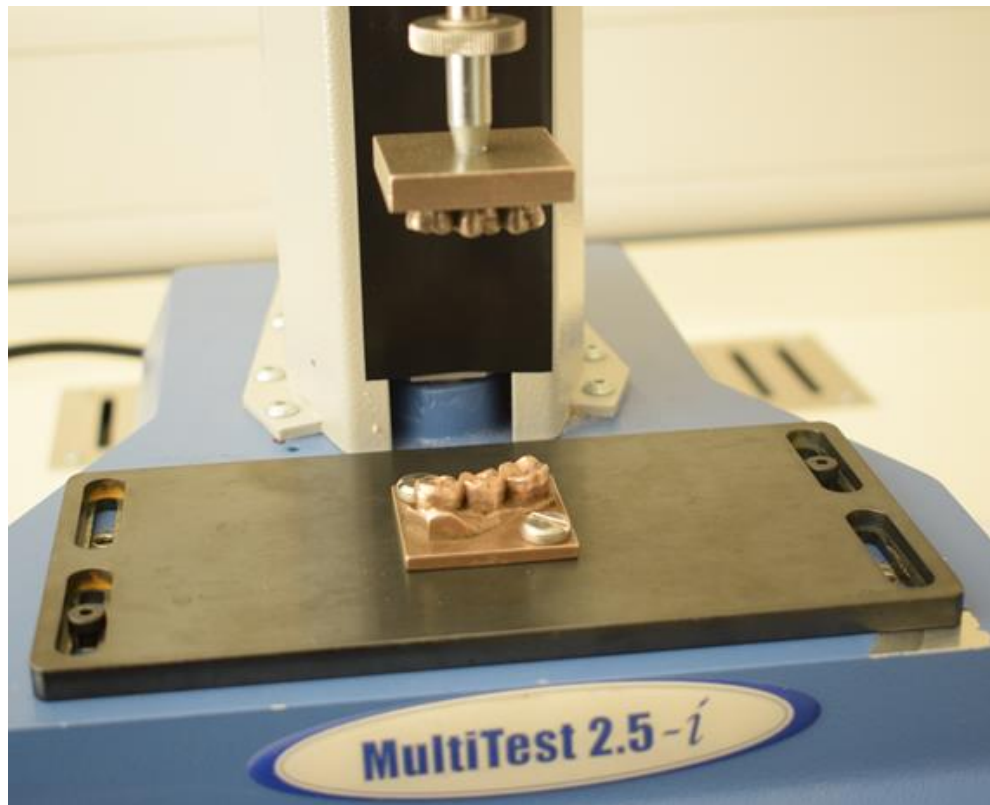
Figure 2.21 Final 3D stainless steel metal print of an upper and lower dental row of a modern *H.sapiens* attached to an attachment plate.

Now that the methodology for designing the dental rows had been established it was necessary to decide on what food items should be used in an investigation of dental function in Hominin evolution and establish a method to consistently place such food on the dentition.

2.6 Creation of artificial food items and designs for placement

Real foods are often highly irregular both in morphology and material properties. This make repeatability of any study of fracture performance difficult; with the reasons behind any difference in dental performance being hidden behind noisy data due to variations in the food items themselves.

As such it was decided that the food items used for this study would also be 3D printed in order to ensure, as much as possible, consistent shape, size, and composition. While the in-house 3D printer previously described, ZPrinter 350 (ZCorporation, SC, USA), was not suitable to recreate the teeth it is ideal to

produce a hypothetical food items. Such an approach has been used before during the investigation of hard food item breakdown (Crofts and Summers 2014; Hunter 2016; Swan 2016). These previous studies have shown that the material produced from the ZPrinter is hard and brittle and allows fracture performance to be compared and replicated. It also allows the user to print large numbers of nearly identical items in standardised conditions.

In terms of the suitability of this food item for an investigation in to hominin dental mechanics, hard objects are frequently associated with traits such as molar expansion in hominins (Demes and Creel, 1980) and primates (Daegling et al 2011). This combined with the limitations of the physical testing equipment (forces can only be applied vertically), makes trying to simulate hard object breakdown appropriate.

2.6.1 Justification of size and shape of food item

Previous studies investigating primate dental function using physical testing have compressed either an upper or lower tooth or dental row into a hemispherical food object stand-in (as done here in section 2.4). Unlike these previous studies, this project will incorporate both an upper and lower dental row in compression. The food item will be crushed between two dental surfaces and as such a hemisphere is not ideal. A sphere would solve this issue and also more closely approximates a natural shape to a food item (such as a nut). Chapter 3 will investigate the relationship between dental size and fracture performance on objects of varying sizes, and whether hominins are adapted to large hard or small hard food items is a topic of debate (Strait et al 2009; Ungar and Sponheimer 2011). As such it is necessary for the method of 3D food replica creation to be able to create objects of varying sizes.

Maximum human gape is approximately 4 cm (Fukui et al. 2002) so for this reason, it was decided that the largest food item would be a sphere of 4 cm diameter. Smaller spheres would be created by halving the size of the next largest sphere, such that there would be four sphere sizes: 4 cm diameter, 2 cm diameter, 1 cm diameter, and 0.5 cm diameter. Importantly, 0.5 cm was near the functional limit

of the ZPrinter. These sizes also neatly replicated various sized hard objects, such as a seed, and were of a size that could realistically be consumed. Ultimately, the 4 cm spheres proved too costly to replicate in large numbers, so these were not included in the study. Instead an intermediate sphere of 1.5 cm in diameter was created. The methods required to design and print spheres of different sizes are outlined below.

2.6.2 Design of food spheres and 3D printing issues

Spheres were created in SolidWorks (Dassault Systemes SolidWorks Corp., MA, USA). A circle of the desired diameter was sketched on a plane. The circle was then bisected with a line from one pole to the opposite. One semicircle was than deleted and the remaining hemisphere revolved around the bisecting line, creating a sphere. This sphere was then saved as a surface file ready for 3D printing. Four different sized spheres were created of 5mm, 10mm, 15mm and 20mm diameters (Figure 2.22).
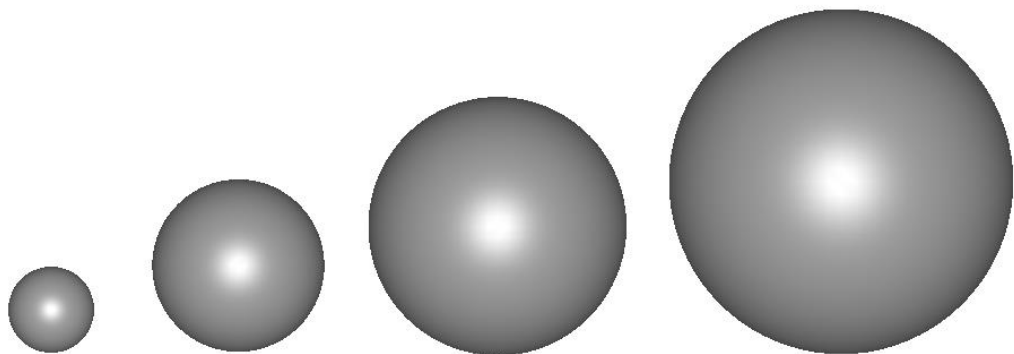
Figure 2.22 Virtual 3D spheres used as food replicas. Spheres vary in size 5mm, 10mm, 15mm and 20mm in diameter (left to right).

The spheres were printed using the ZPrinter 350, but the resulting spheres were surprisingly not spherical (Figure 2.23). After numerous reprints and servicing of the equipment the issue was established. Because of the limits of the technology, most 3D printers, including the ZPrinter 350 used for this study are more or less

incapable of printing spherical objects with an angle less than 45 degrees. If the angle exceeds this the specimen will collapse slightly before it has set. This problem can be overcome with the creation of a simple support. Programs exist to create these supports automatically including Zprinter software (Figure 2.24)

Figure 2.23 Multiple attempts to print the 10mm spheres. Prints ended up egg shaped

objects rather than spheres.

Figure 2.24 Examples of supports for 10mm diameter spheres. The five supports and spheres to the right were created automatically by ZPrint Pro. The small support second from the left was designed by the author. On the far left is a "sphere" printed without a support.

During printing the support (Figure 2.24) counteracts the weight of the powder pressing down upon and pushing out the layers below, preserving the shape of the sphere. Without this support, an egg-shape is produced, rather than a sphere. However, in order to minimise costs bespoke supports were created manually in SolidWorks (Dassault Systemes SolidWorks Corp., MA, USA) along with the spheres (Figure 2.24 2.25 and 2.26). To do this a point along the circumference of the sphere is found such that a 45 degree angle exists between a line parallel to

the horizontal and a line tangent to the circumference (Figure 2.25). On a horizontal plane, a circle with a radius slightly longer, in this case approximately 0.5-1.0 mm longer, than a line in the horizontal from the point found above and the centre of the sphere is drawn. This circle is then extruded from the surface of the sphere by 0.25 mm, that is, it is extruded up from the horizontal plane until it is 0.25 mm from the surface of the sphere, creating a cup-like support for the sphere (Figure 2.25 and 2.26). Bases were created for all the relevant sphere sizes (Figure 2.26) It should be noted that an absolutely perfect sphere is still beyond the capabilities of current 3D printers but the supports do limit the range of variability between 3D printed spheres and produced models which were considered acceptable.
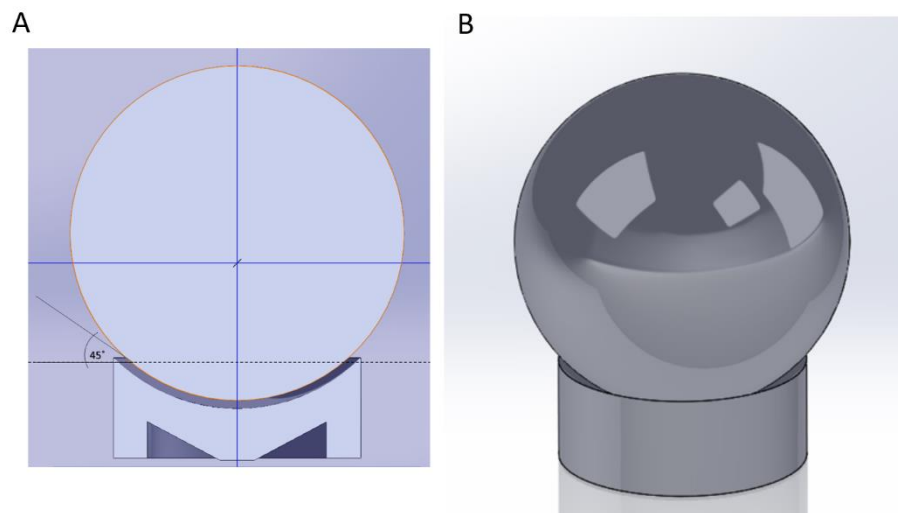
Figure 2.25 Process for the creation of the sphere supports. (A) Measurements used in the process (B) final 3D based produced. This design minimised material and produced a spherical object post print.
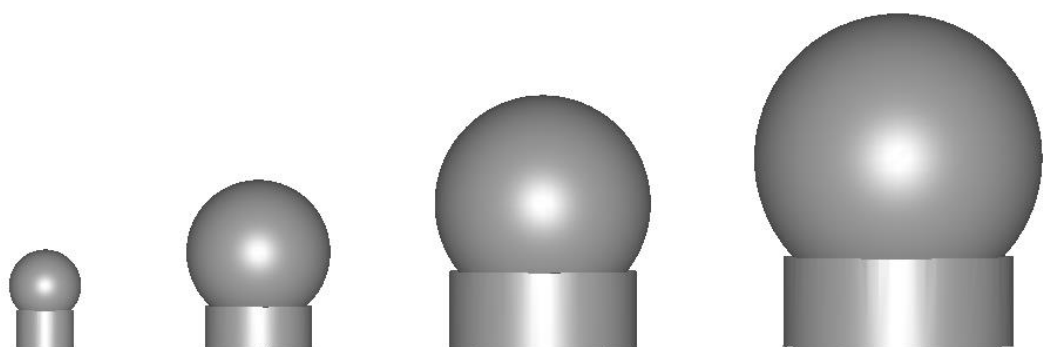
Figure 2.26 Bespoke supports created to minimise cost yet preserve the integrity of the sphere during printing. Supports were created for all sized spheres (5mm, 10mm, 15mm and 20mm left to right)

2.6.3 3D Printing and post processing of the spheres

After the spheres were printed using the ZPrinter 350 they were extracted from the printer and placed in a vacuum oven. The oven was set at 75˚ C, between 15 and 20 Hg. Spheres were left in the oven for 24 hours, and then placed in a desiccating box prior to use. This process kept the spheres hard and brittle. The spheres were printed in batches of between 40 and 80 and all spheres were to be crushed within 12 hours of removal from the vacuum oven.

2.6.4 Placement of food item between the dental rows

Another challenge to overcome was how to reliably and consistently place the sphere on the same point of the tooth, especially between spheres and dental models of different sizes. The location of where food is placed on a tooth may have a big impact on fracture performance (Swan 2016).

After careful consideration of alternative methods for doing this and considering time and monetary constraints, it was decided the spheres would be placed manually and held in position until contact between the teeth and sphere had occurred. The centre of the lower M2 was chosen as the target position for placement. This point was identifiable on the models, and was a natural resting point for some of the spheres, and as such the spheres could be placed with reasonable precision on the same location manually. The centre point was also chosen as it would enable the effects of tooth size and food size on the contact surface area of teeth to be fully explored.

To aid with the vertical placement of the food replica, and to make sure that the vertical reaction force travelled through the sphere in the same way during each bite the sphere's poles (which could be seen on the print due to the additive nature of their manufacture) were used as guides to consistently place the spheres manually in this position (see chapter 3).

Based on the size of the sphere and the teeth the contact surface varied (this would also have been the case of the sphere placement device). For example, the 5 mm sphere tended to fit well between the cusps of the teeth, while the 20 mm sphere was perched on top of the cusps. This in itself formed part of the investigation in to the relationship between tooth size and food size. Ultimately and most importantly the positioning remained consistent for each sphere/tooth combination (chapter 3).

2.7 Conclusion

While other researchers (Berthaume et al. 2010; Crofts and Summers 2014; Hunter 2016; Swan 2016) have carried out physical tests on foods replicas before, this study's design is the first to incorporate both upper and lower dental rows. The processes and stages involved the development of a dental testing rig have been outlined above. The main steps produced a 3D computer model for a human molar row (upper and lower) and a replica food item suitable for crushing. The dental models presented are those of a modern human, however the virtual nature of their design means they can be modified and altered in form (relevant for investigations into size in chapter 3). A method of physical manufacture in a stainless-steel composite was also presented and a sensitivity study carried out confirming their suitability to such studies investigating hard food breakdown. Finally, rather than use real food items this chapter also designed and produced an artificial hard brittle food replica which could be created at different sizes and be placed consistently between runs and models. In summary the development and manufacture process laid out above provides the framework for the next subsequent chapter.

Chapter 3: Testing for Functional Significance of Dental Reduction

3.1 Introduction

Extinct hominins possess a large variety of dental sizes, from the megadont molars of the robust australopithecines to the much smaller molars of *H. habilis* (Table 3.1). Such increases in dental size have often been associated with an increased reliance on more mechanically challenging diets (Ungar 2012). With the emergence of *Homo*, again changes are identified in the molar dentition size, with a sharp decline in size, and a continued trajectory of dental reduction into the present day. This reduction in *Homo*, often associated with the emergence of material culture and extra oral food processing, may signify a significant dietary or cultural shift. Yet the relationship between dental size and food breakdown capabilities has not been fully investigated. We know very little as to whether larger teeth are mechanically more advantageous for small or large food breakdown, and whether small teeth are necessarily disadvantageous. Understanding this relationship between dental form and function may give us a better insight in to the selective pressures faced by our hominin ancestors.

Previous studies have tried to investigate the importance of dental form on food object breakdown in a range of species (Anderson 2009; Crofts and Summers 2014; Hunter 2016; Swan 2016), including hominins (Berthaume et al. 2010). Berthaume et al. (2010) used metal replicas, not dissimilar from the ones used here, of the molar rows of four australopithecine specimens. These replicas were used to crush hollow acrylic domes using a universal testing machine, recording fracture force and displacement at fracture. Unlike this study, Berthaume et al. (2010) complemented their physical testing with an FEA analysis. The results of their study indicated that differences in occlusal surface were not indicative of functional differences in terms of inducing fracture in large hard objects, as often proposed, and instead sugested the differences in the teeth of the specimens may reflect adaptations to limit fractures in the teeth themselves. Importantly, Berthaume et al. was interested not in the size of the teeth but the differences in shape between the species studied. Additionally, they only used one molar row

per specimen, rather than two, so were unable to address the effects of the teeth actually coming into occlusion during their simulated mastication. Laird et al 2015 also examined the effect of tooth size in modern humans on chewing performance. Live participants were given various prepared food items to masticate. The faces of the participants were marked in order to calculate a reasonable estimate of the forces they produced during mastication. The resulting food bolus was then analysed to identify degree of fragmentation. This was compared to the forces generated by the participant to provide a degree of efficiency. Laird et al. (2015) ultimately concluded that the larger-toothed individuals involved in the study were more efficient at mastication, i.e. they produced greater fragmentation at lower forces. In both these studies because different individuals were compared, size effects alone could not be controlled for. Teeth vary in from (size and shape) between and within individuals, and as such differences in dental performance are likely a combination of both aspects of dental form. 3D rapid prototyping therefore offers us an opportunity to isometrically scale teeth, control shape and thus examine the consequence of size only changes in dental functional performance. This chapter will use this approach to create hypothetical hominin teeth, altered in size only, and using physical testing breakdown food items to examine the functional consequence of differences in dental size. The sizes to be investigated span a range of sizes found within the hominin fossil record, but do not attempt to approximate any one specimen or species.

Food object size is also a factor that needs to be considered when examining the relationship between tooth size and food breakdown. Food item size likely played an important role in the evolutionary anatomy of the masticatory morphology in past hominins. Features increasing gape, such as prognathism, can be found when compared to modern *H. sapiens* in many of the extinct hominins, including *Homo neanderthalensis*, *H. heidelbergensis*, and the australopithecines. Masticatory features in these species have been associated, following biomechanical modelling, with wider gapes or more anteriorly positioned bites (Demes 1987; Strait et al. 2009; Godinho et al. 2018). Features such as the anterior nasal pillars in the gracile australopithecine, *Australopithecus africanus*, for example has been

associated with the need to resist bending during premolar anterior bites on large objects (Strait et al 2009). Whether the hominins were frequently feeding on large hard or small hard food items is a topic of debate (Strait et al 2009; Ungar and Sponheimer 2011). However, few people have tried to examine the role teeth play in breaking down objects of different sizes. Given the differences expected in contact surface area when food items of varying sizes contact a tooth it would be reasonable to assume this will impact on the fracture performance (Lucas 2004). If a relationship between tooth size and food size is established this may partly elucidate the functional significance of a dental reduction trend during *Homo* evolution.

In addition to the wide variety of form seen in dentition between species, dentition also exhibits a variety of topographical features and forms within individuals and indeed within different parts of individual teeth (Lucas 2004). Thus, it may also be possible for an individual to completely change the occlusal surface area, the part of the tooth that comes in contact with the food object, by changing the placement of the food object on the tooth. Previous work seems to downplay the effect of this (Swan 2016), though other studies (Constantino et al. 2010), and field observations of cebus monkeys (M D Fogaça 2018, personal communication), suggest this may be of great functional significance. Feeding position may be as important as tooth morphology on fracture mechanics and as such needs to be investigated to gain a fuller picture of the relationship between dental form and food breakdown.

Our primary goal is to understand the functional significance of tooth size and food size and food placement on food breakdown. The point of food item failure is a key parameter to be investigated. How easy it is to break a food item down to aid in food processing and swallowing may offer an important advantage to a species. This ease may come in the form of a low bite force required for the initial break (force at initial fracture) or the total energy used to initiate the fracture (low forces may be needed which would be more optimal but for longer durations which would increase the energy). How the food fragments is also of interest. In some cases to break down the food into a larger number pieces would reduce the need for repetitive mastication, however for some stress resistant food items (such as

those consumes by seed predators) the hardest part, the endocarp may not actually need fragmenting into a large number of pieces as long as the seed is accessible following an initial fracture (Barnett et al. 2016). Here it is assumed that an efficient tooth is defined as one that requires low energy and force to induce fracture and that a significant fragmentation will occur.

The aims of this study are thus to address the following questions:

Q1: How does the size of a tooth effect efficiency?

Q2: Which food item size is more optimal for a given tooth size?

Q3: How much does the placement of the food object on the tooth effect efficiency?

3.1.1 Hypotheses

Associations have previously been made between hard object feeding and postcanine megadontia and enlargement (Goldstein et al. 1978; Strait 1993; Wood and Strait 2004). However, it is here presumed that due to their smaller surface area, which should concentrate forces on a smaller area, smaller teeth will be more optimal for the breakdown of both large and small food items in terms of force at initial fracture, but that fragmentation will be less efficient.

Hypothesis 1: Smaller teeth will require lower forces at initial fracture, expend less energy during failure, and produce smaller amounts of fragmentation compared to larger teeth when breaking down the same sized food item.

Hypothesis 2: For any given tooth size larger food objects will require larger forces at initial fracture and expend more energy during failure and fragment less than smaller food objects.

The final hypothesis predicts that the placement of the food object will have an effect. Varying the placement of a food item, such that the number of cusps or the shape of the cusps in contact with the food item change, will alter the contact surface area. Tooth-food tooth contact between the cusp could act as wedge or have a scissor-like effect, while placement in more flat areas could maximize the contact surface area, distributing forces across the tooth and leading to higher peak forces at fracture.

Hypothesis 3: The placement of the food object so that the food centre is centralised over a tooth cusp rather than the whole occlusal surface will reduce the force at initial fracture.

3.2 Materials and Methods

The hypotheses outlined above will be addressed using methods and materials similar to those used in Chapter 2 to test the suitability of the 3D printed models, based on previous work by Hunter (2016) and Swan (2016). Steel dental replicas will be connected to a Mecmesin Universal Tester and used to crush 3D printed hard brittle hypothetical food items which vary in size. *Homo sapiens* teeth (previously used in chapter 2) will be scaled in size to create three differently sized dental models (normal, large and extra-large). The process for designing the scaled teeth, food items and the rig set-up, including placement of the food items are described below.

3.2.1 Dental Models scaled in size

Studies indicate that human teeth have decreased in size by roughly 20% in the last 35,000 years (Brace et al. 1987; Pinhasi and Meiklejohn 2011), and these trends are magnified when considering earlier *Homo* species or even pre-*Homo* species. Of course, in reality, this reduction in size is accompanied by significant changes in the topography and the exclusion or inclusion of various traits (Bailey

et al. 2017). The modelling of all, or even some of these traits associated with different *Homo* species is beyond the scope of this project. Instead, it was decided to create hypothetically enlarged versions of the model of the modern dentition not to simulate the trend in size reduction observed in human evolution but to exaggerate it in order to better test the effects of tooth size on food object breakdown.

Three models were created: one model at actual size (hereafter referred to as the small model), one model 1.5 times the size of the teeth (the medium model), and one model twice the size of the original teeth (the large model). The enlargement was done using the Transform editor in Avizo Lite (v9.2, Visualization Sciences Group, Burlington, MA, USA). Some dimensions of the resulting teeth are presented in Table 3.1. Though it should be reiterated that these hypothetical models are not meant to accurately replicate the actual dentition of extinct hominins, for reference some average dimensions of earlier hominins have been included in the table. The medium model teeth are somewhat similar in size to *Paranthropus boisei* teeth, and the large model teeth are larger than any known hominin.

Table 3.1 Buccolingual (B-L) and Mesiodistal (M-D) dimensions (mm) of the teeth models (based on *H. sapiens*) and several comparable species (means), taken from Irish et al. 2015.

	UM1	UM2	UM3	LM1	LM2	LM3
Small model	B-L: 9.9 M-D: 9.58	B-L: 9.14 M-D: 10.8	B-L: 8.62 M-D: 9.45	B-L: 9.4 M-D: 11.08	B-L: 8.42 M-D: 10.11	B-L: 8.52 M-D: 9.93
Medium model	B-L: 14.85 M-D: 14.37	B-L: 13.71 M-D: 15.27	B-L: 12.93 M-D: 14.175	B-L: 14.1 M-D: 16.62	B-L: 12.63 M-D: 15.165	B-L: 12.78 M-D: 14.895
Large model	B-L: 19.8 M-D: 19.16	B-L: 18.28 M-D: 20.36	B-L: 17.24 M-D: 18.9	B-L: 18.8 M-D: 22.16	B-L: 16.84 M-D: 20.22	B-L: 17.04 M-D: 19.86
A. africanus	B-L: 13.9 M-D: 12.9	B-L: 15.7 M-D: 14.0	B-L: 15.9 M-D: 14.0	B-L: 13.0 M-D: 14.0	B-L: 14.5 M-D: 15.7	B-L: 14.6 M-D: 16.3
P. boisei	B-L: 15.0 M-D: 14.1	B-L: 16.8 M-D: 15.5	B-L: 17.4 M-D: 14.1	B-L: 14.0 M-D: 15.5	B-L: 15.9 M-D: 17.5	B-L: 15.4 M-D: 18.0
H. habilis	B-L: 13.0 M-D: 12.9	B-L: 14.6 M-D: 13.1	B-L: 14.6 M-D: 12.6	B-L: 11.8 M-D: 13.8	B-L: 13.4 M-D: 15.0	B-L: 13.0 M-D: 15.3

As in 2.5.1, two new pairs of attachment plates were created in SolidWorks (Dassault Systemes SolidWorks Corp., MA, USA), with sides of different lengths corresponding to the size of the teeth: 60 mm for the medium model, and 80 mm for the large model. Again, the base attachment plate was made 5 mm thick. Two holes of 6 mm diameter were placed diagonally in the base attachment corresponding to M6 threaded holes on the baseplate leaving room for the models. However, the large model was in fact too large to fit on the plate without obscuring at least one of these holes slightly, so two additional holes were set into the plate further apart. It was thought that additional holes could be drilled into the attachment plate if the original holes were unusable. Ultimately, this proved unnecessary as the original holes proved workable for the large model regardless.
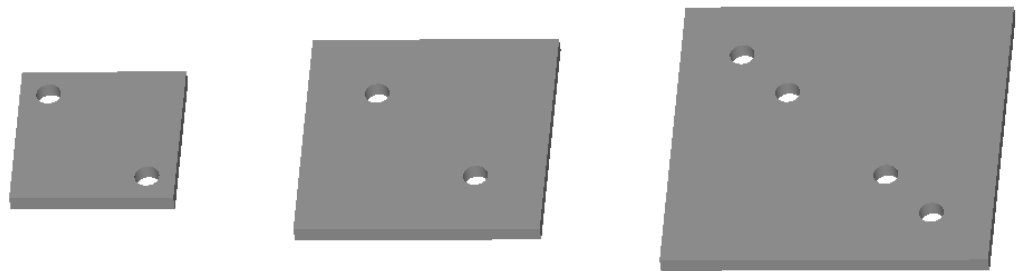
Figure 3.1 Three baseplate prototypes. From right to left: the small model plate (40mm length), the medium model plate (60mm length) and the large model plate (80mmm length), with the two additional holes.

The top plate was created exactly as in the original model (2.5.1), though the dimensions were extended to accommodate the larger teeth, corresponding to those used for the bottom plates.
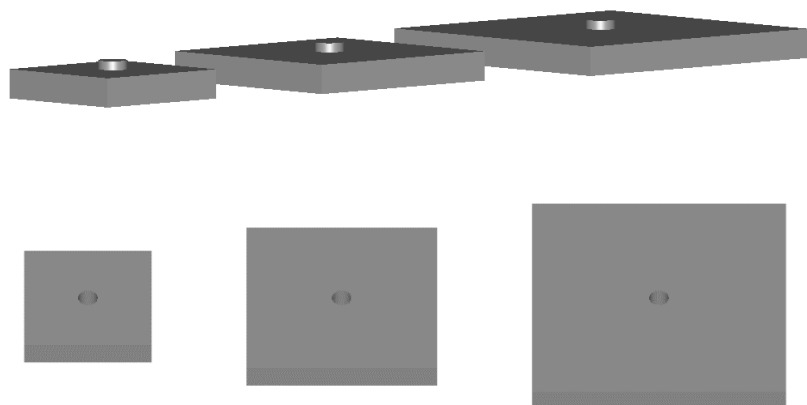
Figure 3.2 Two views of the top plates created in Solidworks. From the left: the small plate, the medium, plate, and the large plate.

The models were merged with the plates as in Ch. 2.5.2. The complete models were then 3D printed in the same stainless steel/bronze composite used for the original sized teeth models by Sculpteo (2.4).
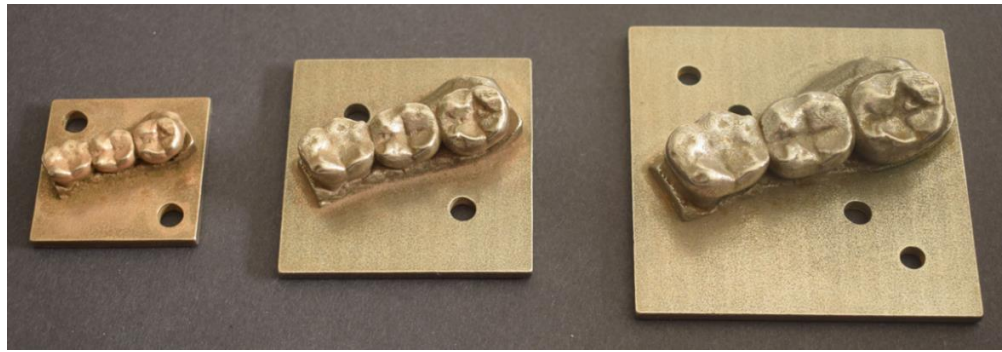
Figure 3.3 Photograph of the final steel 3D printed models used in this study.

3.2.2 Differently sized replica food items (spheres)

Four different sizes of 3D printed spheres were selected to act as food item replicas. Spheres of 5mm, 10mm, 15mm, and 20mm diameters were printed in batches of between 40 and 80. Sometimes batches combining multiple sphere sizes were printed. Following extraction from the ZPrinter 350 they were placed in a vacuum oven at 75˚C, between 15 and 20 Hg for at least 24 hours. They were then extracted and placed in a desiccating box before use, which took place within 12 hours of withdrawal from the oven. The spheres were crushed in groups of 10 to 30 of one diameter, followed by a similar group of a different diameter. Crushing took place over several, non-consecutive days. Each sphere was weighed, crushed, and photographed. The Mecmesin was programmed using the same script used in the sensitivity test described above (2.4.1). 60 iterations were collected for each sphere size. However, due to a data collection error, only 40 usable samples of the 20 mm sphere were collected.

3.2.3. Output parameters – force, energy and fragmentation

As in the sensitivity test (2.4.1) data was collected using the program Emperor (v.1.18408, Mecmesin, Sussex, UK). This program records the force at each moment of displacement at a frequency of 500 Hz. The script entered was set to automatically halt the test after a drop in force of 75% or greater was recorded between two points, as an indication of fracture. In retrospect, this was clearly too high a threshold to set. It was thought, based on previous work (Swan 2016), that the solid domes would likely fracture in a very dramatic way, and thus this break

percentage would be appropriate. In fact, it proved infrequently suitable. Thus, in order to calculate peak force, that is, the highest force experienced before fracture, it was necessary to rely on notes taken during testing indicating the moment of fracture. However, as fracture patterns were relatively inconsistent, it was decided to take the highest forces experienced during the first arc observable in the data as the peak forces. Fragmentation data was recorded in the form of photographs of the crushed spheres. Additionally, the degree of fragmentation was indexed from 1 to 4, with 1 being no fragmentation and 4 being fragmentation into 5 or more pieces. However, because the break percentage used (75%) was too high to accurately end the compression test at the point of initial fracture for many of the test runs, there is no way to accurately compare the fragmentation results. Some are accurate records of initial fracture, but others represent fragmentation from forces well above those required to induce fracture. For this reason, the fragmentation results have been excluded.

3.2.4 Sphere Placement

In order to test the effect of tooth size and food size on food breakdown the M_2 was chosen as the central point to place the food item. The M_2 was chosen as the prefered tooth as it would allow both the distal M_1 and mesial M_3 cusps to contact the food item during the bite simulation if needed. This position was easily replicable with all teeth sizes and all food objects. In order to minimise any additional sources of error in the results the placement of the food item during repeats needed to be as consistent as possible. Unfortunaltey sphere placement devices (described and designed in chapter 2) proved unsuitable due to the shrinkage inherent in the 3D printing process. These devices would have positioned the spheres directly above the precise centre of the lower M2 on the models. Without the placement devices spheres were placed, by hand, as consistently as possible. A visually identifiable pole, indicated in Figure 3.4, was used to manually align the spheres over the lower M2. An artefact of the printing process, this pole was the last layer of powder and binder laid down by the printer. It was used to ensure that the sphere was placed in relatively the same orientation, at least in regards to the horizontal rotation, such that the printed layers were parallel to the occlusal surface. The spheres were held in position and lowered by

hand to find a natural point of rest on the teeth. This final position of the sphere (see Figure 3.4) appeared to be very consistent, particularly between runs of the same sized sphere on the same sized tooth. In all cases (regardless of the size of food or tooth) the sphere's centre lay over the central fossa, with the degree of contact with the two buccal and two lingual cusps varying depending on the food item size vs. tooth size. A larger number of test repeats was chosen to address any minor errors introduced as consequence of placement.

For one of the hypotheses to be tested tooth placement will be examined. Two additional areas of the teeth were selected for the initial placement. One on the approximate centre of the buccal cusp of the lower M2 (the results from this are referred to as Placement 1 or "P1"), and a second over the distal cusps of the lower M1 and the mesial cusps of the lower M2 (Placement 2 or "P2"). Thirty 15mm spheres were crushed by each sized teeth model on each of these placement locations.

Figure 3.4 Photograph of a sphere placed on the tooth model. The arrow indicates the pole used for alignment.
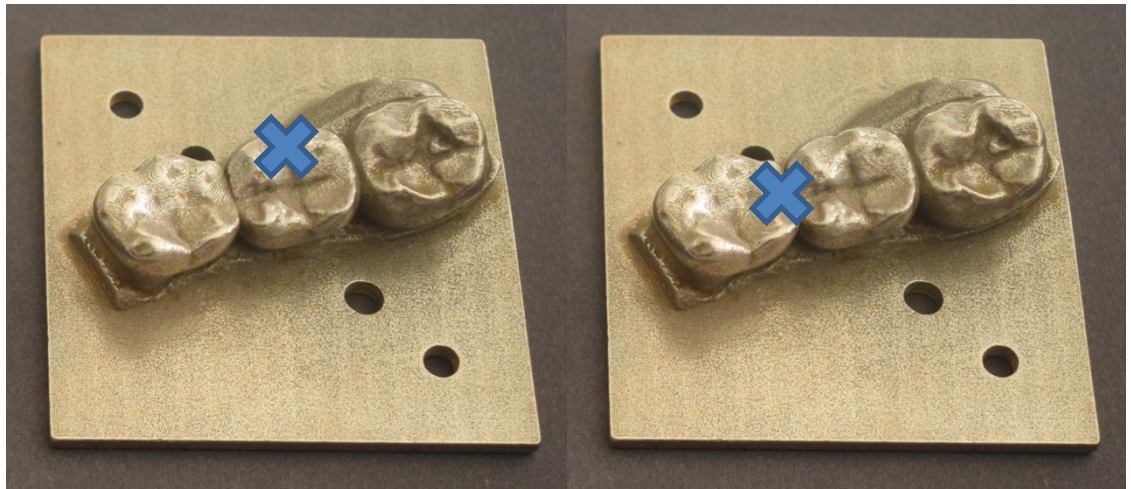
Figure 3.5 The two locations selected for the placement test. Placement 1 on the left and placement 2 on the right.

3.2.5 Experimental runs testing the effect of tooth size, food size and food placement

To test the above three hypotheses each series of repeats was carried out on the following pairing between teeth and food size (Table 1). Note only the 15mm sized food items were examined in relation to the effect of food position.

Table 3.2. Combination of dental model sizes, food item sizes and food placement locations tested. X indicates that 60 repeat compression tests were run for this combination, X* indicates only 40 repeats were collected for this combination, and x indicates 30 test repeats were run for this combination.

Food item size	Tooth models		
	Original size dental model (x1 scale)	Medium dental model (x 1.5 scale)	Large dental model (x2 scale)
Small (5mm)	X	X	X
Medium (10mm)	X	X	X
Large (15mm)	X	X	X
Extra large (20mm)	X*	X*	X*
Placement 1 (15mm)	x	x	x
Placement 2 (15mm)	x	x	x

The results for the above tests are presented below as a series of line graphs plotting the force and displacement recorded for each set of repeats so show the trends and patterns of behaviour during the compression. The point of failure defined as either a 75% break (if registered), or the initial peak in the results, is then extracted and presented as a box plot. All statistical tests were conducted in SPSS (v.22; IBM SPSS Statistics, USA), with a significance of $p<0.05$. Tests for homogeneity of variance and normality were conducted, and based on the results of these tests either an ANOVA, a Welch's T-test, or Tamhane's test were performed on the results, as indicated below, to analyse variance.

3.3 Results: effect of food size and tooth size on food breakdown

Results are given below for each tooth and for all 4 food item sizes followed by a comparison of the three teeth sizes against each other.

3.3.1 Original x1 scale dental model vs all four food item sizes

The results of varying the food item size on the original x1 scale dental model show that while there is some overlap in the results for the two largest spheres, there is a clear differentiation of force and total displacement between sphere sizes (Figure 3.6). The peak forces and displacement at fracture, and thus the energy required to induce fracture is clearly related to the size of the sphere being compressed. The smallest spheres (5mm diameter) require the least energy to fracture and experience the smallest forces and the least displacement, while the largest spheres (20mm diameter) require the greatest energy to fracture and experience both the greatest forces and the most displacement.
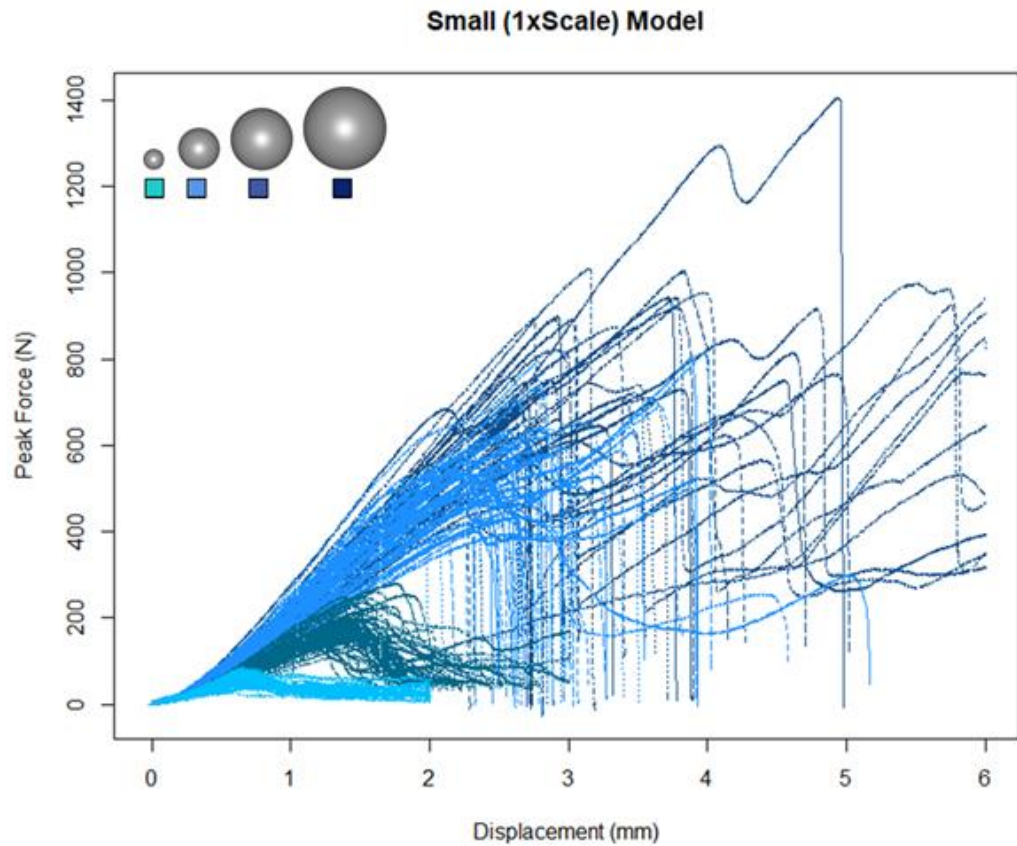
Figure 3.6 Force - Displacement recorded Graph of Force (N) by displacement (mm) for all tests using the small (1xscale) teeth models.

An analysis of variance showed significant differences when comparing the energy required to induce fracture (Welch test, $F_{(5, 91.270)}=685.338$, $p<0.001$), the peak force at fracture (Welch test, $F_{(5, 96.441)}=1152.801$, $p<0.001$), and the displacement at peak force (Welch test, $F_{(5, 97.846)}=1263.399$, $p<0.001$) between the different sphere sizes. In all cases, the larger the sphere's diameter, the greater the mean in each of these categories.
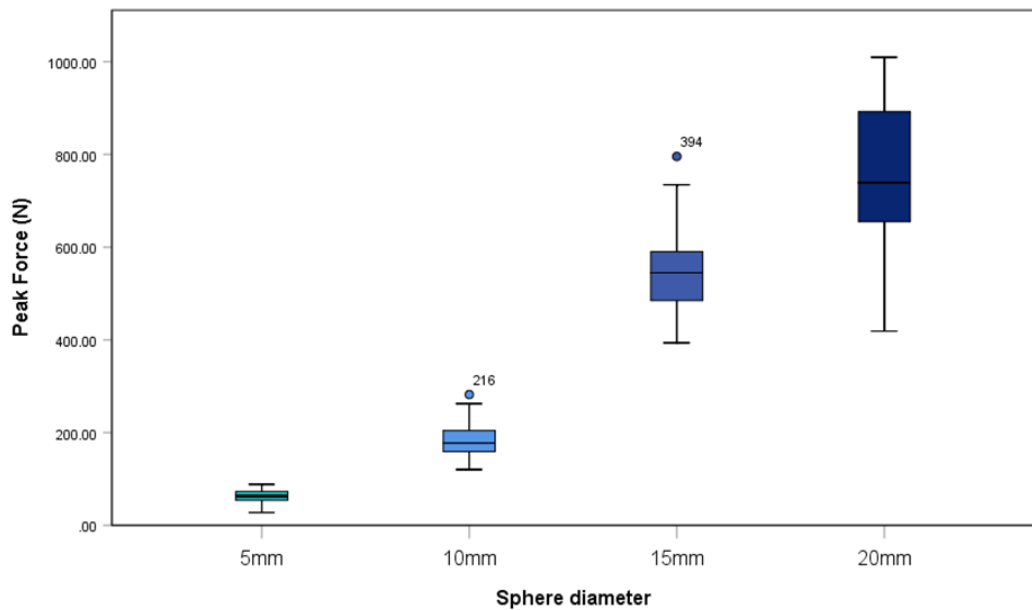
Figure 3.7 Boxplot showing peak forces (N) recorded during fracture of spheres using the modern *Homo* teeth models. Showing, from left to right, the results of the smallest (5mm) diameter spheres to the largest (20mm) diameter spheres.

When looking at the peak forces, the differences between each category were significant (Tamhane test; p<0.001 for any combination). There was some overlap between the forces recorded for the 15 mm spheres (minimum=393.90 N; maximum 795.60 N) and the 20 mm spheres (minimum=418.0 N; maximum=1009.80 N), however, their means (544.5083 N and 750.8675 N, respectively) were still significantly different (Tamhane test; p<0.001). There was no overlap between any other sphere size. Interestingly, the amount of variability within groups increases as the size of the spheres increases, despite the fact that the largest size spheres (20mm) which display the greatest variability also comprise the fewest iterations.
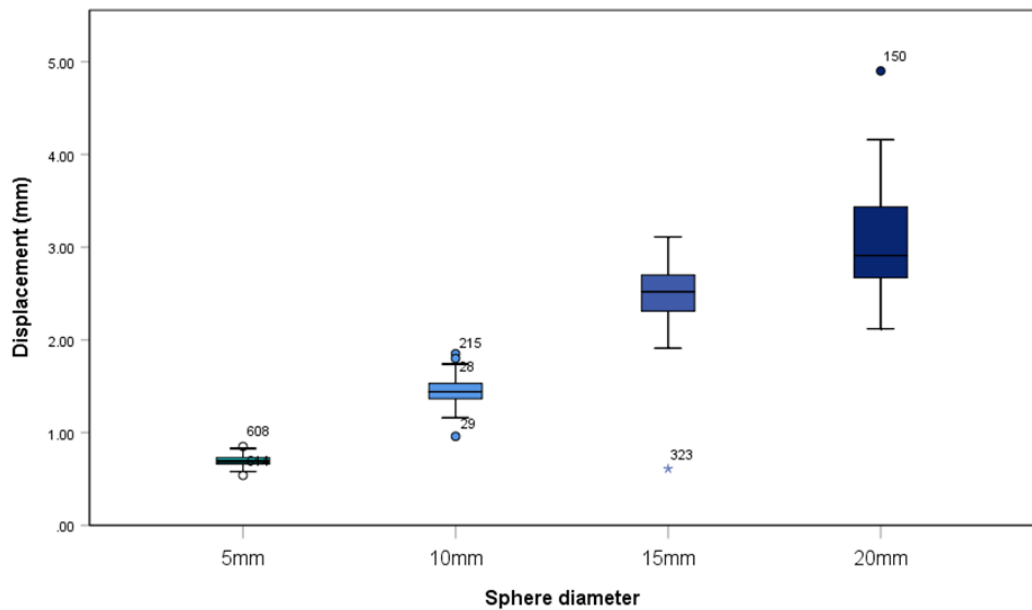
Figure 3.8 Boxplot showing displacement (mm) recorded at peak force during fracture of spheres using the modern *Homo* teeth models. Showing from left to right the results of the smallest (5mm) diameter spheres to the largest (20mm) diameter spheres.

The results for displacement are similarly differentiated, excluding an outlier in the 15 mm sphere tests (labelled 323 in Figure 3.8) which actually falls within the range of displacements experienced by the 5 mm spheres. It should be noted that displacement is a recording of the distance the upper teeth travel down into the sphere following contact with the sphere. It is therefore limited by the size of the sphere, such that a displacement value greater than the diameter of the sphere being compressed could not be recorded. However, these results seem to indicate a clear trend, with the mean displacement roughly paralleling the difference in diameters of the sphere. Thus the mean displacement recorded for the 5 mm spheres (0.6927 mm) is roughly half the mean displacement recorded for the 10 mm spheres (1.4438 mm) which is roughly half the mean displacement recorded for the 20 mm spheres (3.0475 mm), and even the mean displacement for the 15 mm spheres (2.4798 mm) broadly follows this trend, which may be coincidental, or may be a function of the structural mechanics of a sphere.

Figure 3.9 Boxplot showing energy (mJ) required to induce fracture of spheres using the modern *Homo* teeth models. Showing from left to right the results of the smallest (5mm) diameter spheres to the largest (20mm) diameter spheres.

The energy required to induce fracture of the spheres was calculated by finding the area bound by the graph of force by displacement at peak force (Hunter 2016; Swan 2016). As with peak force and displacement, the energy data was clearly differentiated, with only some overlap between the 15mm (minimum= 398.53 mJ; maximum= 1115.74 mJ) and 20mm (minimum= 421.90 mJ; maximum= 2051.63 mJ) data. Again, the means were nevertheless significantly different (Tamhane test; $p < 0.001$).

In summary these results of the original sized teeth strongly suggest that the size of a food object has a significant impact on the forces experienced during fracture, and thus a substantial impact on the energy required to induce fracture. Clearly, the larger an object, the more difficult it is to cause that object to break, assuming the consistency and other physical properties are unaffected by the size.

3.3.2 Medium (1.5xscale) dental model vs all four food item sizes

As can be seen from Figure 3.9, the results of the tests using the medium (1.5xscale) models follow a similar trend to those seen in the small (1xscale) models. Again, the peak forces and displacement seem to be relatively consistent

69

for each sized sphere, though again the larger spheres (15mm and 20mm) seem slightly more confused. An analysis of variance showed significant differences when comparing between the peak forces recorded in the breakdown of all the various sized spheres (Welch Test; $F_{(5,102.915)}=1086.543$, $p<0.001$). Peak force was lowest for the 5mm spheres (minimum=14.92 N; maximum=98.00 N) and highest for the 20mm spheres (minimum=583.50; maximum=1116.80 N). There was no overlap in the ranges except between the 20mm spheres and the 15mm spheres (minimum=383.40 N; maximum=867.90 N). However, their means were significantly different (Tamhane test; $p<0.001$).

Figure 3.10 Force - Displacement recorded Graph of Force (N) by displacement (mm) for all tests using the medium (1.5xscale) teeth models

Statistically significant differences were also observed for displacement at peak force (Welch test, $F_{(5, 100.918)}=1933.826$, $p<0.001$). Tamhane tests revealed significant differences in the means of all possible combinations ($p<0.001$ for all combinations). Again, the displacement scaled with the size of the sphere, with the mean displacement recorded for the 5mm sphere (0.6992mm) roughly half

70

that experienced by the 10mm sphere (1.3655mm), which itself experienced a mean displacement roughly half that of the 20mm sphere (2.9015mm), and about two-thirds that of the 15mm sphere (2.3078mm).

Figure 3.11 Boxplot showing peak forces (N) recorded during fracture of spheres using the medium (1.5xscale) teeth models. Showing, from left to right, the results of the smallest (5mm) diameter spheres to the largest (20mm) diameter spheres.
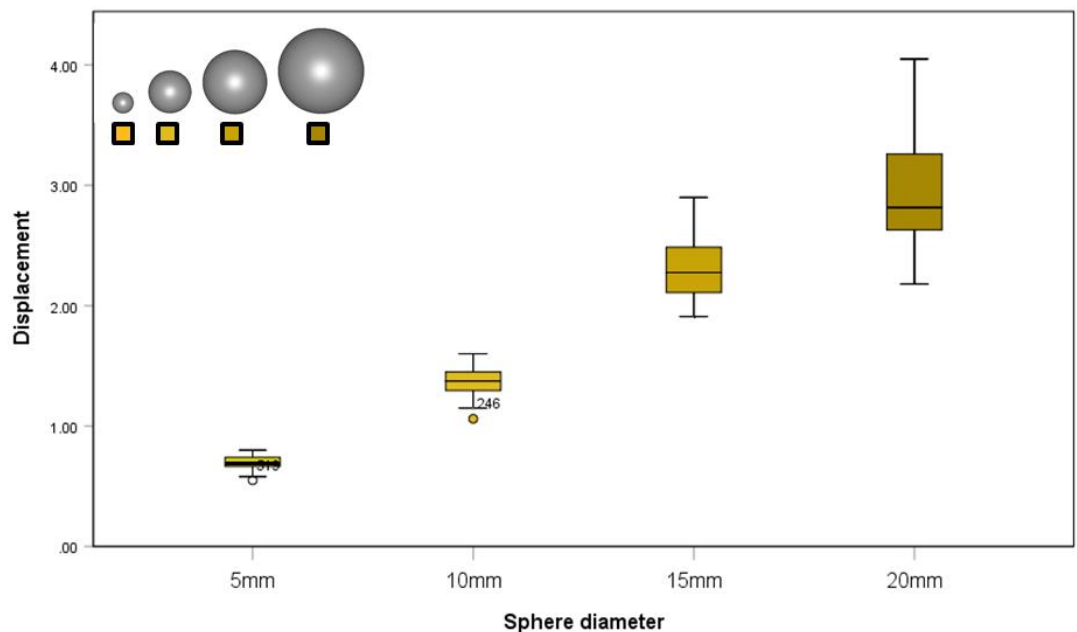
Figure 3.12 Boxplot showing displacement (mm) recorded at peak force during fracture of spheres using the medium (1.5xscale) teeth models. Showing from left to right the results of the smallest (5mm) diameter spheres to the largest (20mm) diameter spheres.

An analysis of variance for the energy (Figure 3.13) produced similar results, again with statistical significant differences observed (Welch test; $F_{(5, 99.667)}=598.845$, $p<0.001$). Tamhane tests revealed statistically significant differences between the means of each sized sphere (Tamhane test; $p<0.001$ for all combinations).
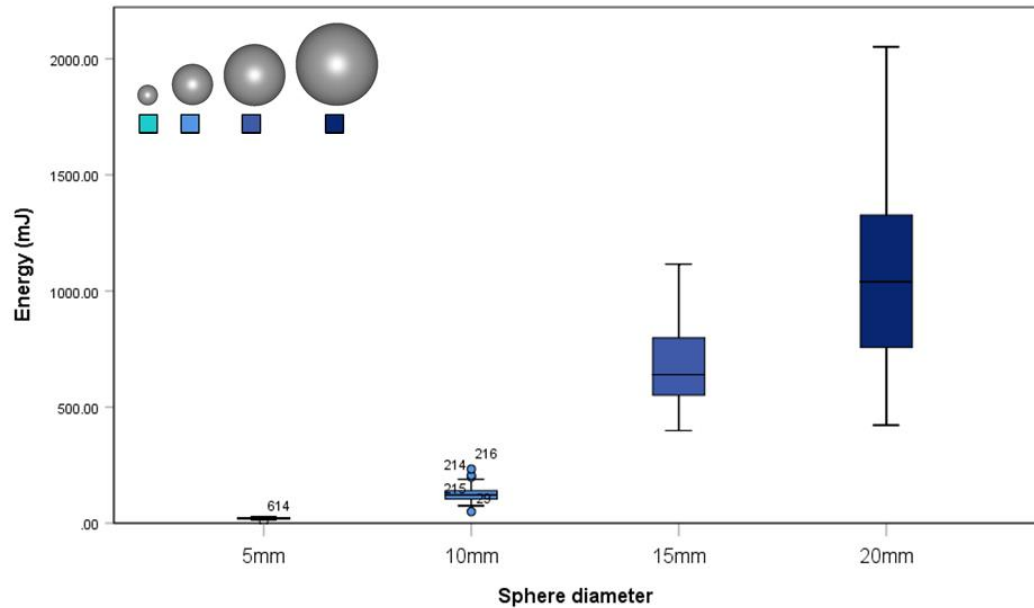

Figure 3.13 Boxplot showing energy (mJ) required to induce fracture of spheres using the medium (1.5xscale) teeth models. Showing from left to right the results of the smallest (5mm) diameter spheres to the largest (20mm) diameter spheres.

These results seem to confirm the idea that the larger the food object, the greater the forces required to induce fracture and the greater the degree of displacement that occurs before this fracture. The actual performance of the medium sized teeth model will be compared to the small teeth model below, but from these results, it seems the medium teeth are performing broadly similarly to the small teeth.

3.3.3 Large (2x scale) dental model vs all four food item sizes

Figure 3.14 shows that the results of the sphere crushing on the large (2xscale) teeth models conforms well with the patterns established on the other two teeth models. The 5mm sphere clearly fractured under the smallest forces and least displacement, while the 20mm sphere experienced significantly greater force at fracture and significantly more displacement. Indeed, unlike the graphs for the

other teeth models, it is clear from Figure 3.13 that the 20mm spheres required a greater force and more displacement to induce fracture than the 15mm spheres, a distinction that though true for the other teeth models was not nearly as clear in their corresponding graphs.
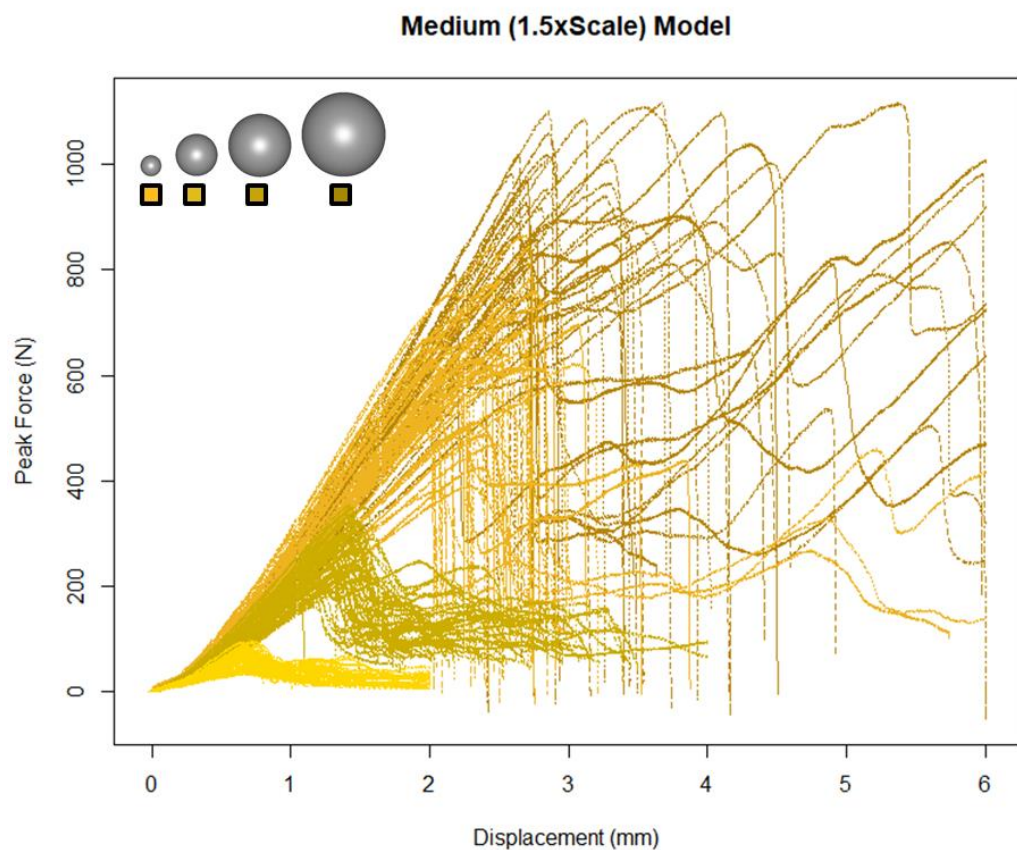
Large (2xScale) Model
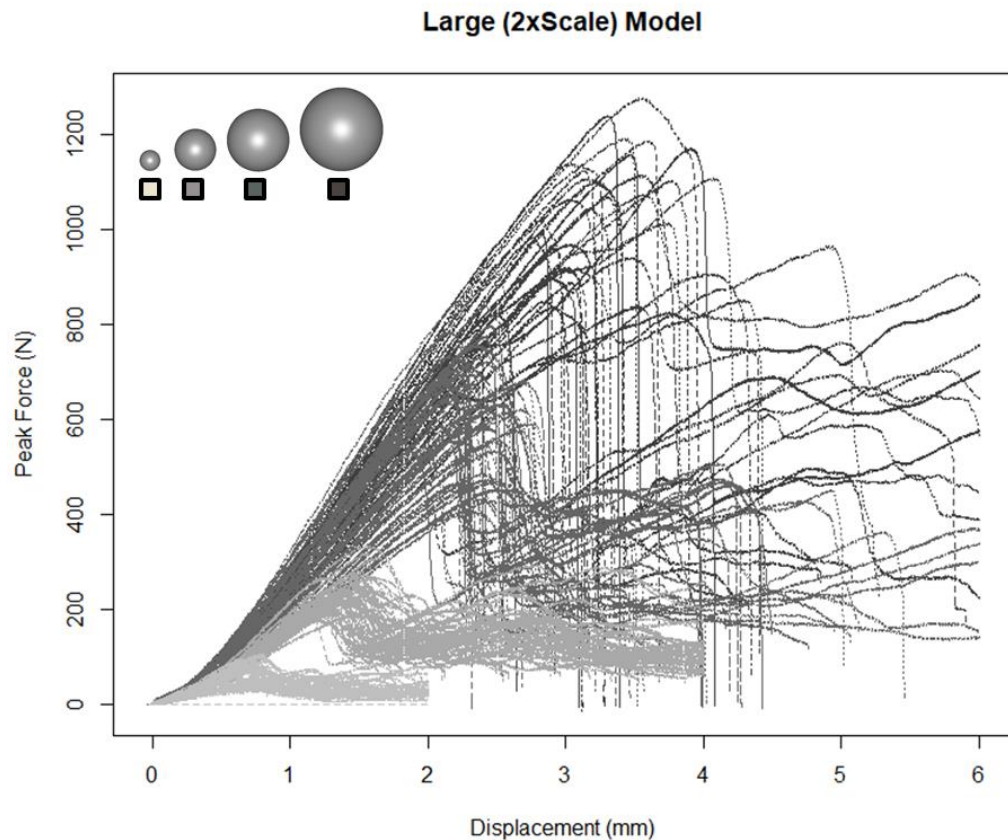
Figure 3.14 Force - Displacement recorded Graph of Force (N) by displacement (mm) for all tests using the large (2xscale) teeth models.

As with the other data from the other models, after testing for homogeneity of variance, analyses of variance were conducted along with Welch tests followed by Tamhane tests. Statistically significant differences were found in the peak force (Welch test, $F_{(5, 100.175)}=975.112$, $p<0.001$), displacement (Welch test, $F_{(5, 109.267)}=454.184$, $p<0.001$), and energy (Welch test, $F_{(5, 91.905)}=793.065$, $p<0.001$) results between sphere sizes.

Tamhane tests revealed statistically significant differences in the means of peak force between all possible combinations of sphere size (Tamhane test; $p<0.001$ for all combinations), indicating a significant difference in the peak forces required to

induce fracture associated with differences in the size of the food object being crushed. As with the other teeth models, the larger the sphere, the greater the forces required to induce fracture.
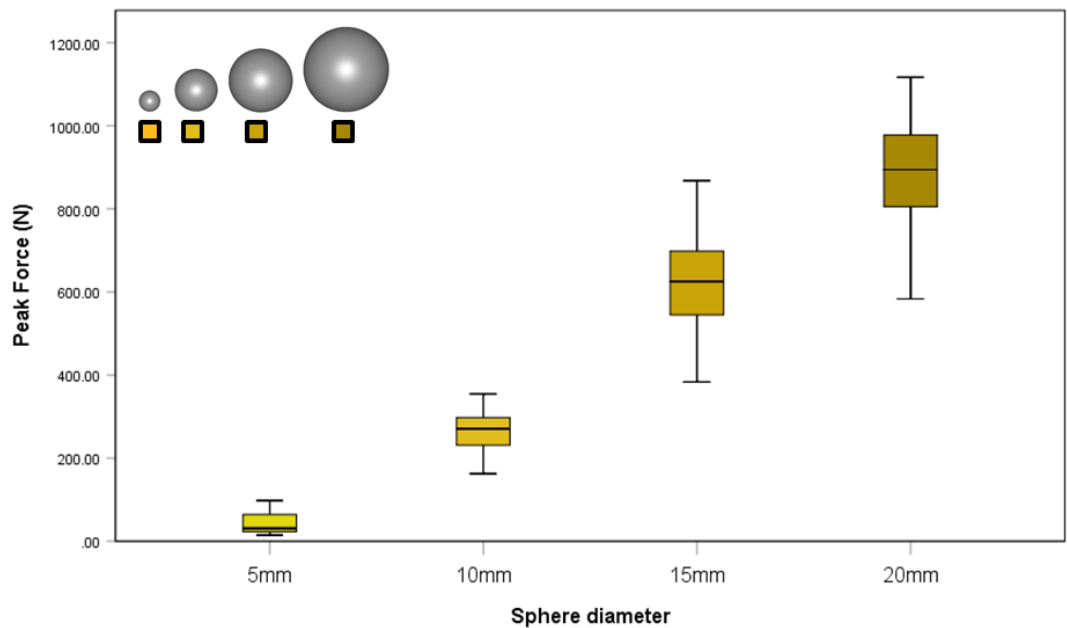

Figure 3.15 Boxplot showing peak forces (N) recorded during fracture of spheres using the large (2xscale) teeth models. Showing, from left to right, the results of the smallest (5mm) diameter spheres to the largest (20mm) diameter spheres.

Statistically significant differences were found between the means of displacement at peak fracture for all combinations of sphere size crushed using the large teeth models (Tamhane test; $p<0.001$ for all combinations). As with the small and medium models, the means of displacement at fracture experienced by the different sized spheres on the large model closely followed the ratios of the size of the spheres. That is, the 5mm spheres (mean=0.7697mm) fractured after roughly half the displacement of the 10mm spheres (mean=1.3943mm), after roughly a third the displacement of the 15mm spheres (mean=23.3332mm), and after roughly a quarter of the displacement experienced by the 20mm spheres (mean=3.1595mm). This seems to confirm that the displacement is a function not of the shape of the tooth but rather the physical properties of the spheres, either due to the shape or the material properties.

Figure 3.16 Boxplot showing displacement (mm) recorded at peak force during fracture of spheres using the large (2xscale) teeth models. Showing from left to right the results of the smallest (5mm) diameter spheres to the largest (20mm) diameter spheres.

There was considerable variation in the range of energy recorded for the 20mm spheres (minimum=531.53 mJ; maximum=2310.76 mJ), indeed, nearly all the results for the 15mm spheres (minimum=423.21 mJ; maximum=1068.03 mJ) fall in this range, though statistically significant differences were observed between all possible combinations of the means (Tamhane test; p<0.001 for all possible combinations).
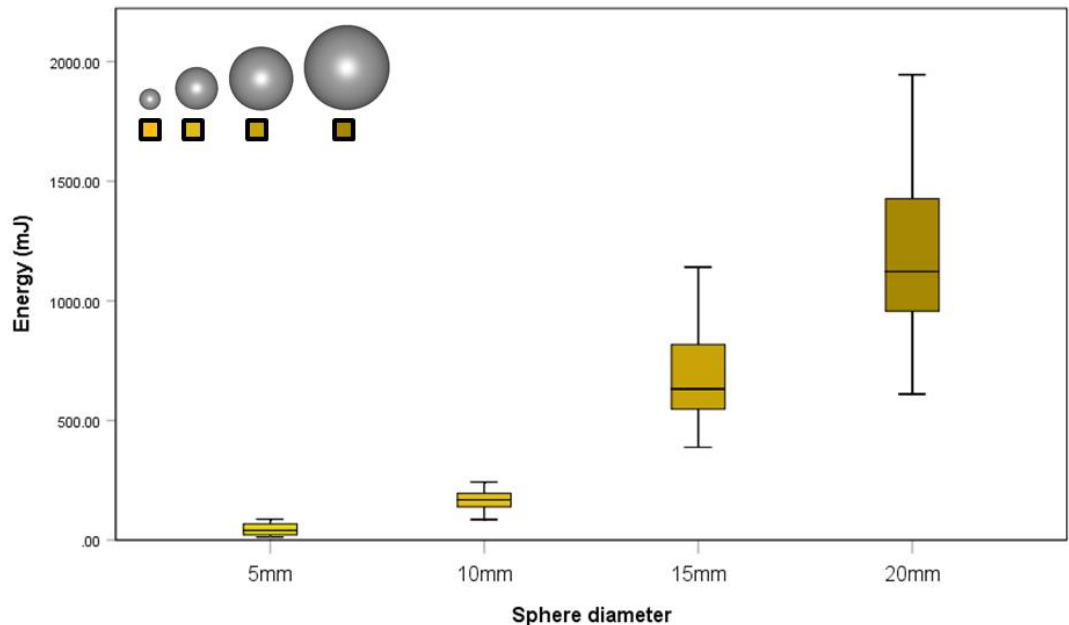
Figure 3.17 Boxplot showing energy (mJ) required to induce fracture of spheres using the large (2xscale) teeth models. Showing from left to right the results of the smallest (5mm) diameter spheres to the largest (20mm) diameter spheres.

The results for the large (2xscale) teeth models display a marked trend towards increased forces, energy expenditure, and displacement to initiate fracture as the size of the food object increases. Additionally, there is increased variance in all three categories as the size of the food object is increased.

3.4 Comparisons between dental model sizes

After having considered the performance of each of the three teeth models against the four different sized spheres (sections 3.3.1-3.3.3), the performance of the three models on each sized sphere against each other are compared here. The data has been re-plotted to more easily make comparisons between the teeth and to investigate the effect of tooth size on performance.

3.4.1 Comparisons between dental model sizes – 5mm sphere

Figure 3.18 displays the graphs of force plotted against displacement for all of the 5mm spheres crushed in this study. The colours of the graphs represent the tooth used to crush the sphere. It is clear from this figure that all three teeth performed relatively similarly on the 5mm spheres, though there appears to be a broader range of forces required to induce fracture for both the medium and large models.

5mm Spheres

Figure 3.18 Force - Displacement recorded Graph of Force (N) by displacement (mm) for all tests using the 5mm spheres.

Figures 3.19-3.21 display the results of the tests as boxplots. The large teeth experienced the lowest mean peak force (mean=59.8068 N), as well as the absolute minimum force experienced on the 5mm spheres (minimum=27.20 N), but also the highest standard deviation (SD=23.28862) and the absolute maximum force (maximum=106.90 N). However, an analysis of variance showed no significant differences between groups in the peak forces experienced by the 5mm spheres when crushed by the different teeth models (Welch test; $F_{(2, 111.078)}$= 1.323, p=0.271).
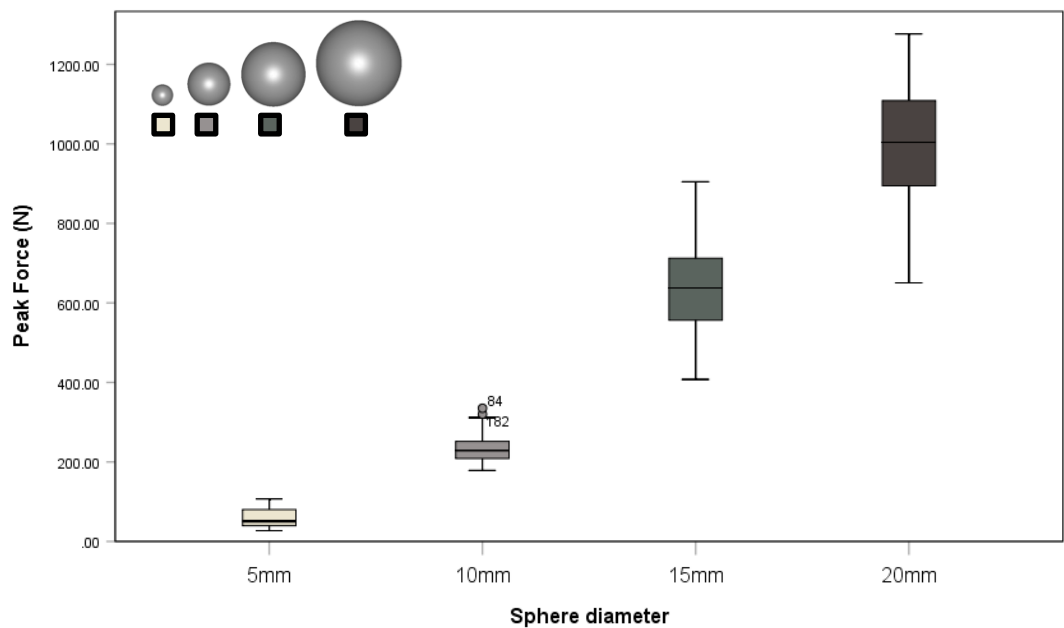
Figure 3.19 Boxplot showing peak forces (N) recorded during fracture of spheres using the 5mm spheres Showing, from left to right, the results of the small, medium, and large teeth models.

An analysis of variance revealed some statistically significant difference between groups for displacement (Welch test; $F_{(2, 115.688)}=3.348$, p=0.039), despite the apparent similarity in results as seen in Figure 3.20. While no statistically significant difference was observed between the small and medium teeth (Tamhane test; p=0.897) or the medium and large teeth (Tamhane test; p=0.129), this difference was observed between the small and large results (Tamhane test; p=0.038). Interestingly, the entire range of the medium results (minimum=0.55mm; maximum=0.80mm) fit within the range of the small results (minimum=0.54mm; maximum=0.85mm).
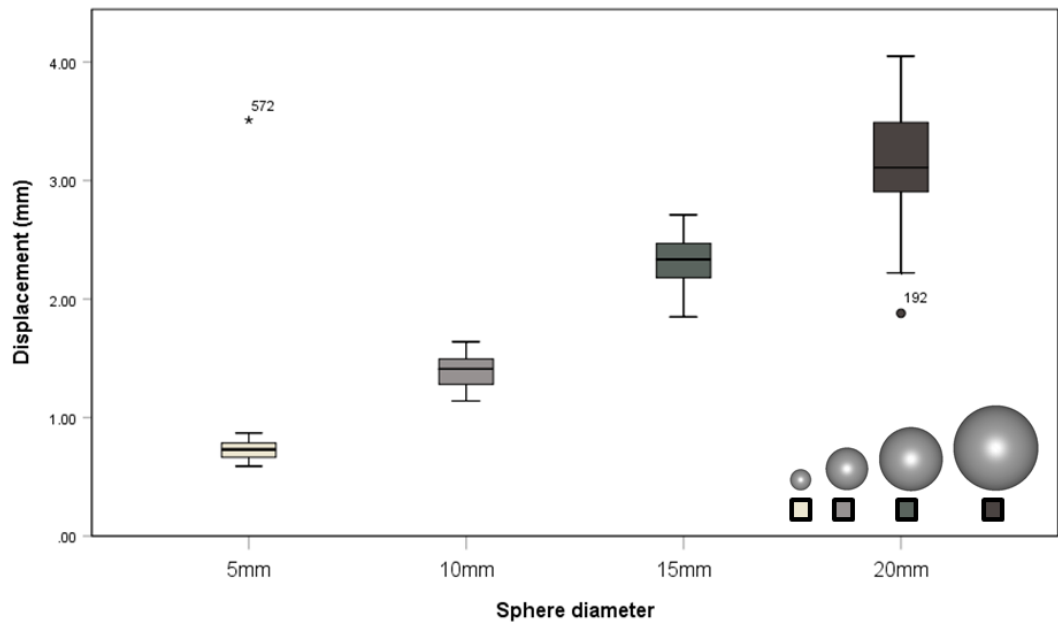
Figure 3.20 Boxplot showing displacement (mm) recorded at peak force during fracture of spheres using the 5mm spheres Showing, from left to right, the results of the small, medium, and large teeth models.

The results of this test are displayed in Figure 3.21 below. The large teeth required the absolute maximum energy to induce fracture (maximum= 40.56mJ) and had the highest standard deviation (SD= 0.90232mJ), though the medium teeth experienced the greatest mean (mean= 22.1998mJ). However, an analysis of variance revealed no statistically significant differences between groups for energy expended to induce fracture (Welch test; $F_{(2, 112.252)}=1.645$, p=0.198).

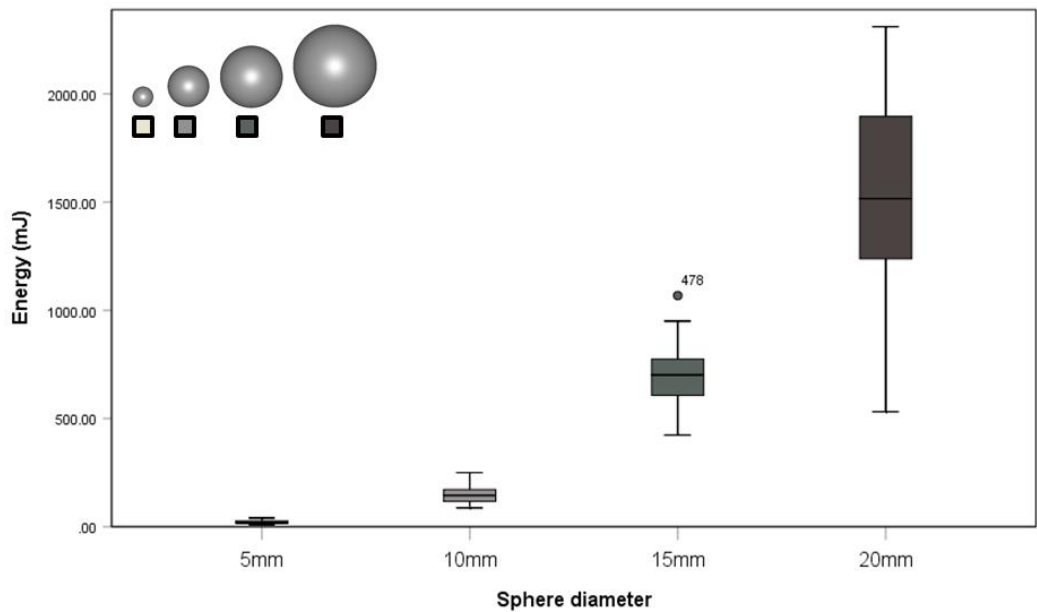**Figure 3.21 Boxplot showing energy (mJ) required to induce fracture of spheres using the 5mm spheres Showing, from left to right, the results of the small, medium, and large teeth models.**

Aside from a slight difference in displacement between the small and large models, this study found no evidence of a significant effect on the fracture of the 5mm spheres due to changes in tooth size.

The results of the 5mm spheres indicate little difference in performance based on tooth size. The medium sized teeth model experienced the highest mean peak force, while the large teeth model experienced the lowest mean, but also the absolute maximum, and the small model was intermediate. Despite some difference in displacement between the small and large teeth models, displacement can likely be considered uniform between teeth models. The energy results were not significantly different between models. From an ecological perspective this indicates no significant advantage to any size of teeth when crushing small hard objects. Likely all three models were able to fully engage the small object, giving no advantage to contact surface area, though further study is required.

3.4.2 Comparisons between dental model sizes – 10mm sphere

From Figure 3.22, some trends in the 10mm sphere data can be observed. Clearly the medium teeth results required a greater force at peak fracture than the small teeth and likely the large teeth as well. There also seems to be considerably less variation in displacement than in force.

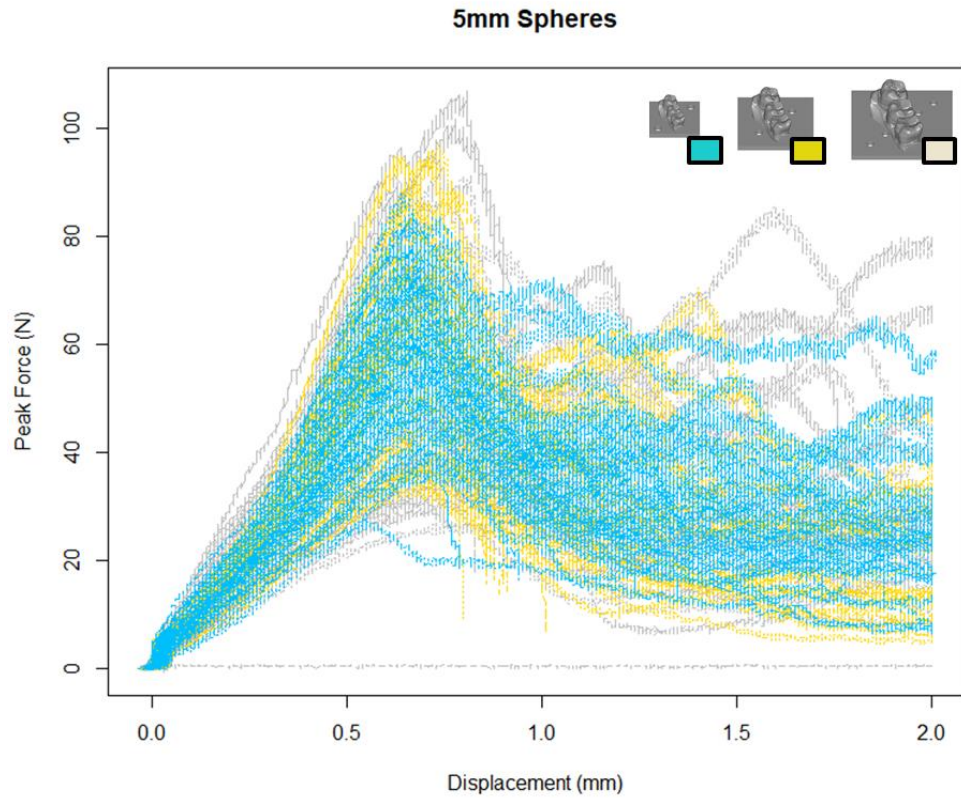**Figure 3.22 Force - Displacement recorded Graph of Force (N) by displacement (mm) for all tests using the 10mm spheres.**

In fact, an analysis of variance revealed statistically significant differences in peak force (Welch test, $F_{(2, 116.278)}=57.672$, $p<0.001$). When comparing between groups, the differences in means were statistically significant between all groups (Tamhane test, $p<0.001$ for all combinations). As Figure. 3.23 shows, the medium teeth models experienced the greatest force (maximum= 354.70 N), the highest mean force (mean=265.9533 N), and the highest standard deviation (SD=46.77694 N). The small teeth experienced the lowest force (minimum=120.40 N) and had the lowest mean force (186.2483 N).
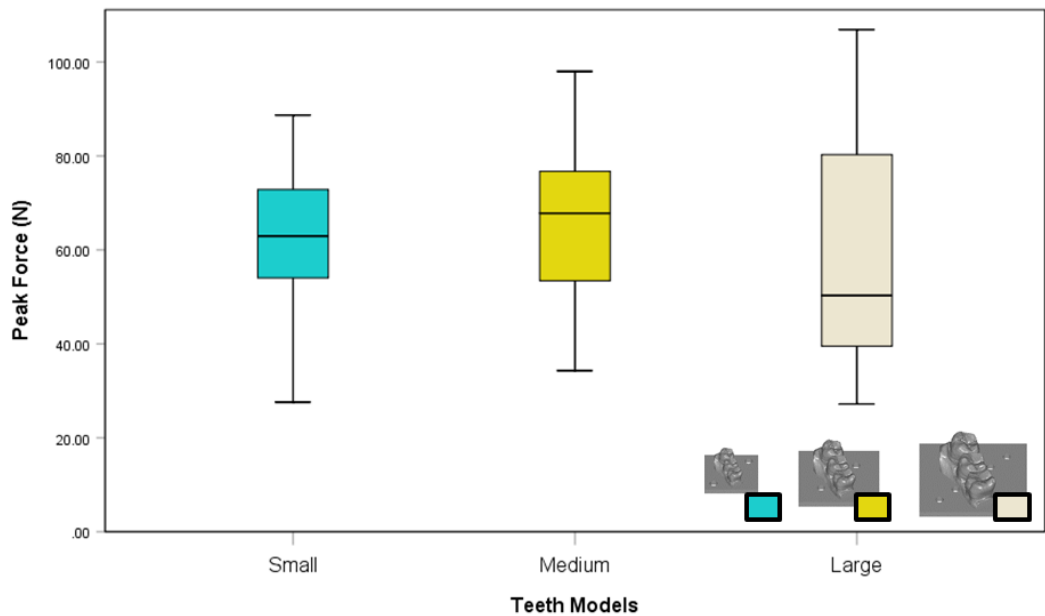
Figure 3.23 Boxplot showing peak forces (N) recorded during fracture of spheres using the 10mm spheres. Showing, from left to right, the results of the small, medium, and large teeth models.

An analysis of variance detected some statistically significant differences between groups for displacement (ANOVA, $F_{(2,177)}=5.161$, $p=0.007$). There was no significant difference between the means of the large teeth and either the small (Tukey HSD test, $p=0.113$) or medium (Tukey HSD test, $p=0.473$) teeth, but there was difference between the means of the small and medium teeth (Tukey HSD test, $p=0.005$). The small teeth had the greatest mean displacement (mean=1.4438mm) as well as the highest standard deviation (SD=0.15882mm) and both the absolute minimum (minimum=0.96mm) and maximum (maximum=1.85mm).
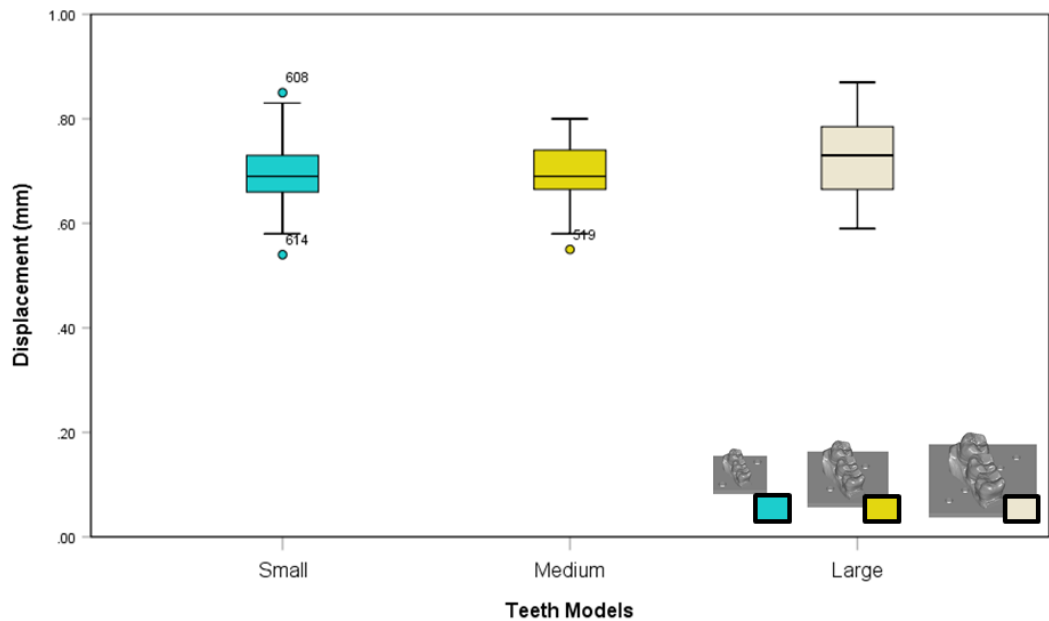
Figure 3.24 Boxplot showing displacement (mm) recorded at peak force during fracture of spheres using the 10mm spheres. Showing, from left to right, the results of the small, medium, and large teeth models.

An analysis of variance revealed statistically significant differences in the energy required to induce fracture of the 10mm spheres between the teeth models (ANOVA, $F_{(2, 177)}=17.301$, $p<0.001$). The mean energy required for the small teeth model was significantly different than both the mean energy for the medium teeth model (Tukey HSD test, $p<0.001$) and the mean energy required for the large teeth model (Tukey HSD test, $p=0.003$). The mean energy required for the medium teeth was also significantly different than the mean energy required for the large teeth (Tukey HSD test, $p=0.031$). The small teeth required the least energy (minimum=49.74 mJ) and the least mean energy (mean=125.9587 mJ). The large teeth required the greatest energy (maximum=250.20 mJ), but the medium teeth model had the greatest mean energy requirement (mean=166.1170 mJ).
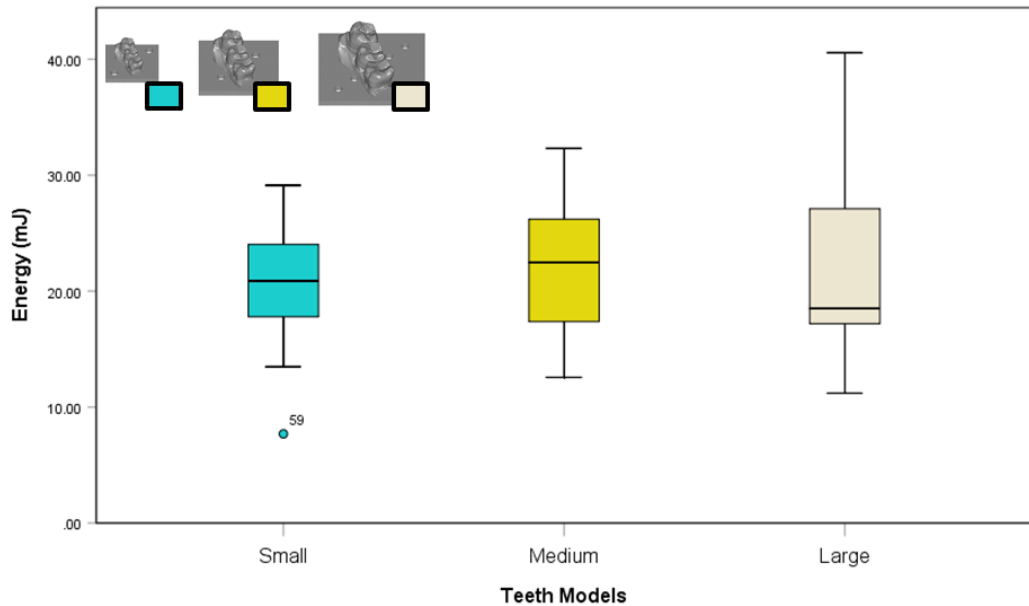
Figure 3.25 Boxplot showing energy (mJ) required to induce fracture of spheres using the 10mm spheres. Showing, from left to right, the results of the small, medium, and large teeth models.

The results of the 10mm spheres indicate some difference in performance based on tooth size. The medium sized teeth model experienced the highest peak force, while the small teeth model experienced the lowest, and the large model was intermediate. Despite some difference in displacement between the small and medium teeth models, displacement can be considered uniform between teeth models. The energy results were similar to peak force, with the medium teeth model performing worst, requiring the greatest energy to induce fracture. From an ecological perspective this would indicate that the medium sized teeth models are the least efficient at crushing the 10mm spheres, requiring more energy than the other two sized teeth.

3.4.3 Comparisons between dental model sizes – 15mm sphere

Figure 3.26 displays the results of the 15mm spheres on the small, medium, and large teeth models. The results are fairly well grouped by teeth model, with the small teeth appearing to have the lowest peak forces, followed by the medium model and the large with the greatest forces. It should be noted that the tall blue peaks around 4mm are not the peak displacement, but rather record forces

experienced as the teeth models continued to compress following an initial fracture of the spheres that was less than the 75% break limit.

15mm Spheres

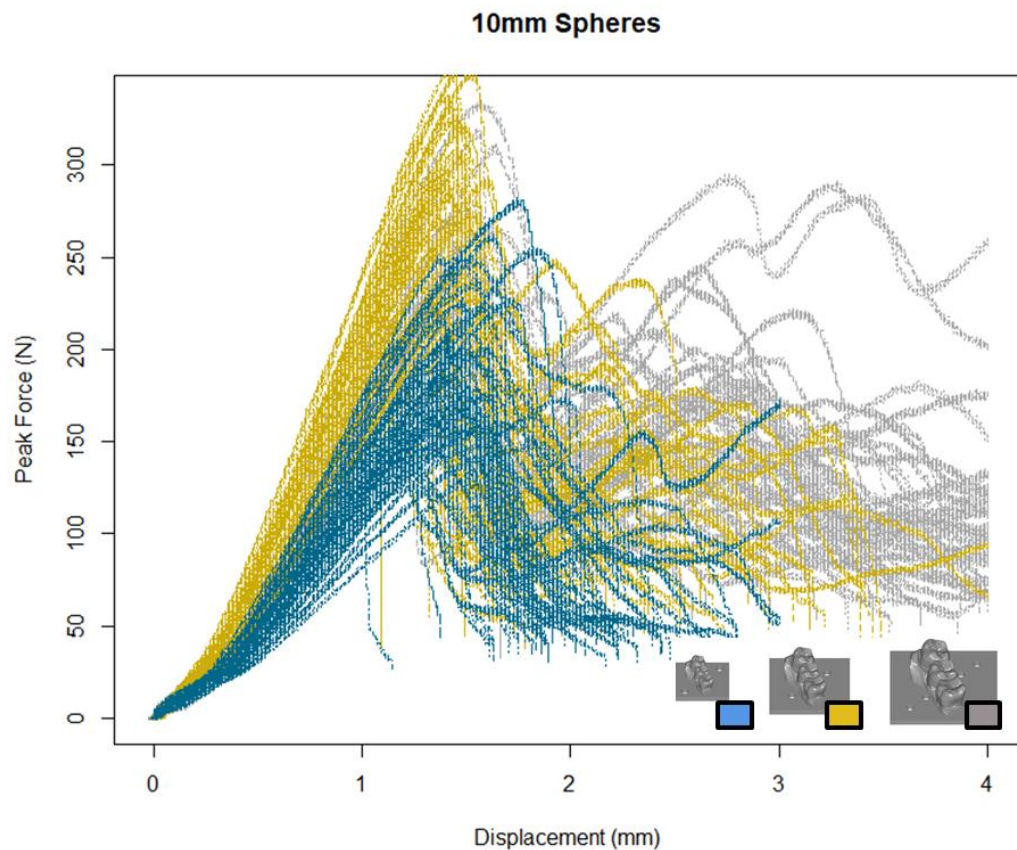**Figure 3.26 Force - Displacement recorded Graph of Force (N) by displacement (mm) for all tests using the 15mm spheres.**

An analysis of variance indicates statistically significant differences in the force data are present between groups (ANOVA, $F_{(2,177)}=14.343$, $p<0.001$). The small teeth produced the lowest mean force (mean=544.5083 N). Though the medium teeth produced the absolute minimum for (minimum=383.40 N), its mean (mean=624.6083 N) was significantly higher (Tukey HSD test, $p<0.001$) than the that of the small teeth. The large teeth, which produced the absolute maximum (maximum=904.80 N) and the highest mean force (mean=636.9000 N) were significantly different from the small teeth (Tukey HSD test, $p<0.001$) but not the medium teeth (Tukey HSD test, $p=0.789$)
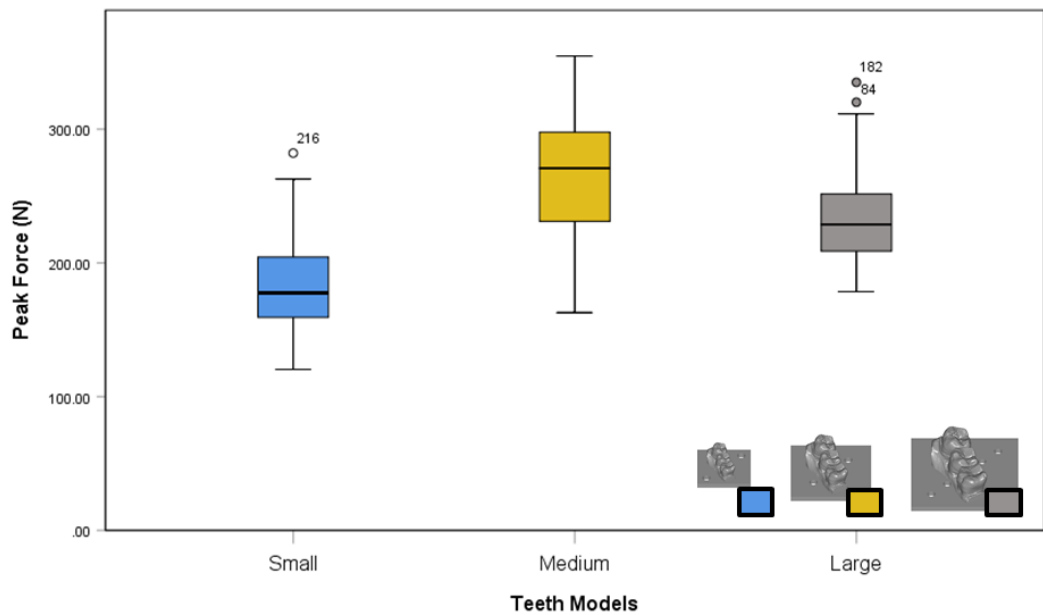
Figure 3.27 Boxplot showing peak forces (N) recorded during fracture of spheres using the 15mm spheres. Showing, from left to right, the results of the small, medium, and large teeth models.

An analysis of variance found some statistically significant difference in the displacement between the teeth models (Welch test, $F_{(2,112.143)}=4.904$, p=0.009). The differences between groups were similar to those observed in the peak force data, with significant differences observed between the small and medium teeth (Tamhane test; p=0.009), the small and large teeth (Tamhane test; p=0.021), but none between the medium and large teeth (Tamhane test; p=0.893). It should be noted that the small teeth also experienced the greatest mean displacement (mean=2.4798mm), the greatest standard deviation (SD=0.36457mm), and both the absolute maximum (maximum=3.11mm) and minimum (minimum=0.61mm).
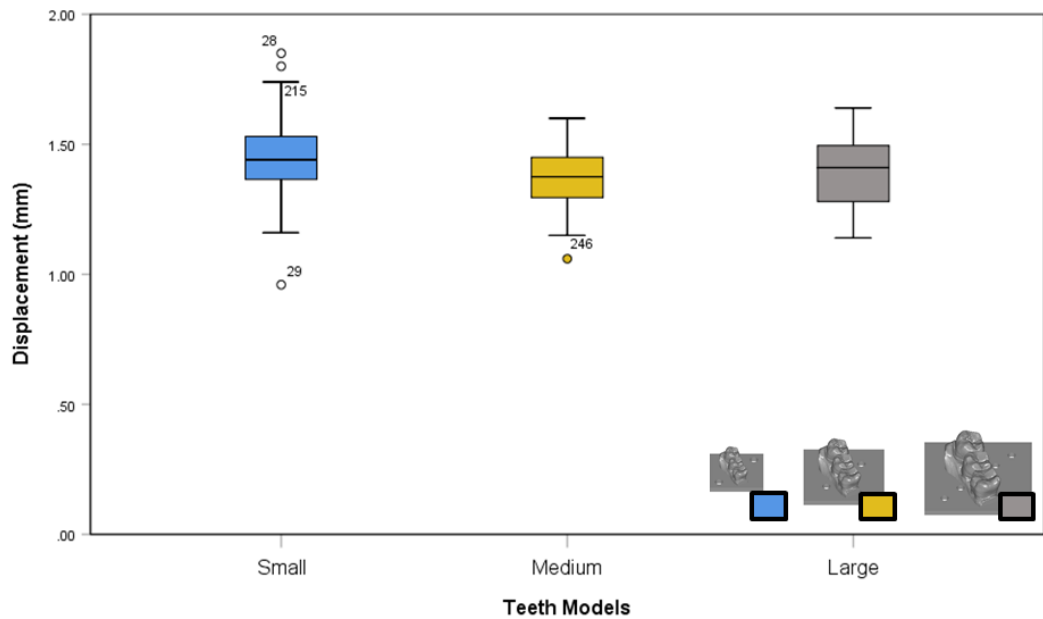
Figure 3.28 Boxplot showing displacement (mm) recorded at peak force during fracture of spheres using the 15mm spheres. Showing, from left to right, the results of the small, medium, and large teeth models.

An analysis of variance found no difference in the energy required to induce fracture between the teeth models (Welch test, $F_{(2, 115.458)}$=0.119, p=0.888). Though, as can be seen from Figure 3.29, the ranges of the small (minimum=398.53mJ; maximum=115.74mJ) and medium (minimum=388.28mJ; maximum=1140.98mJ) models were slightly larger than that of the large model (minimum=423.21mJ; maximum=1068.03mJ).
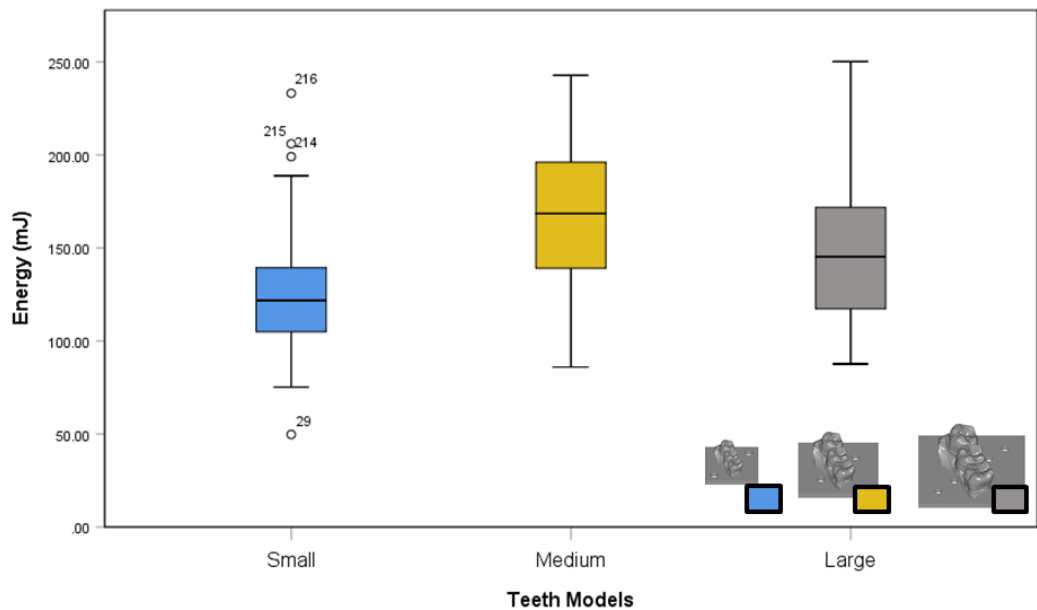

Figure 3.29 Boxplot showing energy (mJ) required to induce fracture of spheres using the 15mm spheres. Showing, from left to right, the results of the small, medium, and large teeth models.

The results of the 15mm sphere indicate no significant effect of tooth size on fracture. All three sized teeth models performed comparably, with no significant difference apparent in the energy required to induce fracture, meaning no size offers a significant advantage in terms of efficiency. The small teeth did experience slightly weaker peak forces, which could convey a slight advantage in mitigating tooth fracture. However, it is likely that though this difference is statistically significant, it does not reflect a real-world difference.

3.4.4 Comparisons between dental model sizes – 20mm sphere

From Figure 3.30 it is clear that the 20mm spheres experienced the greatest forces and displacement, but also the greatest range of the latter. It appears that the small teeth generally required lower peak forces, but this is unclear from the graph.
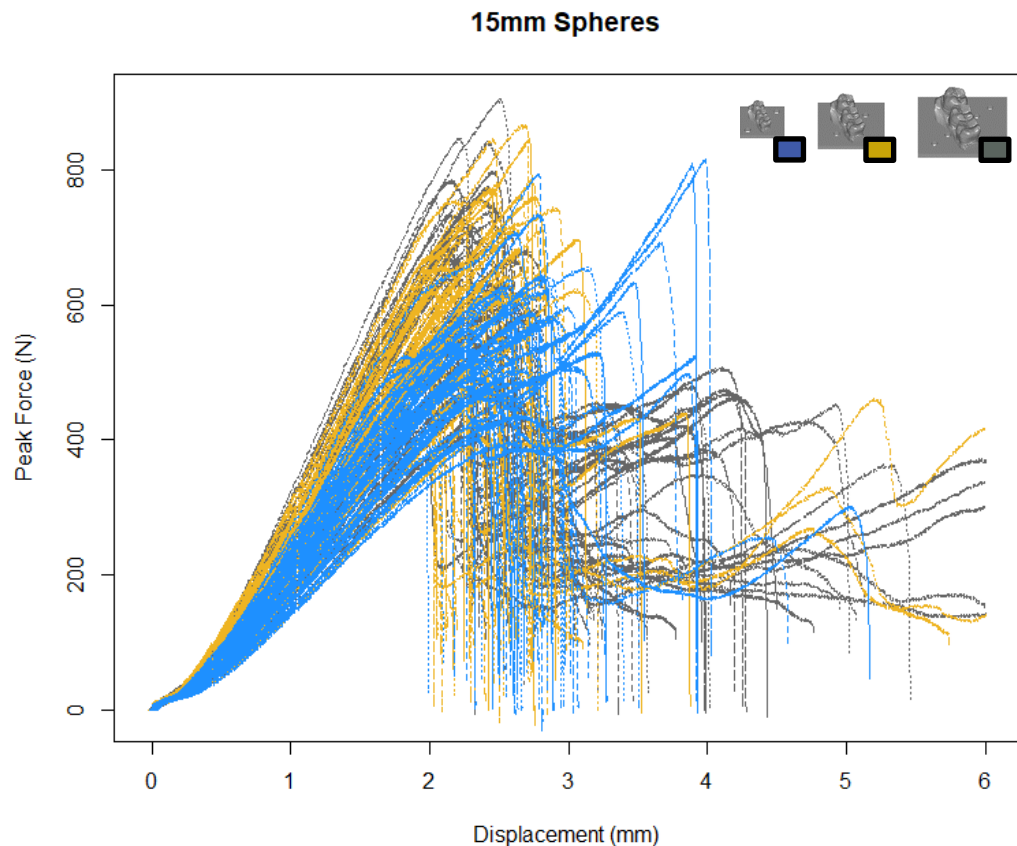

20mm diameter spheres
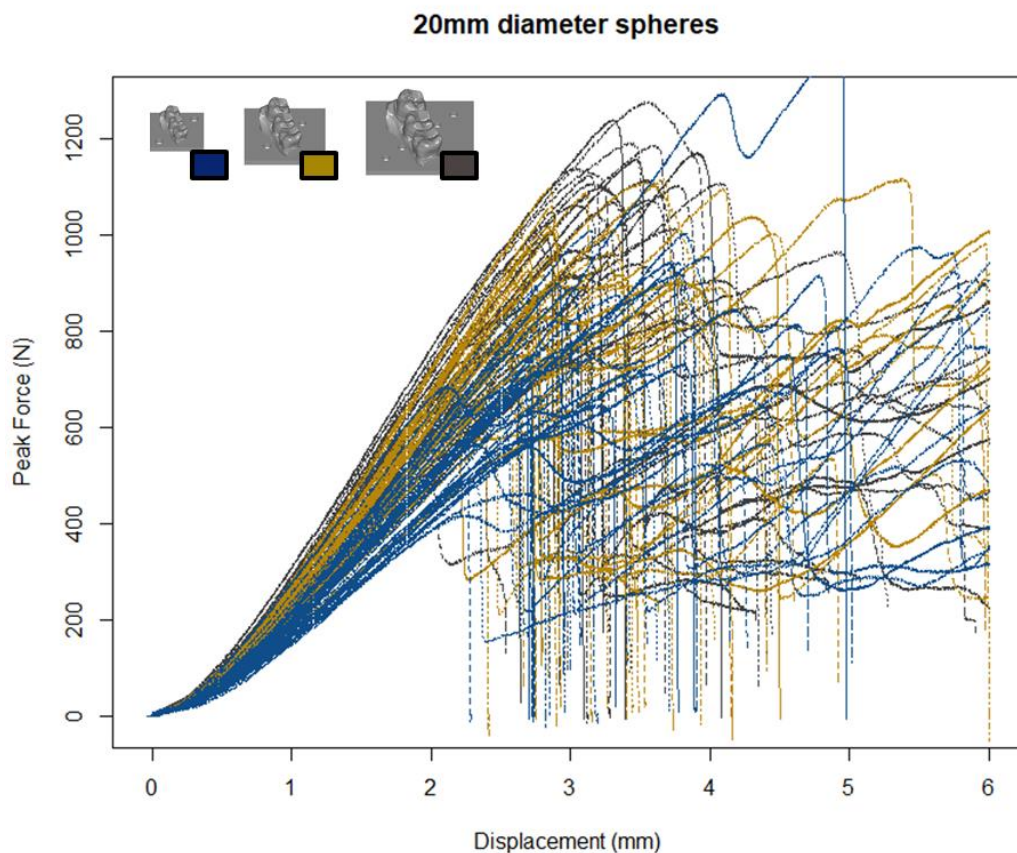
 Figure 3.30 Force - Displacement recorded Graph of Force (N) by displacement (mm) for all tests using the 20mm spheres.

An analysis of variance reveals statistically significant differences in the peak forces at fracture experienced by the 20mm spheres on the different teeth models (ANOVA, $F_{(2, 117)}=28.839$, $p<0.001$). As Figure 3.31 shows, the small teeth experienced the lowest peak force (minimum=418.80 N; mean=750.8675 N), followed by the medium teeth (mean=887.0575 N), and with the large teeth experiencing the greatest forces (mean=993.7825 N; maximum=1276.60 N). Statistically significant differences were observed between the small and medium teeth (Tukey HSD test, $p<0.001$)., the small and large teeth (Tukey HSD test, $p<0.001$)., and the medium and large teeth (Tukey HSD test, $p=0.003$).
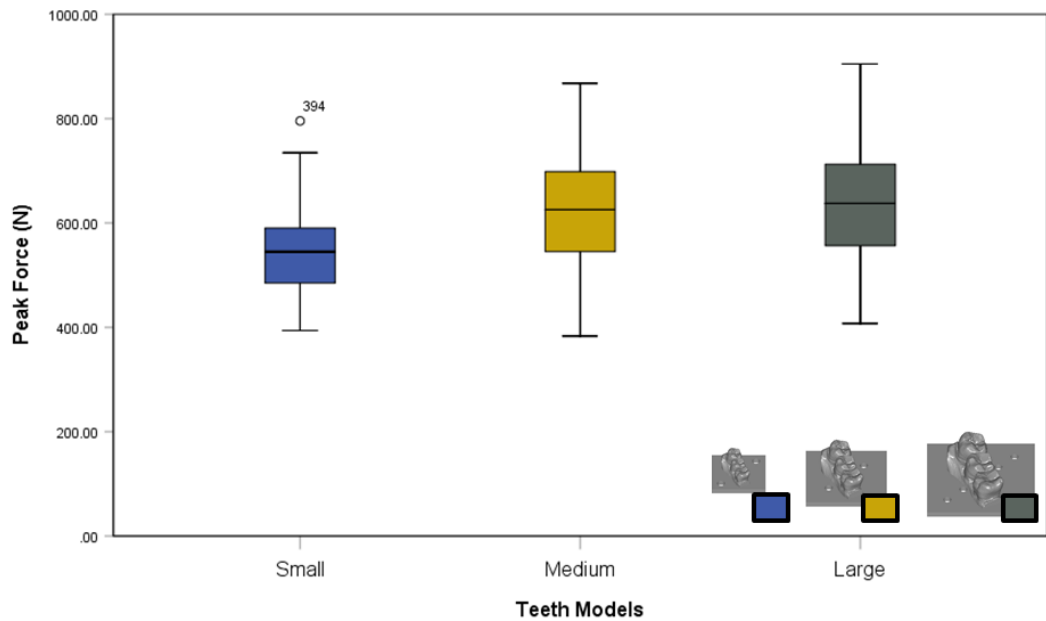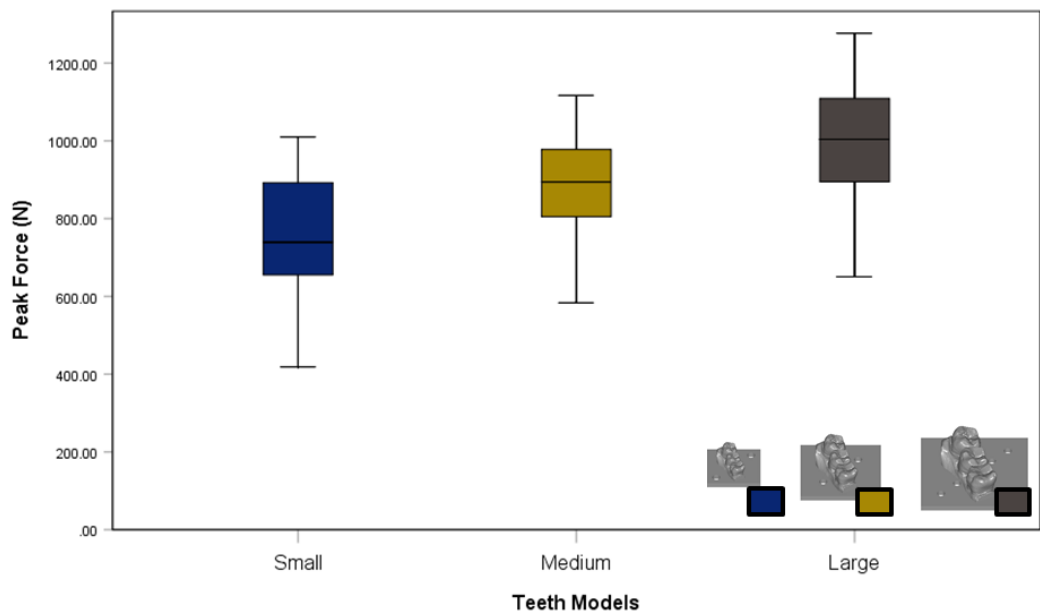

Figure 3.31 Boxplot showing peak forces (N) recorded during fracture of spheres using the 20mm spheres. Showing, from left to right, the results of the small, medium, and large teeth models.

An analysis of variance indicated no statistically significant differences were present in comparisons of the means of the displacement experienced at peak force by the 20mm spheres on the different sized teeth models (ANOVA, $F_{(2, 117)}=2.665$, $p=0.074$).
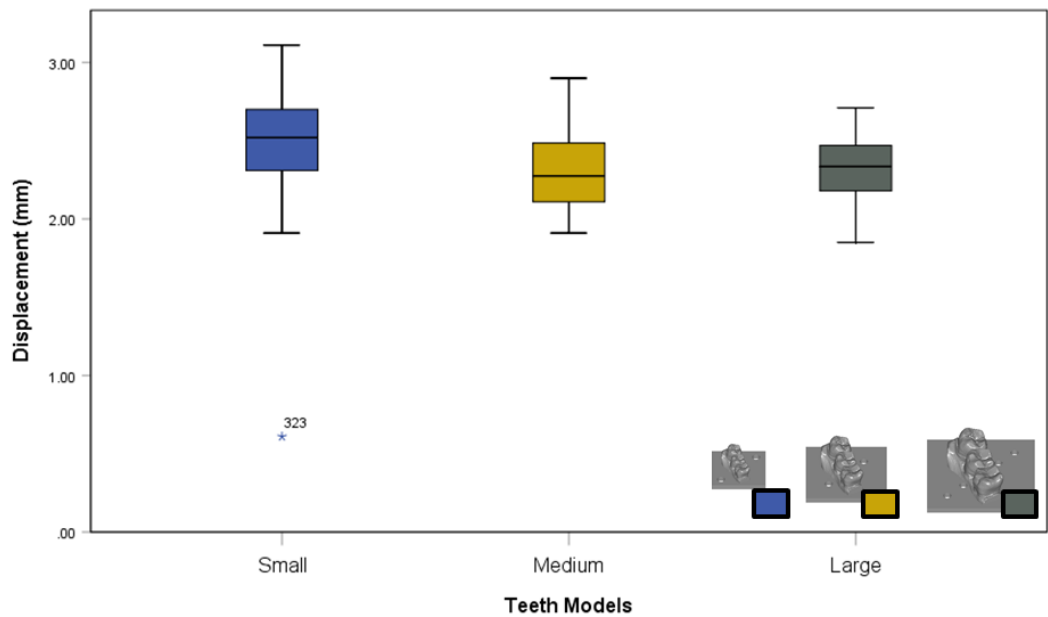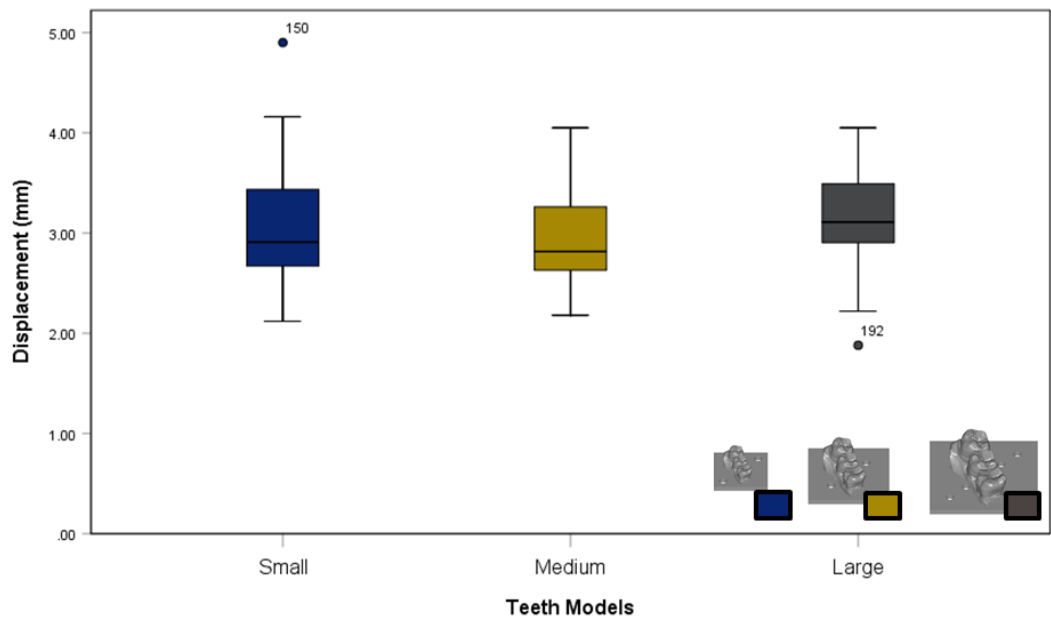
Figure 3.32 Boxplot showing displacement (mm) recorded at peak force during fracture of spheres using the 20mm spheres. Showing, from left to right, the results of the small, medium, and large teeth models.

Statistically significant differences were detected by an analysis of variance in the mean energy required to induce fracture of the 20mm spheres by the different teeth models (ANOVA, $F_{(2, 117)}=13.359$, $p<0.001$). The small teeth required the least energy to induce fracture (minimum= 421.90mJ; mean=1098.1838mJ), followed by the medium teeth (mean=1191.6212mJ), and with the large teeth requiring the most energy (mean=1536.7561mJ; maximum=2310.76mJ). Statistically significant differences were observed in the mean energy required to induce fracture between the small and large teeth (Tukey HSD, $p<0.001$), the medium and large teeth (Tukey HSD, $p=0.001$), but not between the small and medium teeth (Tukey HSD, $p=0.550$).
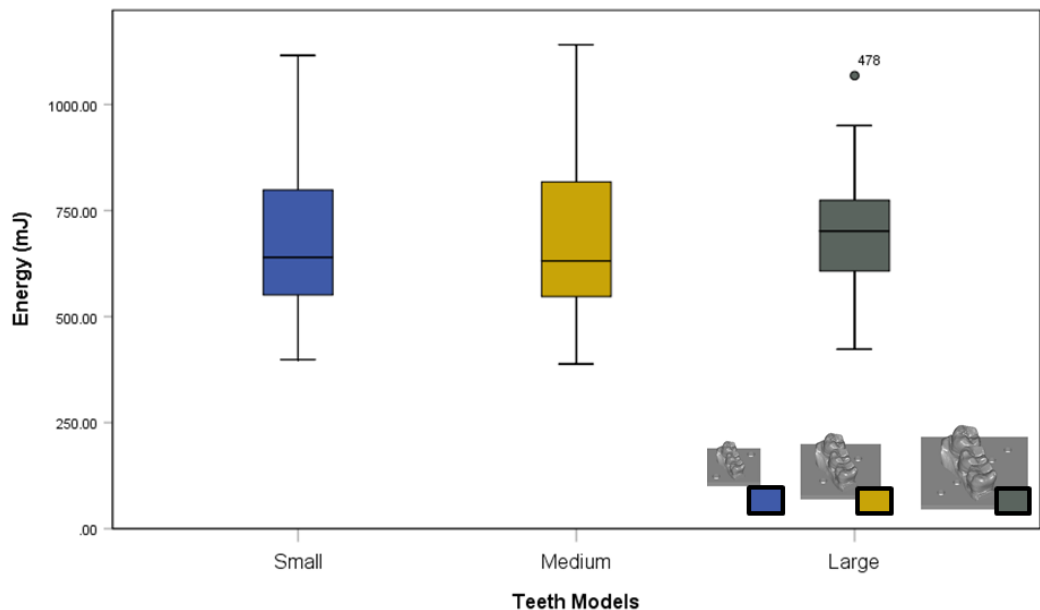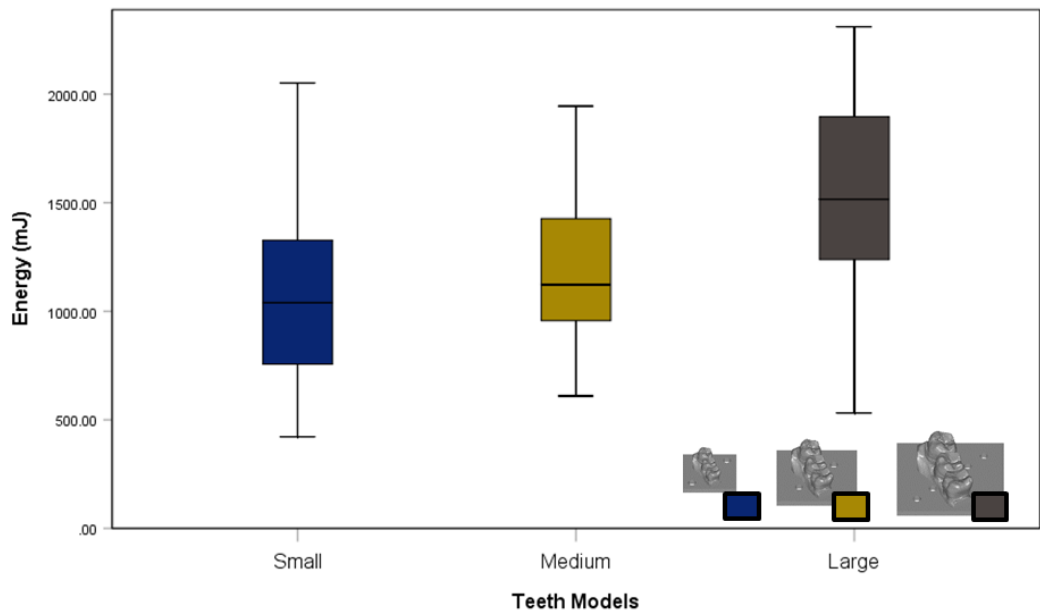
Figure 3.33 Boxplot showing energy (mJ) required to induce fracture of spheres using 20mm spheres. Showing, from left to right, the results of the small, medium, and large teeth models.

The results for the 20mm spheres do indicate a relationship between tooth size and both peak force at fracture and energy required to induce fracture, though no such relationship was recorded for displacement at peak force. According to these results, a smaller tooth has a distinct advantage in both requiring less forces be generated in order to propagate fractures in a food object as well as in the amount of energy expended to induce such fractures. However, in order to understand these relationships, the complete data set produced in this study must be considered.

3.4.5 All Dental size and Tooth size results combined

Figure 3.34 displays the results of all the spheres crushed during this project. The graphs are coloured to reflect which tooth model was used in that particular test, with the blue corresponding to the small model, the gold to the medium model, and the grey to the large. The graphs are also shaded in relation to the size of the sphere used, with the lightest shades indicating the 5mm diameter spheres and the colours getting progressively darker to indicate the 10mm, 15mm, and 20mm diameter spheres. The resulting graph is nevertheless confusing, though it adequately displays the variety in results, as well as the clear effect that sphere

size has on the fracture mechanics. Indeed, it is generally more difficult to distinguish between the teeth used than the spheres, particularly with the smallest (5mm diameter) and largest (20mm diameter) spheres.
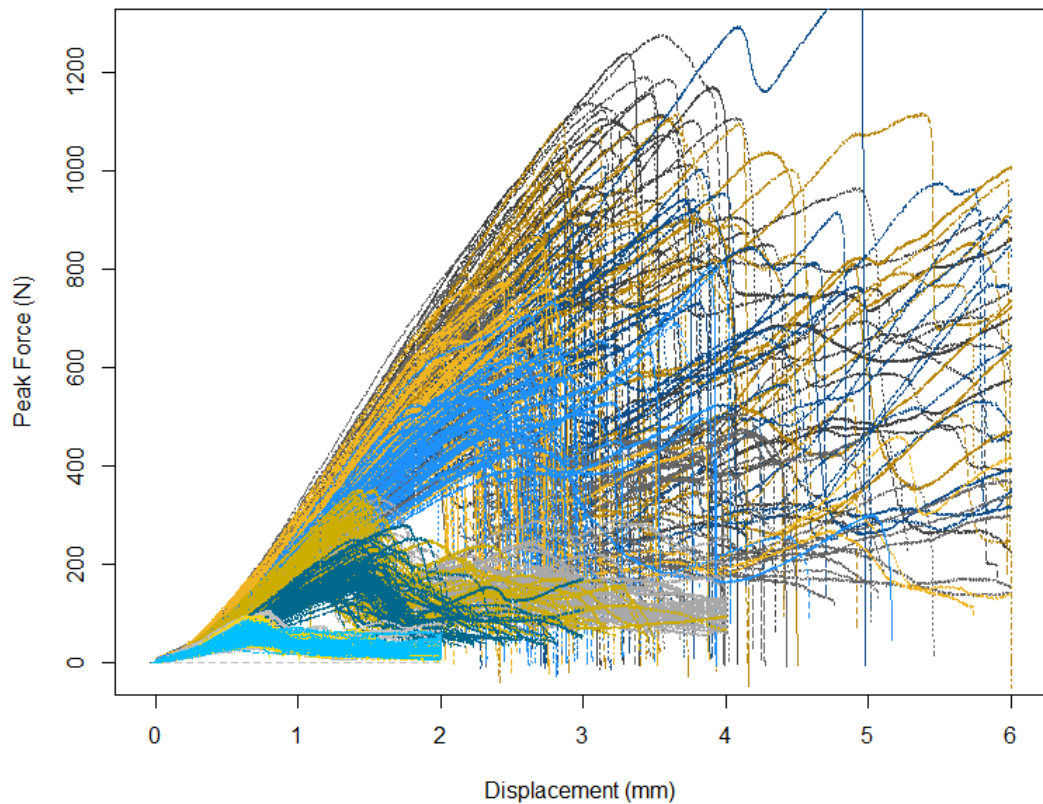
Figure 3.34 Force - Displacement recorded Graph of Force (N) by displacement (mm) for all tests, of all sized spheres using all teeth models.

Figures 3.35-3..37 display boxplots of all the results, grouped by teeth models, and with the colours indicating sphere size. From these graphs a few general trends can be identified. First, it is clear that sphere size has a pronounced influence on fracture mechanics. The larger the sphere, the greater the peak forces, the displacement at peak force, and the energy required to induce fracture, regardless of tooth size.
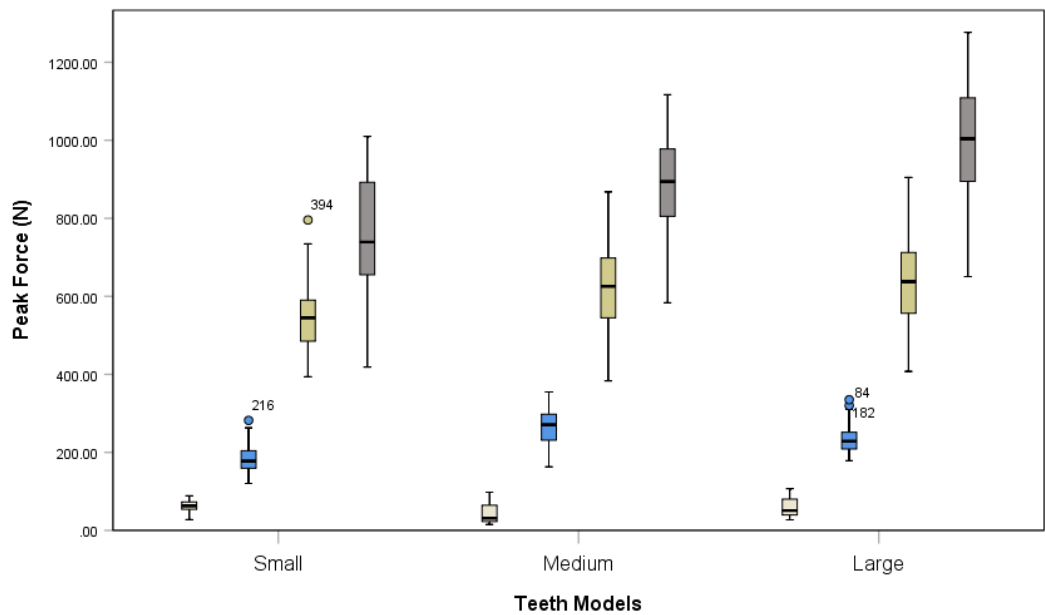
Figure 3.35 Boxplot showing peak forces (N) recorded during fracture of spheres using the modern *Homo* teeth models. Showing, for each tooth, from left to right, the results of the smallest (5mm) diameter spheres to the largest (20mm) diameter spheres.

The second and third trends are far less substantial. There seems to be slight advantage in both peak force and energy for the smaller teeth. Conversely, the small teeth appear to require slightly more displacement before fracture propagation.
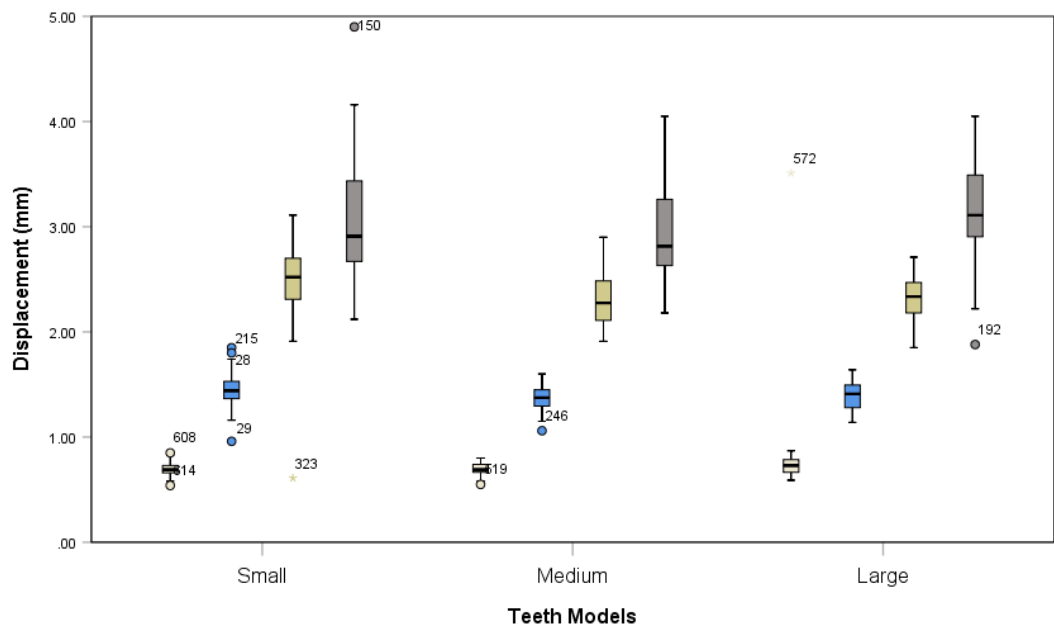
Figure 3.36 Boxplot showing displacement (mm) recorded at peak force during fracture of spheres using the modern *Homo* teeth models. Showing, for each tooth, from left to right the results of the smallest (5mm) diameter spheres to the largest (20mm) diameter spheres.

Importantly, these results do not support the conclusion that the effects of object size are relative to the tooth size. If they were, the results for the 20mm sphere on the large teeth should be similar to the results of the 15mm sphere on the medium teeth and the 10mm sphere on the small teeth model. Instead, the size of the object seems to have an independent effect on the fracture mechanics. This has important implications which will be considered in greater detail in chapter 4.
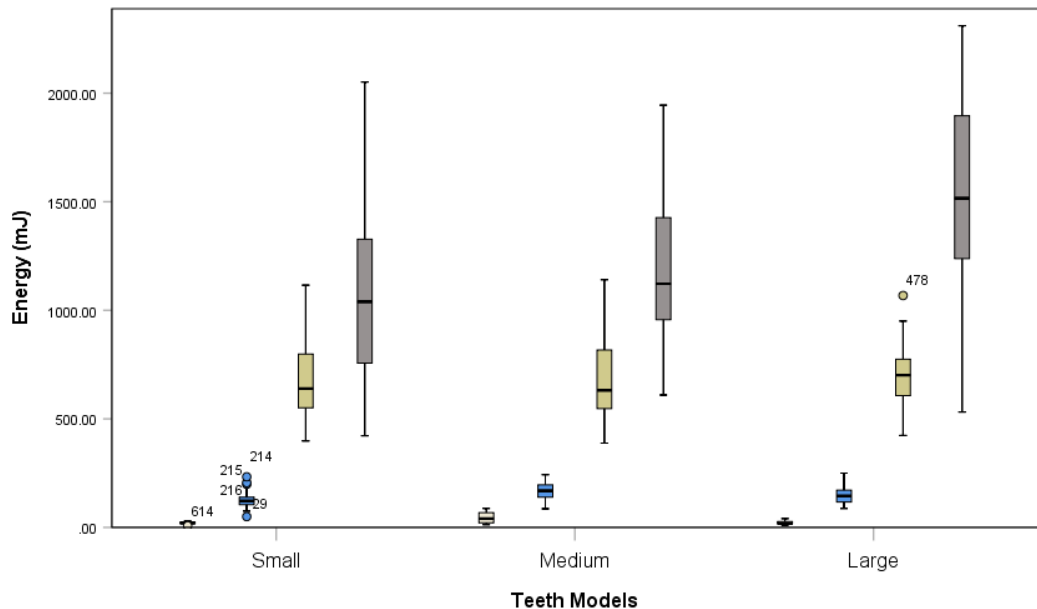
Figure 3.37 Boxplot showing energy (mJ) required to induce fracture of spheres using the small teeth models. Showing, for each tooth, from left to right the results of the smallest (5mm) diameter spheres to the largest (20mm) diameter spheres.

Additionally, it should be noted that the larger the sphere, the greater the standard deviation. This may reflect some physical property that is an artefact of the 3D printing process. Perhaps the larger spheres are more variable in their internal structure, possibly caused by the adhesive binder not drying to the same depth in the larger spheres. This is speculative, though previously addressed by Swan (2016), and is the reason the vacuum oven was incorporated in the sphere processing. It was felt that 24hr would be sufficient to adequately dry the spheres, but this was based on drying times for the hemispheres. Further research is required. Alternatively, the spheres may not be grabbing the larger spheres as well as they did the small spheres. It was observed that the smaller spheres fit neatly between the cusps of the lower teeth, but the larger teeth rested instead on the cusps of the lower teeth. This could lead to slight variations in the position of the

sphere in relation to the teeth, which could result in different fracture mechanics. That said, this effect would be expected to be more pronounced on the small teeth models, which were smaller relative to the spheres than the medium or large models, and thus experienced this change in position on smaller sized spheres.

3.5 Does the placement of the food object on the tooth effect efficiency?

In order to test the effect of varying food object placement (and thus tooth-food-tooth contact), the test was repeated on all three tooth models though with the item placed in one of two different positions. P1 (Placement 1) was located on the buccal edge of the lower M2, midway between the mesial and distal buccal cusps. P2 (Placement 2) was located over the distal cusps of the lower M1 and the mesial cusps of the lower M2. Only the 15mm sphere was used, with 30 iterations on each placement per model (thus, a total of 180 additional results were obtained 60 each on the small, medium, and large teeth).

3.5.1 Results of sphere placement variation

The results of these tests were included in the analyses of variance above (3.3 and 3.4). The boxplots below (Figure. 3.38-3.40) display the results of the two placement tests as well as the results from the 15mm tests above (3.3 and 3.4). The peak forces experienced at fracture for the both the first and second placement tests were significantly different when compared to the results for the 15mm spheres in the original position on all teeth (Tamhane test, $p<0.001$ for all combinations). When comparing the two placement tests against each other, the P1 and P2 results on the small teeth were significantly different (Tamhane test, $p=0.003$), but on the medium (Tamhane test, $p=0.117$) and large teeth (Tamhane test, $p=0.233$) they were not significantly different. For the small teeth, the P1 mean (mean=451.2333 N) was lower than the original placement (mean=544.5083 N), and the P2 mean was lower still (mean=399.4367 N). For the medium teeth the P1 mean (mean=397.2700 N) was lower than both the P2 mean (mean=448.2267 N) and the original placement (mean=624.6083 N). The peak force on the large teeth followed a similar pattern to that on the small teeth, with the P1 results (mean=508.0200 N) lower than the original placement (mean=636.9000 N), but

the P2 results (mean=454.6167 N) lower still. However, it should be noted that the results on the large teeth are all slightly higher than the results of the same placement on the small teeth.
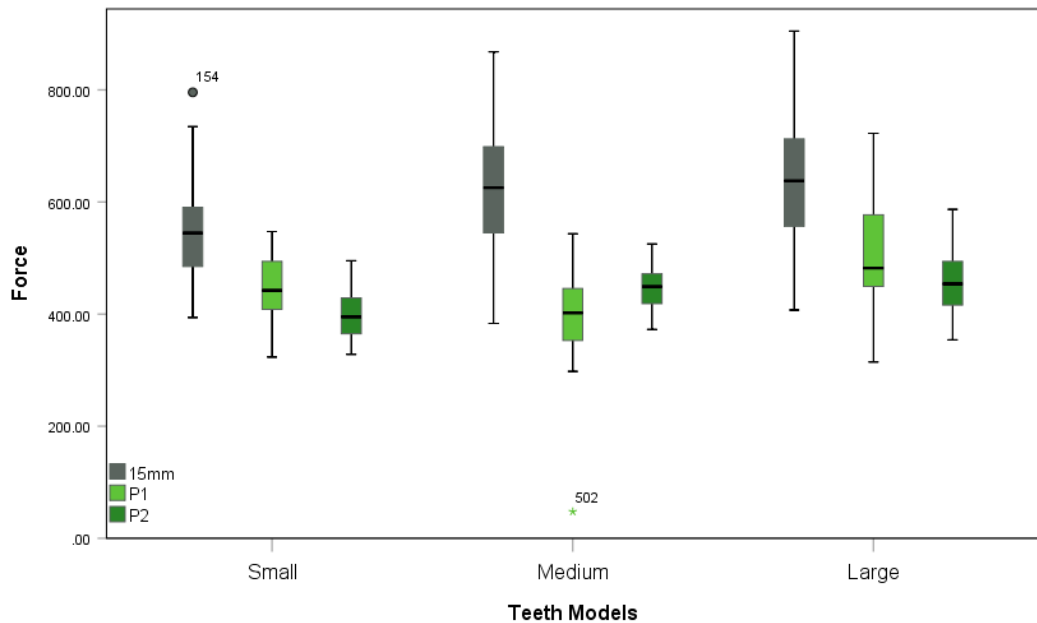
Figure 3.38 Boxplot showing peak force (N) at fracture of the 15mm spheres during the placement tests. 15mm results from the original tests have been included

The P1 displacement results were statistically significantly different than the original 15mm placement results for the small (Tamhane test, p=0.004), medium (Tamhane test, p<0.001), and large (Tamhane test, p<0.001) models. Statistically significant differences were also detected between the P2 displacement results and those for the original placement on the small (Tamhane test, p<0.001), medium (Tamhane test, p<0.001), and large (Tamhane test, p<0.001) teeth. When comparing the P1 and P2 tests, statistically significant differences were observed between the results on the small, medium and large teeth (Tamhane test, p<0.001 for all three). For the small teeth, the P1 results recorded the highest mean displacement (mean=2.7403mm), followed by the original placement (mean=2.4798mm) and the P2 results (mean=2.0583mm). This pattern continued on both the medium and large teeth. Importantly, the mean displacement for the P1 tests on the medium sized teeth model (mean=2.9430mm) was found to be not statistically significantly different (Tamhane test, p=0.972) from the mean of the

20mm spheres crushed in the original placement tests on the medium teeth model (mean=2.9015mm).
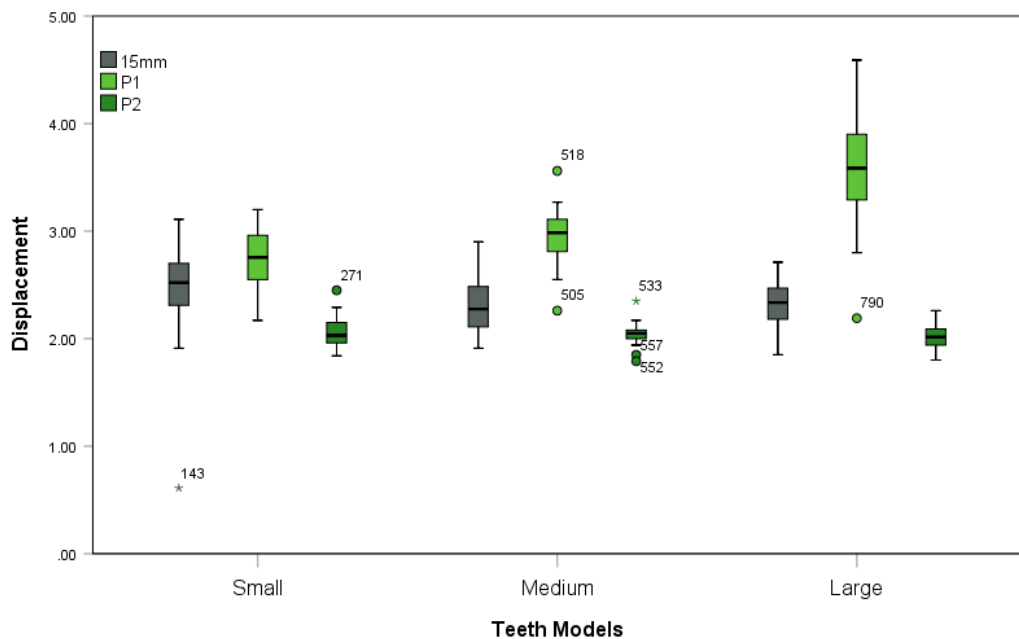
Figure 3.39 Boxplot showing displacement (mm) at peak force for the 15mm spheres during the placement tests. 15mm results from the original tests have been included

Statistically significant differences were detected between the P1 energy results and those for the original placement on the small (Tamhane test, p<0.001) and medium (Tamhane test, p=0.003) teeth models. No statistically significant difference was detected between the P1 energy results and the results of the original placement on the large teeth model (Tamhane test, p=0.229). Statistically significant differences were also detected between the P2 displacement results and those for the small (Tamhane test, p<0.001), medium (Tamhane test, p<0.001), and large (Tamhane test, p<0.001) teeth. Statistically significant differences were also identified between the results of the P1 and P2 tests on the small (Tamhane test, p<0.001), medium (Tamhane test, p<0.001), and large (Tamhane test, p<0.001) teeth models. On the small teeth, the greatest energy was required to induce fracture in the original placement position (mean=682.6395 mJ), followed by the P1 test (mean=534.4721 mJ), and the P2 test (mean=381.7364 mJ) with the least energy requirement. On the medium teeth, the greatest energy was required to induce fracture in the original placement position (mean=683.4414 mJ), followed by the P1 test

(mean=561.0897 mJ), and the P2 test (mean=428.6514 mJ) with the least energy requirement. On the large teeth, the greatest energy was required to induce fracture in the P1 test (mean=807.7673 mJ), followed by the original placement position (mean=694.6977 mJ) and the P2 test (mean=428.7617 mJ) with the least energy requirement.
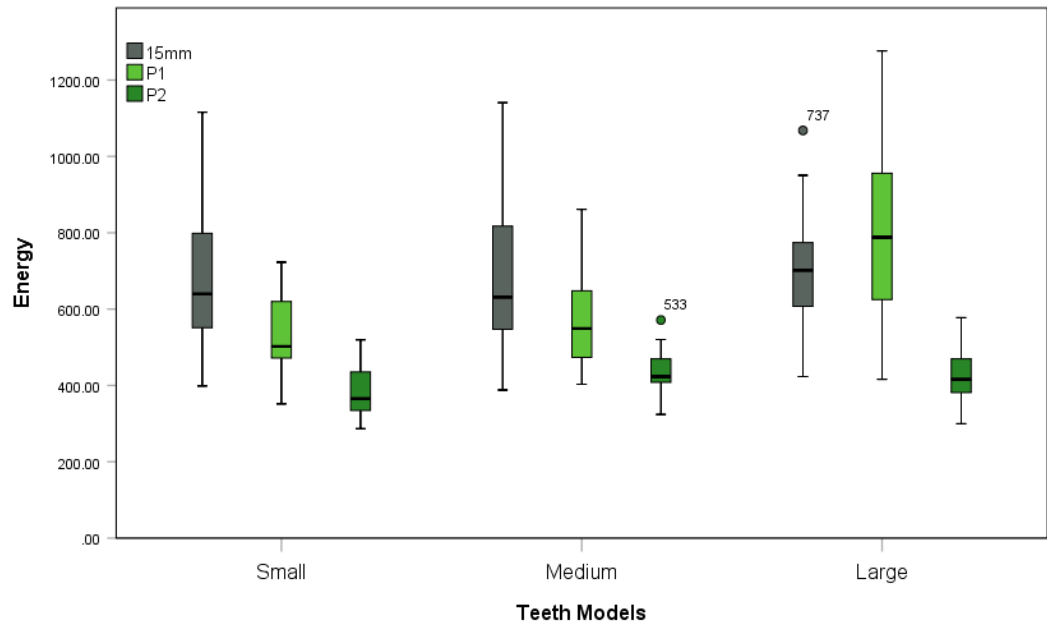
Figure 3.40 Boxplot showing energy (mJ) required to induce fracture of the 15mm spheres during the placement tests. 15mm results from the original tests have been included.

These tests indicate that the placement of the food object on the tooth can have significant effects on the forces, displacement, and energy required to fracture the hypothetical food object. By changing the placement of a food object, efficiency can be increased or decreased dramatically.

Chapter 4: Discussion

4.1 Results

This study set out to investigate the relationship between tooth size, food size and food placement on food breakdown. Given that the hominin dental size has varied considerably and reduced significantly with the emergence of *Homo* the effect of dental size on food breakdown was explored. The hypothesis that smaller teeth will require smaller forces to initiate fracture and expend less energy during failure compared to larger teeth was tentatively met. There is some evidence to support it, though the advantage appears slight and inconsistent.

The second hypothesis predicted that the size of the food object would limit the efficiency at which it could be broken down. The size of the object affects the gape required to masticate it, as well as the degree to which the teeth can come in contact with the object and the number of cusps that can come in contact with it. The smaller objects were limited to come in contact with only the upper and lower M2s, but the larger objects were able to involve the M1s and even parts of the M3s, particularly on the small (1xscale) teeth. It was predicted that the greater the surface area of the teeth involved, and the less the surface area of the sphere involved in the tooth-food-tooth contact, the greater the forces required to induce fracture. Ultimately, the hypothesis that for any given tooth size larger food objects will require larger forces at initial fracture and expend more energy to induce fragmentation was met. Whether the cause for this outlined above is accurate requires further study into the contact surface area.

Finally we also examined how food placement can alter the requirements placed on the masticatory apparatus for food breakdown. We predicted that placement of the food object over a tooth cusp rather than the whole occlusal surface will reduce the force at initial fracture and the energy required to induce fracture. this condition was also rejected. The original placement over the centre of the lower M2, and the P1 placement on the buccal edge of the M2 were the conditions designed to limit contact surface area most, with the P2 placement over the distal cusps of the lower M1 and the mesial cusps of the lower M2 designed to maximize contact surface area. For the hypothesis conditions to have been met, the P2

placement should have experienced the greatest forces and expended the most energy. The opposite was true. It is unclear why this was the case. Additional work could be directed towards better accurately measuring the surface area in contact with the sphere at each placement. It is possible that due to the specific topography of the teeth used, P1, though designed to limit contact surface area, actually maximised it. The buccal edge of the M2 did exhibit some signs of wear that in effect blunted that edge. No practical method of obtaining this measurement was devised for this project.

Overall the reduced size of *Homo* teeth may not be totally disadvantageous

The above results clearly suggest that food object size has a significant and identifiable impact on the forces required to induce fracture. Regardless of the size of the tooth, the energy, peak force, and displacement required to induce fracture increase as the size of the food object being fractured increases. From an ecological perspective, this would indicate that a diet consisting of smaller food objects may require less energy from the animal to consume than a diet consisting of larger food objects.

Additionally, the results seem to follow similar trends, regardless of teeth size. This may indicate that teeth size has a negligible influence on the fracture mechanics, especially when compared to the influence of object size. However, in order to better understand the effect of teeth size on fracture performance, it is necessary to compare between the results for each sphere size when crushed by each of the three models above.

It should be noted that the larger the sphere, the greater the standard deviation. This may reflect some physical property that is an artefact of the 3D printing process. Perhaps the larger spheres are more variable in their internal structure, possibly caused by the adhesive binder not drying to the same depth in the larger spheres. This is speculative, though previously addressed by Swan (2016), and is the reason the vacuum oven was incorporated in the sphere processing. It was felt that 24hr would be sufficient to adequately dry the spheres, but this was based on drying times for the hemispheres. Further research is required. Alternatively, the spheres may not be grabbing the larger spheres as well as they did the small

spheres. It was observed that the smaller spheres fit neatly between the cusps of the lower teeth, but the larger teeth rested instead on the cusps of the lower teeth. This could lead to slight variations in the position of the sphere in relation to the teeth, which could result in different fracture mechanics. That said, this effect would be expected to be more pronounced on the small teeth models, which were smaller relative to the spheres than the medium or large models, and thus experienced this change in position on smaller sized spheres.

4.2 Limitations

There are several limitations inherent in this study. Fundamentally this study only modelled initial fracture. Mastication is a multi-step process, and initial fracture is only one part of that process, and a part that is most important to one type of feeding: hard object feeding. It is debate bale how important hard objects feeding is to human masticatory development. Laird (2015) found that large toothed individuals mere most efficient at mastication, contrary to these results. Perhaps the larger surface area allows for increased fragmentation. Laird also incorporated fragmentation into her calculation of efficiency, which could provide a more result that is more meaningful. Additionally, this study used as a food object a 3D printed sphere. Though the size of the sphere was altered, the material properties were not intentionally or knowingly done so. This was done to preserve replicability and limit variability. However, it is possible that the effects observed in this study are particular to the material properties of the food object. Perhaps the material or the way it is constructed, or perhaps the shape of the food object has an effect on the relationship between fracture mechanics and tooth size.

4.3 Directions for future research

Future research should endeavour to incorporate additional materials. Particularly interesting would be real foods, such as fruits and berries. Meats, particularly the differences between raw and cooked meat would be highly relevant to current discussions about masticatory size reductions, however, meat is highly displacement-limited and therefore not well suited to this testing mechanism. Perhaps some alternative test could be developed.

4.4 Conclusion

The work presented in this thesis developed a novel physical testing rig to compare the fracture performance of teeth of differing sizes on the breakdown of food replicas to examine the relationship between tooth size, food size and breakdown performance. This work presented the design of a protocol for sensitivity studies carried out in order to develop the methodology for subsequent investigations into dental mechanics. The rig was successfully developed and subsequently used to examine trends in the dental reduction size of our own species.

The results of this study suggest that smaller teeth of modern *Homo sapiens* are slightly more efficient, than they could be if larger in size, reducing the force required and energy for all sizes of food. However, compared to the effect of changes in food size and the location of the bite on the tooth, performance differences between the different tooth sizes were minimal. The results suggest that individuals may be able to access different stress resistant food resources by simply changing how they position a food item, but also suggest that dental reduction during human evolution may have had a minimal impact on the ability of the individual to break hard food items of varying sizes. This study highlights the conflicting constraints placed on a tooth and considers the evolutionary, developmental and mechanical mechanisms that may have resulted in the reduced molar size we see during human evolution.

Much work has focused on the effect, generally assumed to be pronounced, extraoral processing, particularly with tools and fire, i.e. cooking, must have had on hominin dental evolution. Logically, the marked trend towards size reduction, coupled with these relatively uniquely human subsistence strategies, must have some causal correlation. However, no such relationship has yet been identified. It has been theorised that cooking and other extraoral processing, such as cutting with tools, leads to a diminished work load for the masticatory apparatus. This would decrease the beneficial effects and competitive advantage of any genetic mutations increasing the ability of the masticatory apparatus of humans to accommodate high loads or work-intensive mastication, decreasing the likelihood these traits are passed on. As cooking techniques, technology, and particularly agriculture, domestication, and modern food processing advanced and developed,

mastication theoretically became easier and easier allowing hominin and eventually human teeth to exist at the sizes seen today (for example, Wrangham et al. 1999).

Interestingly, the results of this study seem to undercut the idea that small teeth are maladaptive to an increased masticatory demand. New developments in the field of genetics and epigenetics seem to support this. The inhibitory cascade effect indicates that epigenetics may have a significant impact on the size of teeth (Evans et al. 2016). Even more convincingly, recent work clearly shows that tooth size has not been positively selected for in recent human evolution (Gomez-Robles et al 2017).

Instead, it is likely that the trend towards tooth size reduction in hominins is a function of other changes to the craniomandibular apparatus and skeletal structure. Indeed, the results of the placement tests seem to indicate that perhaps broad changes in tooth size can be overlooked in favour of changes in topography when searching for indications of dietary change.

References

Aiello, L.C., and Dean, C. (1990) *An Introduction to Human Evolutionary Anatomy*. Academic Press Limited: London.

Aiello, L.C., and Wheeler, P. (1995). The expensive-tissue hypothesis: the brain and the digestive system in human and primate evolution. *Current Anthropology,* 36, 199-221.

Alam, M.K., Hamza, M.A., Khafiz, M.A., Abul Rahman, S., Shaari, R., Hassan A. (2014) Multivariate Analysis of Factors Affecting Presence and/or Agenesis of Third Molar Tooth. *PLoS One* 9(6): e101157.

Anderson, P.S.L. (2009) The effects of trapping and blade angle of notched dentitions on fracture of biological tissues. *Journal of Experimental Biology* 212: 3627-3632.

Anderson, P.S.L. and Rayfield, and E.J. (2012) Virtual experiments, physical validation: dental morphology at the intersection of experiment and theory. *J. R. Soc. Interface* 9:1846-1855.

Bailey, S.E., Weaver, T.D. and Hublin, J.-J. (2017) The Dentition of the Earliest Modern Humans: How 'Modern' Are They?, in Assaf Marom and Erella Hovers (eds.) *Human Paleontology and Prehistory: Contributions in Honor of Yoel Rak*. Springer: London.

Barnett, A.A., Bezerra, B.M., Santos, P.J.P, Spironello, W.R., Shaw, P.J.A., MacLarnon, A., and Ross, C. (2016) Foraging with finesse: A hard-fruit-eating primate selects the weakest areas as bite sites. *American Journal of Physical Anthropology* 160(1), 113-125.

Berthaume, M., Grosse, I.R., Patel, N.D., Strait, D.S., Wood, S. and Richmond, B.G. (2010) The effect of early hominin occlusal morphology on the fracturing of hard food items. *The Anatomical Record* 293: 594-606.

Berthaume, M.A. (2016) Food mechanical properties and dietary ecology. American Journal of Physical Anthropology, 159(S61), pp.79-104.

Birnbaum, N.S. and Aaronson, H.B. (2008) Dental impressions using 3D digital scanners: virtual becomes reality. *Compend Contin Educ Dent*. 29(8): 494-505.

Brace, C.L., Rosenberg, K.R. and Hunt, K.D. (1987) Gradual change in Human tooth size in the Late Pleistocene and Post-Pleistocene. Evolution, 41(4): 705-720.

Brace, C.L., Smith, S.L. and Hunt, K.D. (1991) What big teeth you had grandma! Human tooth size, past and present. *Advances in dental anthropology*, 121, 33-57.

Calcagno, J.M. and Gibson, K.R. (1988) Human dental reduction: natural selection or the probable mutation effect. *American Journal of Physical Anthropology*, 77, 505-517.
Constantino, P.J., Lee, J.J.W., Chai, H., Zipfel, B., Ziscovici, C., Lawn, B.R., and Lucas, P. W. (2010) Tooth chipping can reveal the diet and bite forces of fossil hominins. *Biology letters*, 6, 826-829.

Crofts, S.B. and Summers, A.P. (2014) How to best smash a snail: the effect of tooth shape on crushing load. *J. R. Soc. Interface* 11: 20131053

Curtis N, Kupczik K, O'Higgins P, Moazen M, Fagan MJ (2008) Predicting skull loading: applying multibody dynamics analysis to a macaque skull. The Anatomical Record 291(5): 491-501.

Daegling, D.J., McGraw, W.S., Ungar, P.S., Pampush, J.D., Vick, A.E. and Bitty, E.A. (2011) Hard-object feeding in sooty mangabeys (*Cercocebus atys*) and interpretation of early hominin feeding ecology. *PLoS One*, 6(8), p.e23095.

Daegling, D.J., Judex, S., Ozcivici, E., Ravosa, M.J., Taylor, A.B., Grine, F.E., Teaford, M.F. and Ungar, P.S. (2013) Viewpoints: feeding mechanics, diet, and dietary adaptations in early hominins. *American Journal of Physical Anthropology*, 151(3), pp.356-371.

Dalstra, M. and Melsen, B. (2007) From alginate impressions to digital virtual models: accuracy and reproducibility. *Journal of Orthodontics* 36(1): 36-41.

Demes, B. (1987) Another look at an old face: biomechanics of the neandertal facial skeleton reconsidered. *J Hum Evol* 16, 297-303.

Demes, B. and Creel, N. (1988) Bite force, diet, and cranial morphology of fossil hominids. *Journal of Human Evolution*, 17, 657-670.

Dunsworth, H.M. (2010) Origin of the genus *Homo*. *Evo Edu Outreach* (2010) 3:353–366.

Evans, A.R., Daly, E.S., Catlett, K.K., Paul, K.S., King, S.J., Skinner, M.M., Nesse, H.P., Hublin, J.-J., Townsend, G.C., Schwartz, G.T. and Jernvall, J. (2016) A simple rule

governs the evolution and development of hominin tooth size. *Nature*, 530, pp. 477-480.

Freire Fernandes, T.M., Sathler, R., Natalicio, G.L., Castanha Henriques, J.F. and Pinzan, A. (2013) Comparison of mesiodistal tooth widths in Caucasian, African and Japanese individuals with Brazilian ancestry and normal occlusion. *Dental Press Journal of Orthodontics*, 18(3), 130-135.

Friess, M., 2012. Scratching the surface? The use of surface scanning in physical and paleoanthropology. Journal of Anthropological Sciences, 90, pp.1-25

Fukui, T., Tsuruta, M., Murata, K., Wakimoto, Y., Tokiwa, H. and Kuwahara, Y. (2002) Correlation between facial morphology, mouth opening ability, and condylar movement during opening-closing jaw movements in female adults with normal occlusion. *European Journal of Orthodontics* 24:327-36.

Godinho, R.M., Fitton, L.C., Toro-Ibacache, V., Stringer, C.B., Lacruz, R.S., Bromage, T.G., and O'Higgins, P. (2018) The biting performance of *Homo sapiens* and *Homo heidelbergensis*. *Journal of Human Evolution* 118, 56-71.

Goldstein, S., Post, D. and Melnick, D. (1978) An analysis of cercopithecoid odontometrics. I. The scaling of the maxillary dentition. *American Journal of Physical Anthropology* 49(4), 517-532.

Gomez-Robles, A., Smaers, J.B., Holloway, R.L., Polly, P.D and Wood, B.A. (2017) Brain enlargement and dental reduction were not linked in hominin evolution. PNAS, 114(3), 468-473.

Hublin, J.-J., Ben-Ncer, A., Bailey, S. E., Freidline, S. E., Neubauer, S., Skinner, M. M., Bergmann, I., Le Cabec, A., Benazzi, S., Harvati, K., Gunz, P. (2017) New fossils from Jebel Irhoud, Morocco and the pan-African origin of *Homo sapiens*. *Nature,*546, 289-292.

Hunter, E. (2016) The effect of dental wear on food breakdown during development in a hard-object feeding primate (*Cercocebus atys*).

Irish, J.D., Hemphill, B.E., de Ruiter, D.J. and Berger, L.R. (2015) The apportionment of tooth size and its implications in *Australopithecus sediba* versus other Plio-pleistocene and recent African hominins. *American Journal of Physical Anthropology*, 161, 398-413.

Kay, R.F. (1975) The functional adaptations of primate molar teeth. *American Journal of Physical Anthropology*, 43(2), pp.195-215.

Kay R.F. (1985) Dental evidence for the diet of *Australopithecus. Annual Review of Anthropology,* 14, 315-341.

Khodabakhshian, R. and Emadi, B. (2014) Development of a Finite Element Method Model to Determine Mechanical Behavior of Pumpkin Seed. *International Journal of Food Properties*, 18(2): 231-240.

Laird, M. (2015) Chewing efficiency in modern humans: adaptation and variation of the masticatory complex.

Laird, M., Vogel, E.R., and Pontzer, H. (2016) Chewing efficiency and occlusal functional morphology in modern humans. *Journal of Human Evolution* 93: 1-11.

LeBlanc, S.A and Black, B. (1974) A long term trend in tooth size in the eastern Mediterranean. *American Journal of Physical Anthropology*, 41, 417-422.

Lee-Thorpe, J.A., Sponheimer, M., Passey, B.H., de Ruiter, D.J. and Cerling, T.E. (2010) Stable isotopes in fossil hominin tooth enamel suggest fundamental dietary shift in the Pliocene. *Philosophical Transactions of the Royal Society B: Biological Sciences, 365*(1556), 3389-3396.

Lucas, P.W. (2004) *Dental functional morphology: how teeth work*. Cambridge: Cambridge University Press.

Macho, G.A. and Moggi-Cecchi, J. (1992) Reduction in maxillary molars in *Homo sapiens*: a different perspective. *American Journal of Physical Anthropology*, 87, 151-159.

Nandini, V.V., Venkatesh, K.V. and Nair, K.C. (2008) Alginate impressions: A practical perspective. *Journal of Conservative Dentistry* 11(1): 37-41.

Patterson, N., Richter, D.J., Gnerre, S., Lander, E.S., and Reich, D. (2006) Genetic evidence for complex speciation of humans and chimpanzees. *Nature*, 441, 1103-1108

Pinhasi, R. and Meiklejohn, C. (2011) Dental Reduction and the Transition to Agriculture in Europe, in Ron Pinhasi and Jay T. Stock (eds.) *Human Bioarchaeology of the Transition to Agriculture*. John Wiley & Sons, Ltd. London. pp 451-473.

Pilloud, M.A., Hefner, J.T., Hanihara, T. and Hayashi, A. (2014) The use of tooth crown measurements in the assessment of ancestry. *Journal of Forensic Sciences*, 59(6), 1493-1501.

Ruiz, J. and Arsuaga, J.L. (2017) On the calculation of occlusal bite pressures for fossil hominins. *Journal of Human Evolution*, 102, 67-71.

Schmidt, C.W. (2012) CT scans: balancing health risks and medical benefits. *Environmental Health Perspectives* 120(3): A118-A121.

Sellers, W.I. and Crompton, R.H. (2004) Using sensitivity analysis to validate the predictions of a biomechanical model of bite forces. *Annals of Anatomy Anatomischer Anzeiger,* 186(1), 89-95.

Shi, J., Curtis, N., Fitton, L.C., O'Higgins, P., Fagan, M.J. (2012) Developing a musculoskeletal model of the primate skull: predicting muscle activations, bite force, and joint reaction forces using multibody dynamics analysis and advanced optimisation methods. *Journal of Theoretical Biology,* 310, 21-30.

Slizewski, A., Friess, M., and Semal, P. (2010) Surface scanning of anthropological specimens: nominal-actual comparison with low cost laser scanner and high-end fringe light projection surface scanning systems. *Quartär* 57: 179-187.

Sponheimer, M., Alemseged, Z., Cerling, T.E., Grine, F.E., Kimbel, W.H., Leakey, M.G., Lee-Thorpe, J.A., Manthi, F.K., Reed, K.E., Wood, B.A., Wynn, J.G. (2013) Isotopic evidence of early hominin diets. Proceedings of the National Academy of Sciences, 110(26), 10513-10518.

Strait, S.G. (1993) Differences in occlusal morphology and molar size in frugivores and faunivores. *Journal of Human Evolution* 25(6) 471-484.

Strait, D.S., Weber, G.W., Neubauer, S., Chalk, J., Richmond, B.G., Lucas, P.W. and Grosse, I.R. (2009) The feeding biomechanics and dietary ecology of *Australopithecus africanus. Proceedings of the National Academy of Sciences,* 106(7), 2124-2129.

Strait, D.S., Grosse, I.R., Dechow, P.C., Smith, A.L., Wang, Q., Weber, G.W., Neubauer, S., Slice, D.E., Chalk, J., Richmond, B.G., Lucas, P.W., Spencer, M.A., Schrein, C., Wright, B.W., Byfton, C., Ross, C.F (2010) The Structural Rigidity of the Cranium of Australopithecus africanus: Implications for Diet, Dietary Adaptations, and the Allometry of Feeding Biomechanics, *Anat Rec*, 293, 583-593.

Strait, D.S., Constantino, P., Lucas, P.W., Richmond, B.G., Spencer, M.A., Dechow, P.C., Ross, C.F., Grosse, I.R., Wright, B.W., Wood, B.A. and Weber, G.W. (2013) Viewpoints: diet and dietary adaptations in early hominins: the hard food perspective. *American Journal of Physical Anthropology*, 151(3), pp.339-355.

Swan, K. (2016) Dental morphology and mechanical efficiency during development in a hard object feeding primate (*Cercocebus atys*). Unpublished PhD Thesis, Hull York Medical School.

Teaford, M.F., and Ungar, P.S. (2000) Diet and evolution of the earliest human ancestors. *Proceedings of the National Academy of Sciences*, 97(25), pp. 13506-13511.

Teaford, M.F., Ungar, P.S. and Grine, F.E. (2002) Paleontological evidence for the diets of African Plio-Pleistocene hominins with special reference to early *Homo*. In *Human diet: Its origins and evolution,* 143-166.

Townsend, G., Bockmann, M., Hughes, T., and Brook, A. (2012) Genetic, environmental and epigenetic influences on variation in human tooth number, size and shape. *Odontology*, 100, 1-9.

Unger, P.S., Grine, F.E. and Teaford, M.F. (2006) Diet in early *Homo*: a review of the evidence and a new model of adaptive versatility. *Annual Reviews in Anthropology,* 35, 209-228.

Ungar, P.S., Scott, R.S., Grine, F.F., and Teaford, M.F. (2010) Molar microwear textures and the diets of *Australopithecus anamensis* and *Australopithecus afarensis. Philosphical Transactions of the Royal Society B: Biological Sciences,* 365(1556), 3345-3354.

Ungar, P.S and Sponheimer, M. (2011) The diets of early hominins. *Science* 334(6053), 190-193.

Van der Merwe, N.J., Masao, F.T. and Bamford, M.K. (2008). Isotopic evidence for contrasting diets of early hominins *Homo habilis* and *Australopithecus boisei* of Tanzania. *South African Journal of Science,* 104(3-4), 153-155.

Vukelic, A., Cohen, J.A., Sullivan, A.P. and Perry, G.H. (2017) Extending Genome-wide association study results to test classic anthropological hypotheses: Human third molar agenesis and the "Probable Mutation Effect". *Human Biology*, 89(2).

Williams, S.H., Wright, B.W., Truong, V.D., Daubert, C.R. and Vinyard, C.J. (2005) Mechanical properties of foods used in experimental studies of primate masticatory function. *American Journal of Primatology*, 67(3), pp.329-346.

Wood, B.A. and Stack, C.G. (1980) Does allometry explain the differences between "gracile" and "robust" australopithecines? *American Journal of Physical Anthropology*, 52(1), 55-62.

Wood, B.A. and Collard, M. (1999) Human Genus. *Science*, 284(5411), pp. 65-71.

Wood, B.A. and Strait, D.S. (2004) Patterns of resource use in early *Homo* and *Paranthropus*. *Journal of Human Evolution* 46(2), 119-162.

Wrangham, R.W., Jones, J.H., Laden, G., Pilbeam, D., Conklin-Brittain, N. (1999) The raw and the stolen. *Current Anthropology,* 40, 567-594.

Zhang, H., Shen, L., Lan, H., Li, Y., Liu, Y., Tang, Y., and Wen, L. (2018) Mechanical properties and finite element analysis of walnut under different cracking parts*. International Journal of Agricultural and Biological Engineering*, 11(6), pp 81-88.

Appendix A Jan1

The following is a small excision that formed part of Ch. 2 that details the methods used to create the sphere placement devices and a description of the reason they were not used in the project. If the shrinkage problem could be overcome it is recommended any attempt to replicate this study make use of similar devices.

2.6.4.1 Description of the sphere placement devices

The sphere placement devices consist of a surface with a hole, sized to the diameter of the sphere being placed, supported by four L-shaped legs (Figure 2.27) . The height of the surface or table is dependent on the model and the diameter of the sphere, but is designed so that a sphere held in place will have its horizontal circumference at the midpoint of the width of the table when the sphere is just coming into contact with the teeth below it. The width of the table is also predicated on the diameter of the sphere. The L-shaped legs are designed so that they grip the corners of the square attachment plates on the teeth models. The lengths of the sides of the placement device are thus dependent on the lengths of these attachment plates, though the legs are created with a thickness of 5 mm, so the length of the placement devices are always 10 mm longer than the attachment plates. The placement device is bisected diagonally through two legs, creating two parts that can be pushed together to hold the sphere in position or pulled apart to remove them before crushing the sphere
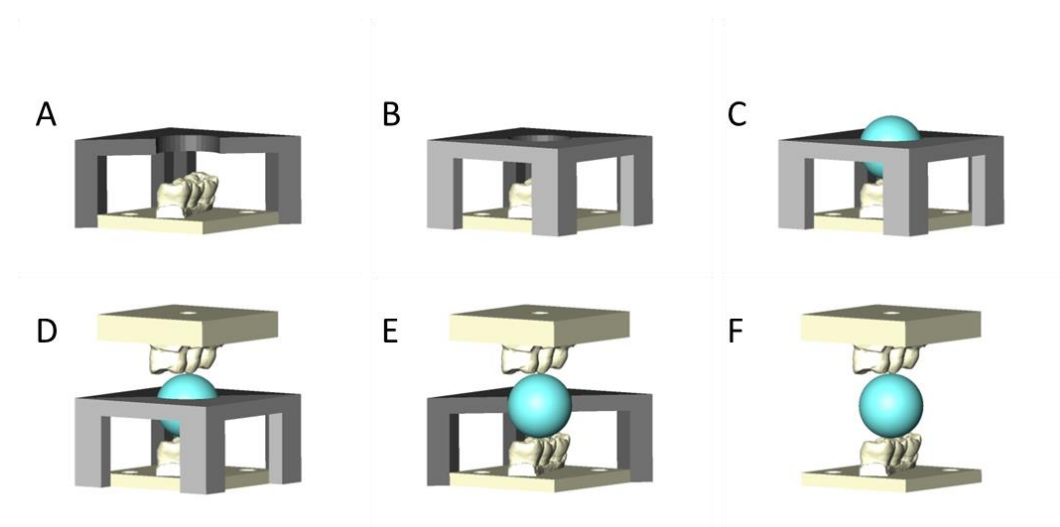
Figure 2.27 Process showing how the sphere placement devise allows the sphere to be placed centrally and consistently above the M2 (A-C). Once the teeth have made contact (D) the device can then be removed (E) leaving the sphere in occlusion (F).

In order to create placement devices to fit all sized spheres, the exact heights of the legs of the device had to be calculated. In Geomagic Studio (v.11; Dassault Systèmes SolidWorks Corp., MA, USA), the sphere of a given size is transformed such that its centre point is directly over the origin. The sphere is then raised or lowered so that it only just touches the ideal point of contact desired on the occlusal surface of the tooth. A Boolean intersect is then performed to create a file that is just the portion of the occlusal surface of the tooth in contact with the sphere. These three files are then uploaded to Avizo (v.9.2; Visualization Sciences Group, Burlington, MA, USA). A landmark set is created with one landmark, a, placed on the intersect and another, b, on the underside of the mandible. The difference in the values of the z dimensions between these points gives the height above the plate at which the sphere first comes into contact with the tooth. The height of the legs, l, of the sphere placement device should be this number plus the distance from the first landmark's z coordinate to a plane through the diameter of the sphere and parallel to the horizontal minus half the width, w, of the table atop the legs of the sphere placement device. The placement of a landmark, c, at the centre of the sphere is useful to assist in these calculations. Thus:

$$|a_z - b_z| + |a_z - c_z| - \frac{w}{2} = l$$

.

For each sphere diameter and teeth model these numbers will be different. Finally, in SolidWorks (Dassault Systemes SolidWorks Corp., MA, USA) a square is sketched with lengths 10 cm longer than the lengths of the attachment plates of the model. A circle is sketched from the midpoint of this square with a diameter the exact size of the diameter of the sphere being placed. The square is then extruded the desired width, leaving enough of the sphere exposed for the mandibular tooth to grip when lowered. For the 10 mm, 15mm, and 20 mm spheres this was 5 mm. For the 5 mm spheres this was naturally too thick, and so instead a 2 mm thick table

was created. L-shapes were then sketched in each corner, and extruded to a length, *l*, obtained using the formula above. A plane was then created bisecting the device diagonally and cutting through two corners. In this way, two parts, each with three legs to stand on were created. The sphere placement device was 3D printed and proved to be highly successful (Figure 2.28).
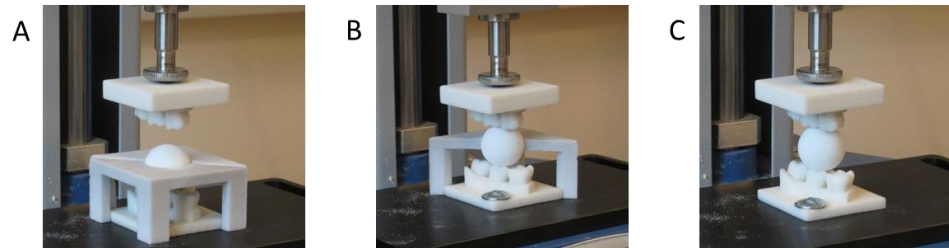

Figure 2.28 3D printed sphere placement device allows the sphere to be placed centrally and consistently above the M2 (A). Once the teeth have made contact (B) the device can then be removed leaving the sphere in occlusion (C). Note prototype dental models are used here rather than the final metal models.

2.6.4.2 Abandonment of sphere placement device and metal model shrinkage

At the point of completion of the above ZPrinter sphere placement devices (Figure 2.28) we were still awaiting delivery of the final metal dental models (Figure 2.21). Unfortunately after the metal dental models had been delivered it was noted that they experienced a slight degree of shrinkage (<4%), and though this was expected, it turned out to be slightly unpredictable and not uniform. There were slight variations in the degree of shrinkage, with some dimensions experiencing as little as <2%, and others as much as 5%.

While this shrinkage seemed to make little impact on the tooth models, such that the upper and lower teeth still fit together perfectly in occlusion, the error produced was enough to render the powder composite sphere placement devices unsuitable for the metal dental models. They no longer fit perfectly and thus rendered their aim, which was absolutely accurate placement of the sphere, unattainable. One option was to also get the sphere placement devices manufactured simultaneously in metal, which might retain the same shrinkage and thus allow the locking of the legs around the attached bases. While this was

considered, due to time and budgetary constraints it was not possible to get all the sphere placement devices made in metal. As such the use of a sphere placement device for accurate placement, wanted for chapter 3, was abandoned.